2018-06-18

Damage and Remodelling in Recruitment-Based Models for Biological Tissues

Hamedzadeh, Amirhossein

UNIVERSITY OF CALGARY

Damage and Remodelling in Recruitment-Based Models for Biological Tissues

by

Amirhossein Hamedzadeh

A THESIS

SUBMITTED TO THE FACULTY OF GRADUATE STUDIES

IN PARTIAL FULFILLMENT OF THE REQUIREMENTS FOR THE

DEGREE OF DOCTOR OF PHILOSOPHY

DEPARTMENT OF MECHANICAL AND MANUFACTURING ENGINEERING

CALGARY, ALBERTA

June, 2018

Abstract

This thesis focuses on the continuum mechanical modelling of soft biological tissues seen as composite material reinforced by collagen fibres. The fibres have a progressive recruitment mechanism, and the tissue can undergo damage or remodelling. The thesis consists of two major parts. In the first part of the thesis, the recruitment and damage of soft tissues are modelled by introducing a rigorous continuum treatment of the fibre seen as a bundle of fibrils. The fibrils have different initial undulation, and this is represented by the means of a recruitment probability distribution. By exploiting the recruitment distribution, we construct a recruitment and damage model, where the fibrils are progressively recruited and damaged. The model is implemented in a Finite Element package and, as an example, the damage of a human Achilles tendon is studied. The Finite Element model is capable of capturing the qualitative behaviour of the tendon under uniaxial tension. The second part of the thesis focusses on the remodelling of biological tissues in the framework of the theory of material uniformity. A constitutive evolution model is introduced, including fibre recruitment and reorientation, and subjected to the entropy inequality, which enforces the Second Principle of Thermodynamics. The model is applied to a numerical example describing a pressurised fibre-reinforced cylinder, roughly representing an artery, and is able to capture the major characteristics of remodelling in arteries, as reported in the literature. To summarise, this thesis provides a framework for modelling of the interaction of fibril recruitment and damage and of whole fibre recruitment and remodelling, and constitutes a promising starting point for a more general model capable of studying the interaction of damage, remodelling and healing.

Acknowledgements

My journey as a PhD student was full of ups and downs, but the only consistent thing that I had during this journey was the great support of my supervisory committee. First and foremost, my great supervisor, Dr. Salvatore Federico, has been supportive beyond measure in every aspect imaginable. I am greatly indebted to Dr. Marcelo Epstein, not just for the scientific guidance, but also for shaping my thoughts. Dr. Elena Di Martino (Civil Engineering) was very kind and welcoming whenever I needed help on the biomechanical aspects of this research.

I would like to thank Dr. Richard Wan (Civil Engineering) for a great course on geomaterials which I took during my PhD and for being on my examining committee. I would also like to thank Dr. David Steigmann (University of California Berkeley, USA) for accepting to serve as the external examiner of my thesis defence.

I would like to acknowledge the financial support of the Canadian Society for Biomechanics, which provided me with the opportunity to travel to Sweden as a visiting student. I would like to thank Dr. T. Christian Gasser for hosting me at the KTH Stockholm (Sweden) in 2016 and for his help in developing the numerical analysis part of my thesis, and Dr. Alfio Grillo (Politecnico di Torino, Italy) for the help in the development of the remodelling part of the thesis. I am also thankful to Dr. Walter Herzog (Kinesiology), Dr. Mike Kallos and his postdoctoral fellow Dr. Fraz Anjum (Department of Biological Sciences), my MSc supervisor Dr. Nigel Shrive (Civil Engineering) and Dr. Francesco dell'Isola (Università di Roma La Sapienza, Italy) for great scientific discussions on different subjects.

Last, but not least, I am also grateful for all the help and feedback that I received from all my fellow group members, particularly Mawafag Alhasadi, Kotaybah Hashlamoun, Dr. Eng Kuan Moo and Scott Sibole.

Table of Contents

List of Tables

List of Figures and Illustrations

Chapter 1

Introduction

A biological tissue is comprised of a group of cells that have the same functionality and are embedded in an extracellular matrix, composed of several types of macromolecules and water (Fung, 1995). The most common protein in fibrous tissues is collagen, which makes up a large part of the extracellular matrix (Fratzl, 2008) and heavily influences their material properties. A collagen fibre is a hierarchical structure, comprised of bundles of collagen fibrils, which resemble spring-shape structures that are bound together (Fratzl, 2008).

Biological tissues are profoundly different from commonplace engineering materials in that they are highly complex multi-phasic materials, with non-linear, anisotropic, inhomogeneous, time-dependent behaviour (Fung, 1995). Their hierarchical structure plays a key role in their response to external stimuli, such as mechanical forces, electrical signals, and heat. Moreover, the cells can alter the behaviour of the tissue in which they are embedded, as they respond to the external stimuli. This response can be in the form of adaptation and reorganisation (remodelling) of the tissue's internal structure.

Throughout the past decades, Continuum Mechanics has been employed as a tool to study the behaviour of biological tissues. The constitutive models for biological tissues can be divided in two broad categories, namely structural and phenomenological models (Gasser et al., 2006). Structural models account for information regarding the underlying histology (Zulliger et al., 2004; Humphrey, 2003; Holzapfel et al., 2000) and have shed light on the functions of tissues and provided insight into their response to a given mechanical loading. Moreover, structural models have been enhanced with the capability of capturing the effect of the dispersion in the orientation of the collagen fibres by adopting probability distribution functions (Lanir, 1983; Federico et al., 2005; Federico and Herzog, 2008; Gasser et al., 2006).

The load-bearing properties, damage mechanisms and remodelling mechanisms of a biological tissue can be described by considering the arrangement of the collagen fibres embedded in the otherwise isotropic matrix material. It is assumed that the collagen fibrils constituting a particular collagen fibre progressively straighten under stretch before each of them can carrying a load (Hurschler et al., 1997; Martufi and Gasser, 2011).

The goal of this thesis is to propose a framework for the description of damage and remodelling, considering the progressive recruitment the structural elements (either of fibrils in a collagen fibre or of a fibre as a whole).

The failure and damage mechanisms of soft biological tissues arise from the microstructure of the tissue. Despite increasing experimental and analytical efforts, failure-related irreversible phenomena of soft biological tissue have not been fully understood, and there is no consensus on a univocal definition of damage in soft tissues (Gasser, 2011). Common damage models from engineering materials might not fit biological tissues, whose microstructure must be taken into account carefully. In order to build our soft tissue damage model, we take, as a point of departure, some recent works by Gasser (2011) on damage of biological tissues, by Martufi and Gasser (2011) on progressive recruitment of collagen fibrils, and by several groups on biological tissues with statistical orientation of collagen fibres (e.g., Lanir, 1983; Hurschler et al., 1997; Gasser et al., 2006; Federico and Herzog, 2008; Federico and Grillo, 2012).

The collagen fibres are the main actors also when remodelling is considered. In general, growth and remodelling are two interconnected aspects (e.g., Epstein and Maugin, 2000). Growth (mass increase) and resorption (mass decrease) correspond to a change in mass density, whereas remodelling is the rearrangement of the internal structure. When a fibre-reinforced material, such as a biological tissue, undergoes remodelling, the collagen fibres reorient driven, by a particular measure of stress called *Mandel stress* (Epstein and Elzanowski, 2007). Among the several different approaches for growth and remodelling, in

this thesis we follow that of *material uniformity*, introduced by Noll (1967), and further studied by, e.g.,Epstein and Maugin (1990, 2000). Our goal is to study the remodelling of a biological tissue in which not only the orientation of the collagen fibres evolves with time, but also the waviness of the fibres does. This implies a "relaxation", which has been observed experimentally (Kamiya and Togawa, 1980).

1.1 Objectives

The objectives of this thesis project are to:

1. Establish a rigorous continuum treatment of fibril recruitment models;
2. To construct damage and unloading models based on the newly proposed recruitment model;
3. To implement the recruitment-damage model in a Finite Element package;
4. To study the continuum treatment of remodelling of fibrous tissues in the framework of material uniformity theory.

Objectives 1, 2 and 3 were the goal of a paper that has been accepted for publication, Hamedzadeh, A., Gasser, T.C., Federico, S., 2018, On the constitutive modelling of recruitment and damage of collagen fibres in soft biological tissues, *Eur. J. Mech. - A/Solids*, in press, DOI: 10.1016/j.euromechsol.2018.04.007
and, in this thesis, are addressed in Chapters 3, 4 and 5, respectively.

1.2 Synopsis

In the remainder of this chapter, we briefly recall the notation that we employ. In Chapter 2, we report a literature review on the hierarchical structure of soft tissues, their mechanical

behaviour and testing, continuum damage mechanics, damage of biological tissues, growth and remodelling of soft biological tissues from the point of view of Continuum Mechanics.

In Chapter 3, we propose a rigorous continuum treatment of fibril recruitment and its kinematics, and we discuss the notion of recruitment probability density function and its properties. We correct the model previously proposed by Martufi and Gasser (2011) and we prove its uniqueness, considering the assumption made on the constitutive stiffness. Finally, we generalise the newly proposed model and show its equivalence to the model previously proposed by Hurschler et al. (1997). In Chapter 4, we construct a progressive damage model based on the recruitment model we proposed in Chapter 3 and we prove its equivalence to the damage model proposed by Hurschler et al. (1997). Moreover, we construct an unloading model based on the exclusion of the damaged fibrils. In Chapter 5, we implement the damage model into a Finite Element package and regularise the model to make it mesh-independent. As an example of application, we study the damage of Achilles tendons under uniaxial tension.

In Chapter 6, we discuss the premises of the theory of material evolution in the framework of *theory of uniformity* and we introduce an admissible evolution law. In Chapter 7, we solve the problem of the remodelling of a pressurised fibre-reinforced cylinder (mimicking an artery), based on the model introduced in Chapter 6. In addition, we study the sensitivity of the model to the initial mean fibre orientation angle and fibre straightening stretch.

In Chapter 8, we summarise the findings of our thesis and discuss the limitations and the possible future work.

1.3 Notation and Continuum Mechanics Basics

In this section we introduce basic notation that has been used in this thesis. Generally, we follow the notion from the text by Marsden and Hughes (1983), in which uppercase symbols and indices are used for material quantities (in the reference configuration) and lowercase

symbols and indices are used for spatial quantities (in physical space).

The physical space is represented by a three-dimensional affine space (Epstein and Maugin, 2010), denoted by $\mathcal{S}$. At each point $x \in \mathcal{S}$, we define the tangent space $T_x\mathcal{S}$ as the vector space of all vectors emanating from x. The (disjoint) union of all tangent spaces, for all $x \in \mathcal{S}$ is called tangent bundle $T\mathcal{S}$. The dual spaces are the cotangent space $T_x^\star\mathcal{S}$ and the cotangent bundle $T^\star\mathcal{S}$. The space $\mathcal{S}$ is endowed with a metric tensor $\boldsymbol{g} : T\mathcal{S} \times T\mathcal{S} \to \mathbb{R}$, which is a tensor field valued in the tensor space $[T\mathcal{S}]_2^0 = T^\star\mathcal{S} \otimes T^\star\mathcal{S}$, and has (covariant) components g_{ab}. The inverse metric tensor $\boldsymbol{g}^{-1} : T^\star\mathcal{S} \times T^\star\mathcal{S} \to \mathbb{R}$ is valued in the tensor space $[T\mathcal{S}]_0^2 = T\mathcal{S} \otimes T\mathcal{S}$ and has (contravariant) components g^{ab}. The metric tensor and its inverse define the scalar products between vectors and covectors, respectively, i.e., $\boldsymbol{u}.\boldsymbol{v} = \boldsymbol{g}(\boldsymbol{u},\boldsymbol{v}) = \boldsymbol{u}\boldsymbol{g}\boldsymbol{v} = u^a g_{ab} v^b$, $\boldsymbol{\varphi}.\boldsymbol{\psi} = \boldsymbol{g}^{-1}(\boldsymbol{\varphi},\boldsymbol{\psi}) = \boldsymbol{\varphi}\boldsymbol{g}^{-1}\boldsymbol{\psi} = \varphi_a g^{ab} \psi_b$, and are used to lower or raise the indices of any tensor. The fully covariant and contravariant counterparts of an arbitrary tensor are denoted by a flat "$\flat$" and a sharp "$\sharp$", respectively. For instance, for a "mixed" second-order tensor $\boldsymbol{a}$, its "covariant" counterpart $\boldsymbol{a}^\flat$ has components $g_{ab}a^b{}_c$ and $\boldsymbol{a}^\sharp$ has components $a^a{}_b\, g^{bc}$. Moreover, a low dot "$.$" denotes the single contraction of two tensors performed by means of the appropriate metric tensor, e.g., for a fully "contravariant" second order tensor $\boldsymbol{b}$ and a vector $\boldsymbol{y}$, the contraction $\boldsymbol{b}.\boldsymbol{y}$ has components $b^{ab} g_{bc} y^c$.

A body is represented by one of its placements in space, elected as the reference configuration $\mathcal{B}$, assumed to be an open subset of $\mathcal{S}$. The reference configuration $\mathcal{B}$ is equipped with the metric tensor $\boldsymbol{G}$ with inverse $\boldsymbol{G}^{-1}$, with properties analogous to the metric $\boldsymbol{g}$ of the physical space $\mathcal{S}$.

The motion of the body $\mathcal{B}$ is an invertible differentiable map, called configuration, which maps every material points $X = (X^1, X^2, X^3)$ into spatial points $x = (x^1, x^2, x^3)$, at each given time t:

$$\chi(\,\cdot\,, t) : \mathcal{B} \to \mathcal{S} : X \mapsto x = \chi(X, t). \tag{1.1}$$

The differential of the configuration is called *deformation gradient* $\boldsymbol{F} : T\mathcal{B} \to T\mathcal{S}$, and has

components $F^a{}_A = \chi^a{}_{,A}$, where comma denotes partial differentiation. As a two-point tensor field, $\boldsymbol{F}$ maps points $X \in \mathcal{B}$ into the space $T\mathcal{B} \otimes T^\star\mathcal{S}$. The algebraic transpose of $\boldsymbol{F}$ is valued in $T^\star\mathcal{B} \otimes T\mathcal{S}$, and has components $(\boldsymbol{F}^T)_A{}^a = F^a{}_A$.

The *shifter* (Eringen, 1980; Marsden and Hughes, 1983) is defined as the tensor $\mathbf{1} : T\mathcal{B} \to T\mathcal{S}$ that, at every X, parallel-transports vectors from $T_X\mathcal{B}$ to $T_x\mathcal{S}$. The shifter $\mathbf{1}$ is orthogonal in the *metric* sense (Federico, 2012), i.e., $\mathbf{1}^{-1} = \boldsymbol{G}^{-1}\mathbf{1}^T\boldsymbol{g}$. When there is no deformation, the deformation gradient coincides with the shifter, i.e., $\boldsymbol{F} = \mathbf{1}$.

We define the right and left Cauchy-Green deformation tensors, denoted by $\boldsymbol{C}$ and $\boldsymbol{b}$ and their inverses, the Piola deformation tensor $\boldsymbol{B}$ and Finger deformation tensor $\boldsymbol{c}$ as pull-backs and push-forwards of the appropriate metric tensors:

$$\boldsymbol{C} = \chi^*\boldsymbol{g} = \boldsymbol{F}^T\boldsymbol{g}\boldsymbol{F} = \boldsymbol{F}^T.\boldsymbol{F}, \tag{1.2a}$$

$$\boldsymbol{b} = \chi_*\boldsymbol{G}^{-1} = \boldsymbol{F}\boldsymbol{G}^{-1}\boldsymbol{F}^T = \boldsymbol{F}.\boldsymbol{F}^T, \tag{1.2b}$$

$$\boldsymbol{B} = \chi^*\boldsymbol{g}^{-1} = \boldsymbol{F}^{-1}\boldsymbol{g}^{-1}\boldsymbol{F}^{-T} = \boldsymbol{F}^{-1}.\boldsymbol{F}^{-T}, \tag{1.2c}$$

$$\boldsymbol{c} = \chi_*\boldsymbol{G} = \boldsymbol{F}^{-T}\boldsymbol{G}\boldsymbol{F}^{-1} = \boldsymbol{F}^{-T}.\boldsymbol{F}^{-1}. \tag{1.2d}$$

The determinant of the two-point deformation gradient tensor $\boldsymbol{F}$ is defined, in terms of the components of $\boldsymbol{F}$ and of the metric tensors $\boldsymbol{g}$ and $\boldsymbol{G}$, as (Marsden and Hughes, 1983; Federico, 2015b)

$$J = \det\boldsymbol{F} = \sqrt{\det[\![g_{ab}]\!]}\,\det[\![F^a{}_A]\!]\,\frac{1}{\sqrt{\det[\![G_{AB}]\!]}}. \tag{1.3}$$

By comparing the pulled-back metric $\boldsymbol{C}$ with the undeformed metric $\boldsymbol{G}$, we can define the standard measure of strain, known as Green-Lagrange strain $\boldsymbol{E}$, as the material tensor

$$\boldsymbol{E} = \tfrac{1}{2}(\boldsymbol{C} - \boldsymbol{G}). \tag{1.4}$$

The stress tensors, Cauchy $\boldsymbol{\sigma}$, first Piola-Kirchhoff $\boldsymbol{T}$ and second Piola-Kirchhoff $\boldsymbol{S}$ are related to each other by

$$\boldsymbol{\sigma} = J^{-1}\boldsymbol{T}\boldsymbol{F}^T = J^{-1}\boldsymbol{F}\boldsymbol{S}\boldsymbol{F}^T. \tag{1.5}$$

In hyperelasticity, the first and second Piola-Kirchhoff stresses can be given as the derivatives of an *elastic strain energy* or *elastic potential* $\hat{W}$ with respect to the conjugate measure of deformation (or strain), i.e.,

$$\boldsymbol{gT} = \frac{\partial \hat{W}}{\partial \boldsymbol{F}}(\boldsymbol{F}), \tag{1.6a}$$

$$\boldsymbol{S} = \frac{\partial \hat{W}}{\partial \boldsymbol{E}}(\boldsymbol{E}) = 2\frac{\partial \hat{W}}{\partial \boldsymbol{C}}(\boldsymbol{C}). \tag{1.6b}$$

Most biological tissues are assumed to be incompressible due to presence of fluid in the matrix. Therefore, the modified hyperelasticity equations for incompressibility must be used, i.e.,

$$\boldsymbol{gT} = -p\, J\, \boldsymbol{F}^{-T} + \frac{\partial \hat{W}}{\partial \boldsymbol{F}}(\boldsymbol{F}), \tag{1.7a}$$

$$\boldsymbol{S} = -p\, J\, \boldsymbol{C}^{-1} + \frac{\partial \hat{W}}{\partial \boldsymbol{E}}(\boldsymbol{E}), \tag{1.7b}$$

$$\boldsymbol{\sigma} = -p\, \boldsymbol{g}^{-1} + J^{-1}\boldsymbol{F}\left[\frac{\partial \hat{W}}{\partial \boldsymbol{E}}(\boldsymbol{E})\right]\boldsymbol{F}^{T}, \tag{1.7c}$$

where p is the Lagrange multiplier arising from the kinematical constraint of isochoric (volume-preserving motion: $J = 1$).

Chapter 2

Literature Review

In this chapter we review a collection of studies on the mechanical behaviour of soft biological tissues, focusing on the role of collagen fibres. First, we briefly elaborate the hierarchical structure of tissues and collagen fibres and its significance with respect to the unique characteristics of biological tissues. Second, we outline the approaches used to form constitutive relations for biological tissues, in the context of Continuum Mechanics.

2.1 Hierarchical Structure of Biological Tissues

The hierarchical structure of biological tissues is of great importance as it ultimately determines their unique mechanical behaviour and their capacity to adapt and remodelling (Fratzl et al., 1997). Collagenous tissues are mainly built from collagen fibrils as the basic structural element. The thickness of fibrils is in the range of 50 to 500 nm. The fibrils provide a biomechanical scaffold for cells and other macromolecules (such as proteoglycans, elastin, etc) to attach and maintain the shape of the tissue (Kadler et al., 1996). Figure 2.1 shows the hierarchical structure of a tendon, as an example. The subcomponents of tendons include fascicles, fibrils and molecules. Collagen molecules are triple-helical protein chains with a length of around 300 nm and a width of 1.5 nm. They are staggered next to their neighbours, with a repeating banding pattern (also called D-period) of 64 nm to 67 nm (Hulmes, 2002), as shown in Figure 2.1. Each polypeptide chain contains one or more regions identified by the repeating amino acid pattern Gly-X-Y, where Gly denotes glycine, and X and Y can be any other amino acids. This pattern allows the chains to produce a right-handed triple-helical structure (Beck and Brodsky, 1998).

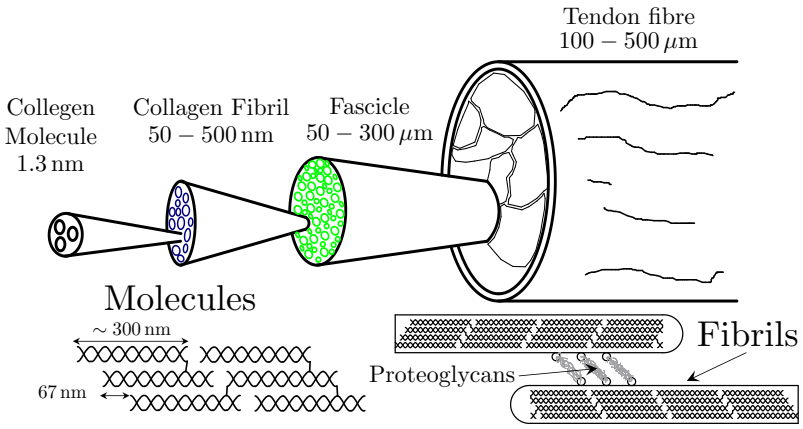

Figure 2.1: Hierarchical structure of fibres (Fratzl, 2008)

In humans, 28 types of proteins have been identified as collagen so far (Kadler et al., 2007; Myllyharju and Kivirikko, 2004). Collagen can be grouped into subfamilies based on their molecular compositions. Type I collagen is the most common collagen found in skin, tendon, bone and cornea. Type II has a more specific tissue distribution, which is mostly limited to cartilage. Type III is mostly present in relatively elastic tissues such as embryonic skin and lung. The other types of collagen are less abundant and they have specific roles in the structure of tissues, which have been discussed in Born and Richardson (1990) and Mendler et al. (1989).

2.2 Mechanical Testing of Biological Tissues

In mechanical modelling, we first need to make some assumptions regarding the general behaviour of the material, which consists in the statement of constitutive relations. The second step is to obtain the material parameters featuring in the constitutive equations through appropriate mechanical tests. Mechanical testing of biological tissues is particularly challenging, given the large variety of parameters needed to be taken into account. The difficulties in the testing of biological tissues can be attributed to many factors, including the small size of the specimens, the compositional inhomogeneity, the damage caused by clamping of the specimen (Sasaki et al., 1999). In addition to these common problems, there are also

difficulties in identifying the material axes and variability of mechanical characteristics among specimens, which will make the analysis of the experimental results more complex.

The typical non-linear stress-strain curve for soft tissues has a J-shape with a toe region (collagen fibres not yet recruited), an elbow region (collagen fibres being recruited) and a linear region (collagen fibres all recruited) and is obtained from uniaxial testing, as reported by numerous studies (Roeder et al., 2002; Tower et al., 2002; Fung, 1993; Hansen et al., 2002). Considering the anisotropic nature of biological tissues, biaxial testing is a better tool for studying their characteristics. However, in biaxial testing, extreme care needs to be taken to produce reliable results. For instance, the specimen should be clamped in a such a way that the edges can expand freely in the lateral direction under the "Poisson effect" caused by the stretch in the orthogonal direction (this is usually achieved by using multiple hooks rather than clamps). The region from which the displacement data is collected should be small compared to the size of the specimen and it should be located away from the outer edges, in order to minimise border effects. Moreover, the strain should be measured optically to avoid any mechanical interference (Sasaki et al., 1999).

Lanir (1983) and Fung (1987) were among the first researchers who carried out biaxial tests on biological tissues. In order to measure the strain without interference, they marked the specimens by evenly spaced pairs of lines along both axes, and measured the distance between the strips in both directions, using a video dimensional analyser (VDA). Their experimental results from their tests showed high non-linearity and anisotropy of the skin tissue. Later on, Fung and Liu (1989) developed the celebrated constitutive models, known as Fung-type, which will be discussed in Section 2.3.

Variability in the material parameters is another concern, which requires close attention. The sources of variability can be associated with inevitable experimental noise, numerical instability of the fitting algorithms due to the non-linearity and the strain-history-dependent nature of the tissues (Hoffman and Grigg, 1984). In order to address these issues, Yin et al.

(1987) introduced a statistical-based approach to examine the sources of variability and to eventually incorporate their effects in the material parameters. They performed residual analysis on experimental data obtained by Chew et al. (1986) and concluded that the strain-history dependent nature of the tissue shadowed other sources of variability, which makes it difficult to obtain the direction of anisotropy.

Identifying the axes of material symmetry is crucial in biaxial testing. In biological tissues, the axes of material symmetry can be identified by observation of the macroscopic fibre orientation. However, if the fibres are too small, other approaches need to be followed. Choi and Vito (1990) developed a practical technique in which a circular specimen is stretched radially. They performed a constant-tension biaxial stretching, and marked the specimen along each direction of loading, with a pair points being equally apart from the centre. Then, they released the specimen from tension and the pairs of points on the tissue formed an ellipse, whose major and minor axes are the material symmetry axes. It is noteworthy that, in this approach, the micro-structure of the material is not of concern and the method can be applied to any material with an unknown substructure.

Biaxial testing is evidently more insightful than uniaxial testing. However, it has some limitations. In planar biaxial tests, the thickness of specimen should be small, and therefore the results from planar biaxial tests are insufficient to produce fully three-dimensional models, an obvious fact that is overlooked in some studies (Sun and Leong, 2003). To address this mistake, Holzapfel and Ogden (2007) pointed out that it is theoretically impossible to determine the material properties of a three-dimensional anisotropic material from biaxial tests, unless some assumption is made to provide more information regarding the behaviour of material. The membrane model cannot capture the complex features of a three-dimensional body such as the variation of radial stress through the thickness and torsional deformation. Another issue is the location-dependence of the material properties (Novak et al., 1994), which is pronounced in cardiac tissue and is reported by numerous studies (Novak et al.,

1994; Sacks and Chuong, 1993; Yin et al., 1987). Anisotropy is observed in all regions of the heart. However, the orientation of the fibres and the degree of anisotropy within the cardiac tissue vary significantly (Demer and Yin, 1983). It should be noted that torsion, shear and radial stress can be studied through different testing methods, such as triaxial shear test (Dokos et al., 2000) or simultaneous extension, torsion and inflation (Humphrey et al., 1993).

It is worth to note that, from the experimental point of view, a constitutive model which requires a smaller number of parameters (such as that by Humphrey and Yin (1987), with only 4 parameters) might be more practical as it limits errors in experimental testing. This will be discussed further in Section 2.3. We should note that there are physical and mathematical constraints associated with each and every model; these should be addressed accordingly in order to produce a sound constitutive model.

2.3 Anisotropic, Fibre-Reinforced Models

In this section, we outline some of the significant works on modelling of soft biological tissues. as noted, biological tissues are of great complexity both in ultra structure and micro structure levels. In past, histology of biological tissues was not known as of today, hence, the modelling of biological tissues relied towards phenomenological description of material behaviour. Having said that, the postulated constitutive models were valid only under specific conditions. In general, even with the presence of considerable knowledge on histology of biological tissues, the construction of universal model that can predict the behaviour of tissues, is not viable. Moreover, the existence of water in porous structure of extra cellular matrix, results in internal flow of water through the pores, which affects the behaviour of the tissue significantly. Taking into account that our knowledge on material properties of biological tissues is limited, a constitutive model that requires several material constants is not desirable. Thus, rather than using a full mixture theory, the models are

formed within contexts of nonlinear elasticity (Federico and Herzog, 2008), viscoelasticity (Best et al., 1994; Bischoff et al., 2004) or poroelasticity (Federico and Grillo, 2012).

Perhaps Fung was the first to employ finite elasticity in modelling of soft biological tissues. Fung (1967), introduced a one-dimensional model based on experimental data on axial tension of thin collagenous membrane in the abdomen. The data admits a linear relationship between stress and stretch. In addition, despite of exhibiting creep, the behaviour of membrane is not affected by strain rate. Fung (1967, 1968) introduced the first Piola-Kirchhoff stress as

$$\frac{\mathrm{d}\hat{T}}{\mathrm{d}\lambda}(\lambda) = c_1 + c_2\,\hat{T}(\lambda), \tag{2.1}$$

in which c_1 and c_2 are material parameters, and λ is the stretch. The corresponding equation (2.1) is a simple ordinary differential equation, which suggests an exponential stress-stretch relationship. Later on, Fung expanded his model for 3D case, using strain energy function:

$$\hat{W}(\boldsymbol{E}) = c_1(\exp(\mathcal{Q}(\boldsymbol{E})) - 1) = c_1(\exp(\tfrac{1}{2}\boldsymbol{E} : \mathbb{Q} : \boldsymbol{E}) - 1) \tag{2.2a}$$

$$\boldsymbol{S} = \frac{\partial \hat{W}}{\partial \boldsymbol{E}}(\boldsymbol{E}) = c_1 \exp(\mathcal{Q}(\boldsymbol{E}))\,\mathbb{Q} : \boldsymbol{E} \tag{2.2b}$$

In which $\boldsymbol{E}$ is Green strain tensor and $\mathcal{Q}$ is a quadratic form in $\boldsymbol{E}$ with fourth-order tensor $\mathbb{Q}$. Later on Fung (1990); Fung et al. (1993) introduced the incompressible version of his model, imposing the constraint $J = 1$ describing isochoric (volume-preserving) motion. It should be noted that other scholars attempted to generalise Fung's model to three dimensional problems, such as Goudreau and Taylor (1972); Demiray (1972), using strain energy exponential functions of strain invariants. It is worth mentioning that a similar approach was taken by Hayashi et al. (1985), who used a logarithmic strain energy function, and considered the uniform strain hypothesis, i.e.,, the arterial wall has a constant circumferential strain over the cross section. These generalised Fung-type potentials are described by Federico et al. (2008).

As mentioned before, a significant portion of tissue mechanics is dedicated to the study of cardiovascular tissues. Several constitutive models have been specifically tailored for

arterial tissue. Since the histology of arterial wall is layer-dependent, structural models are good candidates for modelling. Contrary to phenomenological models, structural models consider information from underlying histology. Wuyts et al. (1995) introduced a structural model of blood vessels, considering mechanically important constituents, including collagen, elastin and smooth muscle. The model had four material constants, namely, the Young's modulus of a collagen fibre, the Young's modulus of combined smooth muscle and elastin network, a parameter accounting for strain in the high stiffness region, and an indicator for the degree of collagen fibre stretching. This model adopted the Lorentz distribution function to account for variability of engagement stretch of collagen fibres, and was one of the first approaches to incorporate the collagen crimping. The model assumed that fibres were linearly elastic. Holzapfel et al. (1996) introduced a decoupled hyperelastic model, which accounted for isotropic contribution using an isotropic part representing the non-collagenous matrix, and an anisotropic part

$$\hat{W}(\boldsymbol{C}) = \hat{W}_{\text{iso}}(\boldsymbol{C}) + \hat{W}_{\text{aniso}}(\boldsymbol{C}), \tag{2.3}$$

representing the contribution of the collagen fibres. As discussed before, the behaviour of arteries is characterised by the mechanical properties of individual layers. Numerous studies (e.g. see Demiray and Vito, 1976; von Maltzahn et al., 1981) restricted the study to two layers, media and adventitia, since the intima is often regarded as structurally irrelevant. Each layer is characterised as an isotropic, homogeneous material.

In structural models, the fibres are assumed to be embedded in an isotropic matrix, which is considered to be elastin. These models are transversely isotropic, with the incompressibility constraint. Holzapfel et al. (2000) extended his previous work to account for different fibre orientations and postulated the existence of an elastic potential written as a function of the Green-Lagrange strain $\boldsymbol{E}$ and N structure tensors $\boldsymbol{A}_\alpha = \boldsymbol{M}_\alpha \otimes \boldsymbol{M}_\alpha$, each describing the direction of one family of fibres. Then for the numerical part, they considered only two

families of fibres, which induces 8 invariants, as reported by Spencer (1984):

$$I_1(\boldsymbol{C}) = \mathrm{Tr}(\boldsymbol{C}), \tag{2.4a}$$

$$I_2(\boldsymbol{C}) = \tfrac{1}{2}[\mathrm{Tr}(\boldsymbol{C})^2 - \mathrm{Tr}(\boldsymbol{C}^2)], \tag{2.4b}$$

$$I_3(\boldsymbol{C}) = \det(\boldsymbol{C}), \tag{2.4c}$$

$$I_4(\boldsymbol{C}) = \boldsymbol{C} : \boldsymbol{A}_1, \quad I_5(\boldsymbol{C}) = \boldsymbol{C}^2 : \boldsymbol{A}_1, \tag{2.4d}$$

$$I_6(\boldsymbol{C}) = \boldsymbol{C} : \boldsymbol{A}_2, \quad I_7(\boldsymbol{C}) = \boldsymbol{C}^2 : \boldsymbol{A}_2, \tag{2.4e}$$

$$I_8(\boldsymbol{C}) = \boldsymbol{C} : (\boldsymbol{A}_1.\boldsymbol{A}_2). \tag{2.4f}$$

The number of required invariants goes down from 8 to 7 for the case of incompressible materials ($\det(\boldsymbol{C}) = 1$). However, Holzapfel et al. (2000) used only I_4 and I_6, which measure the stretch in the direction of the two fibre families, and assumed an anisotropic potential in the form

$$\hat{W}_{\mathrm{aniso}}(I_4, I_6) = \frac{c_1}{2c_2} \sum_{i=4,6} \left[\exp[c_2(I_i - 1)^2] - 1\right]. \tag{2.5}$$

The structural models developed by Holzapfel et al. (2000) and Zulliger et al. (2004) neglect the effect of dispersion of collagen fibres. Therefore, as argued by Gasser et al. (2006), in case of deformations orthogonal to the plane containing the directions of the fibres, there will be no contribution from embedded collagens, which can result in large errors in numerical models. This can explain the reason behind the poor performance of the aforementioned models for stiffening of the adventitial strips, while they work well for uniaxial stretching of the media, based on the fact that media has a small dispersion of fibres (Canham et al., 1989). This can justify the need for developing models with statistical distribution, which have the ability to incorporate the dispersion of fibres.

2.4 Soft Tissues with Statistical Fibre Orientation

We can think of a biological tissue as a composite material comprised of two constituents, namely, matrix and the fibres. The simplest way of studying composite material is to employ

superposition (Federico and Herzog, 2008; Federico, 2015a). Herein, the value of any arbitrary quantity W relative to the whole composite is obtained using some weighted-average function of the values of the same physical quantity for each individual constituent. The weight function of each constituent is considered as its volumetric fraction. In this framework, all constituents are assumed to attain the same motion, denoted as χ. In case of fibrous tissues, the change in the orientation of fibres is characterised by the same deformation gradient $\boldsymbol{F}$. The volume fraction of constituent α, denoted by ϕ_α is an absolutely positive measure, from which the portion of current configuration V_α can be obtained from Equation (2.6):

$$\int_{\chi(\mathcal{B},\cdot)} \phi_\alpha = \int_{\mathcal{B}} J\ \phi_\alpha = \int_{\mathcal{B}} \Phi_\alpha = V_\alpha, \tag{2.6}$$

where $\Phi_\alpha = J\ \phi_\alpha$. We can adopt mass density ρ as the measure function as well. In both material and spatial picture, the volumetric fractions should admit (2.7).

$$\sum_{\alpha=1}^{N} \phi_\alpha = 1, \qquad \sum_{\alpha=1}^{N} \Phi_\alpha = 1. \tag{2.7}$$

Now similarly to what Holzapfel et al. (2000) did for the case of two families, the elastic potential for a tissue with several fibre families, each characterised by referential orientation $\boldsymbol{M}_\alpha \in \mathbb{S}^2\mathcal{B}$ and $\boldsymbol{A}_\alpha = \boldsymbol{M}_\alpha \otimes \boldsymbol{M}_\alpha$ can be introduced as (Federico and Herzog (2008))

$$W = \hat{W}(\boldsymbol{C}, \boldsymbol{A}_1, \ldots, \boldsymbol{A}_n) = \Phi_0 \hat{W}_0(\boldsymbol{C}) + \sum_{\alpha=1}^{N} \Phi_\alpha \hat{W}_\alpha(\boldsymbol{C}, \boldsymbol{A}_\alpha), \tag{2.8}$$

where $\hat{W}_0$ represents the potential for isotropic matrix and $\hat{W}_\alpha$ represents constitutive function for the α-th fibre family oriented in direction $\boldsymbol{M}_\alpha$.

If the fibres have statistical orientation, we can adopt a probability distribution

$$\Psi : \mathbb{S}^2\mathcal{B} \to \mathbb{R}_0^+ : \boldsymbol{M} \mapsto \Psi(\boldsymbol{M}), \tag{2.9}$$

defined over the material unit sphere $\mathbb{S}^2\mathcal{B} = \{\boldsymbol{M} \in T\mathcal{B} : \|\boldsymbol{M}\| = 1\}$, assigning the probability to find a fibre with orientation $\boldsymbol{M}$, at a point in the body. It should be noted that Ψ should be normalised over the sphere and should be invariant with respect to reflection of $\boldsymbol{M}$, i.e.,

$$\int_{\mathbb{S}^2\mathcal{B}} \Psi(\boldsymbol{M}) = 1, \qquad \Psi(-\boldsymbol{M}) = \Psi(\boldsymbol{M}). \tag{2.10}$$

If all fibres have the same properties, so that only one constitutive function $\hat{W}_1$ is necessary, the summation over α in Equation (2.8), changes to an integral over the material unit sphere and the constitutive equation for statistically oriented fibre can be given as Federico and Herzog (2008)

$$W = \hat{W}(\boldsymbol{C}) = \Phi_0 \hat{W}_0(\boldsymbol{C}) + \Phi_1 \int_{\mathbb{S}^2_{\mathcal{B}}} \Psi(\boldsymbol{M})\, \hat{W}_1(\boldsymbol{C}, \boldsymbol{A}), \tag{2.11}$$

where

$$W_e = \hat{W}_e(\boldsymbol{C}) = \int_{\mathbb{S}^2_{\mathcal{B}}} \Psi(\boldsymbol{M})\, \hat{W}_1(\boldsymbol{C}, \boldsymbol{A}), \tag{2.12}$$

is called the *ensemble potential* of the fibre family.

An alternative method to account for fibre dispersion was proposed by Gasser et al. (2006), who took the average of the structure tensor $\boldsymbol{A}$, rather than of the fibre potential $\hat{W}_1$. Therefore, their potential is, in our notation (and employing volumetric fractions),

$$W = \hat{W}(\boldsymbol{C}) = \Phi_0\, \hat{W}_0(\boldsymbol{C}) + \Phi_1 \hat{W}_1(\boldsymbol{C}, \boldsymbol{H}), \tag{2.13}$$

where

$$\boldsymbol{H} = \int_{\mathbb{S}^2_{\mathcal{B}}} \Psi(\boldsymbol{M}) \boldsymbol{A} \tag{2.14}$$

is the average of the material structure tensor $\boldsymbol{A}$. Federico and Herzog (2008) proved that their method reduces to that by Gasser et al. (2006) when the fibres have a dominant direction with weak dispersion, or for fibre potentials $\hat{W}_1$ that are affine in $\boldsymbol{A}$.

2.5 Continuum Damage Mechanics

Continuum Damage Mechanics is the branch of general continuum theories that studies failure and damage of materials. The occurrence of damage in a body can be observed at different scales. Hence, it can be treated in different manners. In Damage Mechanics, the focus is placed on the development and progression of damage at the mesoscopic and macroscopic scales (Murakami, 2012). In this context, the deterioration of the material is

treated as an internal variable, the damage parameter $D \in [0, 1]$. When $D = 0$, the body is intact, whereas, when $D = 1$, the body is fully ruptured.

The mechanical description of damage is important in the construction of constitutive damage models. At the mesoscale, damage can be associated with the number of broken bonds or the plastic enlargement of microcavities. The damage parameter can be defined with the aid of a representative volume element (RVE) at an arbitrary point x, and a plane passing by x, with normal (co)vector $\boldsymbol{n}$ Lemaitre and Chaboche (1975) (Figure 2.2). The intersection of the RVE and the plane is a surface with area δS, which will contain damaged portions (voids) and undamaged portions. The area of the damaged portions of δS is denoted δS_D. Note that δS_D depends on the direction of $\boldsymbol{n}$. The damage parameter $D_{\boldsymbol{n}}$ can be introduced as $\frac{\delta S_D}{\delta S}$ for an arbitrary $\boldsymbol{n}$. Then, the actual damage parameter D can be introduced as the maximum of $D_{\boldsymbol{n}}$ for every $\boldsymbol{n}$. One of the fundamental concepts in damage

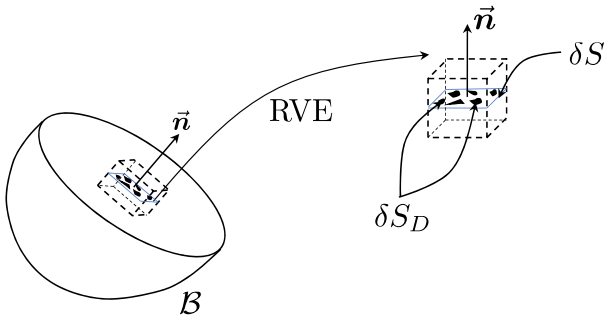

Figure 2.2: RVE model (Lemaitre and Chaboche, 1975)

mechanics is the notion of effective stress, denoted by $\tilde{\sigma}$, and introduced by Kachanov (1986). With reference to Figure 2.2, the damaged area δS_D in the RVE cannot take any load, hence the effective area in the RVE, denoted by $\delta\tilde{S}$ is given by

$$\delta\tilde{S} = \delta S - \delta S_D \tag{2.15a}$$

$$\delta\tilde{S} = (1 - D)\delta S \tag{2.15b}$$

With the aid of Equation (2.15b), the effective stress is introduced as the field

$$\tilde{\sigma} = \frac{\sigma}{1 - D} \tag{2.16}$$

such that

$$\delta F = \int_{\delta \tilde{S}} \frac{\sigma}{1 - D} \, \mathrm{d}S = \int_{\delta \tilde{S}} \tilde{\sigma} \, \mathrm{d}S \tag{2.17}$$

in which δF is the force acting on the surface. It is obvious that $\tilde{\sigma}$ is always greater than σ, as it is magnified by the factor $1/(1 - D)$.

As stated above, in the early development of damage continuum mechanics, damage was described as a single variable that was postulated to obtain the effective stress. However, as it has been discussed in numerous studies (e.g., Ju, 1989; Rabier, 1989; Cauvin and Testa, 1999), even for isotropic damage, one damage variable is not sufficient to elucidate the microscopic mechanisms of damage development. Moreover, as it is clear from the notion of damage, whatever the form of the damage variable $\mathcal{D}$, it should be invariant for reflections of $\boldsymbol{n}$, i.e., $\mathcal{D}(\boldsymbol{n}) = \mathcal{D}(-\boldsymbol{n})$. Murakami (1988) studied the anisotropic damage for a three-dimensional damaged body, considering a symmetric damage tensor, denoted by $\mathfrak{d}$ and showed that the effective stress in this case is given (in our notation) by

$$\tilde{\boldsymbol{\sigma}} = \boldsymbol{g}^{-1} \, (\boldsymbol{g}^{-1} - \mathfrak{d})^{-1} \boldsymbol{\sigma}. \tag{2.18}$$

Equation(2.18) shows that the effective stress tensor is not symmetric (except in the very special case in which $\boldsymbol{g}^{-1} - \mathfrak{d}$ and $\boldsymbol{\sigma}$ are coaxial), which is inconvenient for the formulation of constitutive equations. Several methods have been proposed to symmetrise $\tilde{\boldsymbol{\sigma}}$, by Betten (987b).

One of the fundamental bricks of Continuum Damage Mechanics is the *hypothesis of strain equivalence*, postulating that the inelastic constitutive equation of a damaged body can be replaced by and equivalent constitutive equation for an undamaged body by replacing the stress tensor by the effective stress tensor. Using this hypothesis, we obtain an equivalent undamaged body, having the same strain at each point, but different stress. In figure 2.3,

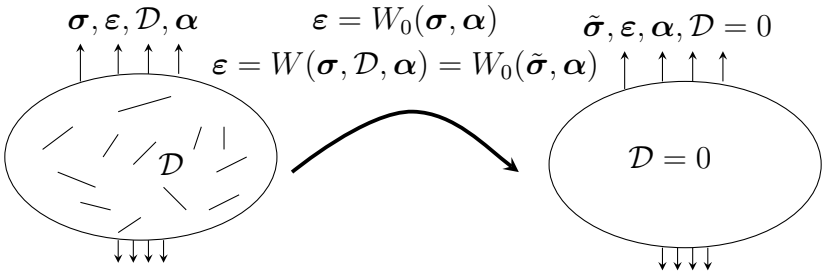

Figure 2.3: Hypothesis of strain equivalence

$\boldsymbol{\varepsilon}$ is the infinitesimal strain and $\boldsymbol{\alpha}$, is the collection of other internal variables (hardening, etc). The elastic potential $\hat{W}_0$ describes the undamaged configuration. If we replace $\boldsymbol{\sigma}$ by the effective stress $\tilde{\boldsymbol{\sigma}}$, then we have the constitutive relation for the damaged body. It should be noted the damaged constitutive relation is entirely dependent on the choice of damage parameter $\mathcal{D}$. For instance, if we consider linear elastic deformations, we can obtain the strain from Equation (2.19), as

$$\boldsymbol{\varepsilon} = \mathbb{S}_0 : \tilde{\boldsymbol{\sigma}}, \tag{2.19a}$$

$$\boldsymbol{\varepsilon} = \mathbb{S}(\mathcal{D}) : \boldsymbol{\sigma}, \tag{2.19b}$$

$$\mathbb{S}(\mathcal{D}) = \mathbb{S}_0 : \mathbb{M}(\mathcal{D}), \tag{2.19c}$$

where $\mathbb{S}_0$ and $\mathbb{S}(\mathcal{D})$ are the (fourth-order) elastic compliance tensors for undamaged and damaged body, respectively, and $\mathbb{M}(\mathcal{D})$ is the fourth-order damage tensor.

The notion of strain equivalence can be represented in energetic terms, yielding the *hypothesis of energy equivalence* (Cordebois and Sidoroff, 1982). In this approach, there is no concern for the symmetrisation of the damage-dependent tensors, as all tensors obtained in the theory are inherently symmetric:

$$\hat{W}_0(\boldsymbol{\varepsilon}) = \frac{1}{2}\boldsymbol{\varepsilon} : \mathbb{C}_0 : \boldsymbol{\varepsilon}, \tag{2.20a}$$

$$\hat{W}(\boldsymbol{\varepsilon}, \mathcal{D}) = \frac{1}{2}\boldsymbol{\varepsilon} : \mathbb{C}(\mathcal{D}) : \boldsymbol{\varepsilon}, \tag{2.20b}$$

$$\boldsymbol{\sigma} = \frac{\partial \hat{W}_0}{\partial \boldsymbol{\varepsilon}} = \mathbb{C}_0 : \boldsymbol{\varepsilon}, \tag{2.20c}$$

$$\tilde{\boldsymbol{\sigma}} = \frac{\partial \hat{W}}{\partial \boldsymbol{\varepsilon}} = \mathbb{C}(\mathcal{D}) : \boldsymbol{\varepsilon}. \tag{2.20d}$$

In Equations (2.20), $\mathbb{C}_0$ and $\mathbb{C}(\mathcal{D})$ are the elasticity tensors, $\hat{W}_0$ and $\hat{W}$ are the elastic potentials.

Damage and plastic deformation of a continuum body is substantially related to thermodynamic evolution of material. Kestin and Rice (1969) introduced the *principle of local state* which has been extensively adopted in continuum thermodynamical models. This hypothesis postulates that the thermodynamic state of a material element in a continuum can be completely characterised by a set a of state variables, regardless of whether the system is in equilibrium or not. Generally speaking, inelastic deformations are mainly associated with irreversible internal changes which can be represented in terms of change in internal variables. The rules for the change of internal variable are examined in the context of thermodynamical potential functions and the Clausius-Duhem inequality. Early studies on classical plasticity and damage are mostly done in the framework of small deformation, in which the total strain tensor is given as the sum of elastic and plastic strain(Gurson, 1977; Chaboche, 1986; Murakami et al., 1998), i.e., $\boldsymbol{\varepsilon} = \boldsymbol{\varepsilon}^e + \boldsymbol{\varepsilon}^p$.

The Helmholtz free energy per unit mass is considered as a function of the total strain ($\boldsymbol{\varepsilon}$), the temperature (θ), the elastic strain ($\boldsymbol{\varepsilon}^e$) and a set of N internal variables collected in the "vector" $\{\mathcal{V}_k\}_{k=1}^N$, i.e.,

$$\psi = \psi(\boldsymbol{\varepsilon}, \theta, \boldsymbol{\varepsilon}^e, \mathcal{V}_k), \qquad \{\mathcal{V}_k; k = 1, 2, ..., n\}. \tag{2.21}$$

The time derivative of ψ can is

$$\dot{\psi} = \frac{\partial \psi}{\partial \boldsymbol{\varepsilon}^e} : \dot{\boldsymbol{\varepsilon}}^e + \frac{\partial \psi}{\partial \theta}\, \dot{\theta} + \frac{\partial \psi}{\partial \mathcal{V}_k}\, \dot{\mathcal{V}}_k. \tag{2.22}$$

The Clausius-Duhem inequality should valid both for elastic and plastic conditions, which leads to

$$\boldsymbol{\sigma} = \rho \frac{\partial \psi}{\partial \boldsymbol{\varepsilon}^e}, \;\; s = -\rho \frac{\partial \psi}{\partial \theta} \tag{2.23a}$$

$$\boldsymbol{\sigma} : \dot{\boldsymbol{\varepsilon}}_p + \mathcal{A}^k \dot{\mathcal{V}}_k + \frac{1}{\theta} \langle \boldsymbol{\mathfrak{h}} | \boldsymbol{q} \rangle \geq 0, \tag{2.23b}$$

where

$$\mathcal{A}^k = -\rho \frac{\partial \psi}{\partial \mathcal{V}_k}, \qquad \mathfrak{h} = -\text{grad}\, \theta. \tag{2.24}$$

Now we can represent the Clausius-Duhem inequality (2.23b) in terms of the product of a *generalised force vector* $\boldsymbol{\mathcal{X}}$ and a *generalised flux vector* $\boldsymbol{\mathcal{J}}$, i.e.,

$$\boldsymbol{\mathcal{X}} = \{\boldsymbol{\sigma}, \mathcal{A}^k, \mathfrak{h}/\theta\}, \tag{2.25a}$$

$$\boldsymbol{\mathcal{J}} = \{\dot{\boldsymbol{\varepsilon}}^p, \dot{\mathcal{V}}_k, \boldsymbol{q}\}, \tag{2.25b}$$

$$\langle \boldsymbol{\mathcal{X}} | \boldsymbol{\mathcal{J}} \rangle \geq 0. \tag{2.25c}$$

In order to complete the damage model, we need to construct a scalar dissipation function describing the evolution of $\boldsymbol{\mathcal{J}}$ (Rice, 1971; Lemaitre and Chaboche, 1975):

$$W_d = \hat{W}_d(\boldsymbol{\mathcal{X}}; \mathcal{V}_k, \theta), \tag{2.26a}$$

$$\dot{\boldsymbol{\varepsilon}}^p = \dot{\xi} \frac{\partial \hat{W}_d}{\partial \boldsymbol{\sigma}}, \qquad \dot{\mathcal{V}}_k = \dot{\xi} \frac{\partial \hat{W}_d}{\partial \mathcal{A}^k}, \qquad \boldsymbol{q} = \dot{\xi} \frac{\partial \hat{W}_d}{\partial (\mathfrak{h}/\theta)}. \tag{2.26b}$$

In Equation (2.26), $\dot{\xi}$ is conceptually similar to the plasticity multiplier (Lubliner, 1986). We also note that $\hat{W}_d$ is a non-negative convex function of $\boldsymbol{\mathcal{X}}$ and that, for $\boldsymbol{\mathcal{X}} = \mathbf{0}$, the dissipation function equals zero.

It is important to remark that, for large deformation plasticity, the deformation must be treated in terms of the deformation gradient and its multiplicative decomposition, rather than in terms of the infinitesimal strain and its additive decomposition. A possible treatment is in terms of the "physical metric", intended as the spatial metric $\boldsymbol{g}$, and its pull-back, the right Cauchy-Green deformation $\boldsymbol{C}$ (Miehe, 1988; Valanis, 1995; Sim et al., 2007).

Constitutive models of damage in soft biological tissues are in principle similar to the damage models that have been introduced for engineering materials. However, the pronounced anisotropy and large deformations lead to quite more complex models. In general, damage models for soft biological tissues are obtained by introducing a choice of damage parameter which is adjusted to fit the available experimental data.

2.6 Damage Mechanics of Soft Biological Tissues

Constitutive models of damage in soft biological tissues are in principle similar to the damage models that have been introduced for engineering materials. However, the pronounced anisotropy and large deformations lead to quite more complex models. In general, damage models for soft biological tissues are obtained by introducing a choice of damage parameter which is adjusted to fit the available experimental data.

The damage aspects of soft tissues can be attributed to different phenomena, such as relaxation (Davis and De Vita, 2012), fatigue (Schwartz et al., 2007), creep (Sasaki et al., 1999), viscoelasticity (Decraemer et al., 1980; Weiss et al., 2002; Peña et al., 2008), etc. Hence, the approaches taken by the scholars in modelling the damage vary based on their initial assumptions. Damage models have been developed for various types of biological tissues, such as tendons and ligaments (Hurschler et al., 1997; Arnoux et al., 2002; Sverdlik and Lanir, 2002; Natali et al., 2005a; Peña et al., 2008), arteries (Balzani et al., 2006; Hokanson and Yazdani, 1997; Alastrué et al., 2007), arteries undergoing arterial clamping (Gasser and Holzapfel, 2007; Calvo et al., 2007). Similarly to the elastic models, the damage models can be either phenomenological (e.g., Hokanson and Yazdani, 1997; Peña et al., 2008; Calvo et al., 2007) or structural (e.g., Hurschler et al., 1997; Rodríguez et al., 2006; Alastrué et al., 2007; Rodriguez et al., 2008). In both phenomenological and structural models, the damage can be considered either for both the matrix and the fibres (e.g., Rodríguez et al., 2006; Alastrué et al., 2007; Peña et al., 2008) or for the fibres only (e.g., Hurschler et al., 1997; Hokanson and Yazdani, 1997; Balzani et al., 2006; Gasser, 2011).

A well-known approach in structural modelling of the fibre damage is using the statistical distribution of fibre length to account for various states of crimp among the fibres. This pioneering idea was first introduced by Lanir (1983) for the recruitment of fibres. Hurschler et al. (1997) followed an approach similar to that proposed by Lanir (1983) for the description of fibril recruitment and then based their structural damage model on excluding the fibres

that have an effective stretch greater than a certain failure stretch. They adopted a linear constitutive law for the single fibril and a Wei bull probability density function (PDF) for the distribution of the straightening stretch of the fibrils in the tissue. They calibrated their model to the experiments conducted on the healing rat medial collateral ligament. Following a similar approach, Liao and Belkoff (1999) introduced a failure model for ligaments, using a Gaussian PDF. Their model had less parameters compared to the model developed by Hurschler et al. (1997).

This idea has been employed in more recent studies by Natali et al. (2005b,a); Rodríguez et al. (2006) with appropriate modifications to account for other aspects of the mechanical behaviour of the tissues in which they were interested. Natali et al. (2005b) introduced an elasto-damage constitutive model for the response of the periodontal ligament, which accounted for anisotropy and large strains of the fibres. The model consisted of three parts, namely the isotropic contribution of the matrix, the anisotropic contribution of the collagen fibres and the interaction between two constituents, which was described as a function of four invariants. The interaction part of the model was ignored in the numerical modelling as it was demanding extra parameters that could not be obtained with simple testing methods. The damage factor for the fibres was considered as the ratio of the number of damaged fibre to the total number of fibres. Natali et al. (2005a) adopted a Gaussian distribution to account for the distribution of fibre waviness and also extended their model to the anisotropic case. They studied the mechanical behaviour of healthy tendons under physiological loading. In this model the damage is only considered for the fibres.

Rodríguez et al. (2006), Alastrué et al. (2007) and Rodriguez et al. (2008) employed the worm-chain model, previously introduced by Kratky and Porod (1949). Rodríguez et al. (2006) developed a three-dimensional finite strain damage model, assuming the damage is characterised by the maximum value previously attained by the strain energy of the undamaged material. The energy for the bundle of fibres was introduced as the integration over the

energy of single fibres, and the model was implemented into a Finite Element (FE) package to study the case of torsion-extension. Alastrué et al. (2007) compared a stochastic damage model and a phenomenological continuum model, through Finite Element modelling and concluded that they predict a similar behaviour.

Martufi and Gasser (2011) considered a triangular distribution for the recruitment of fibrils, and a constitutive model for the single fibril that was linear in the logarithmic strain. Their integration was based on the stiffness of the fibrils, which we will discuss in detail. Rausch and Humphrey (2016) used a Weibull distribution energy function similar to that used by Hurschler et al. (1997) to model early venous thrombus. In their model, the fibres are neo-Hookean elastic. The scale parameter of the distribution is used to capture the Mullins-type damage phenomenon. The common ground among all these models is the representation of the crimped state of the fibrils as a distribution function and the stress or the energy as an integral that sums up the stress or the energy for the whole fibre. The models by Hurschler et al. (1997) and Martufi and Gasser (2011) constitute the starting point for our theory of recruitment and damage developed in Chapters 3, 4 and 5.

2.7 Growth and Remodelling in Biological Tissues

It is well known that biological beings undergo growth and remodelling through the course of their lives constantly (Cowin and Hegedus, 1976; Rodriguez et al., 1993). The fundamental problem is to find the driving force for these two interconnected phenomena. This problem can be tackled from different viewpoints. One could postulate that living organisms try to optimise their structure to adapt to their environment, which sounds reasonable from the standpoint of evolutionary biology. Whether we embrace or dismiss this view, we should acknowledge that this postulate does not automatically provide a mathematical framework for studying growth and remodelling, that these phenomena are very complicated, both at microscopic and macroscopic levels, and that the governing laws of growth and remodelling

vary amongst different species, such as between plants and animals (Huxley et al., 1932). Constitutive models describing growth and remodelling have been formulated for a variety of biological tissues and physiological conditions, e.g., heart muscle (Taber, 1998c,b,a), fusiform aneurysms (Baek et al., 2006), embryonic cells (Brodland, 2002), effect of topology and physical properties of environment on cell growth (Cavalcanti-Adam et al., 2007; Rumpler et al., 2008), plants (Cosgrove, 1985, 1986).

One of the earliest attempt to model biological growth has been made by Hsu (1968). They considered the general mass balance law, including both mass source (volumetric growth) and mass flux. They considered a case of homogenous growth, in which the strength and the orientation of the newly added mass are the same at every point. This condition can be achieved if, and only if, the stresses and body forces are uniform throughout the body. They pictured growth as a very slow process, meaning that inertia effects of the growth or resorption were ignored. At the constitutive level, they assumed that the material grows isotropically with a fading memory (in the sense of Coleman and Noll, 1961) and that its unconstrained growth properties are independent of the stress history. In this framework, the rate of mass density can be conjugated with the stress or it can be constant. Generally speaking, this framework ignores the role of configurational forces in the growth process.

Among the first attempts to approach the problem of growth and remodelling from the continuum mechanical perspective are the seminal works by Cowin and Hegedus (1976) and Hegedus and Cowin (1976), which were devised to study the bone remodelling. This theory, which was called *adaptive elasticity*, considers bone as a mixture of three basic components: bone cells, extracellular fluid and solid extracellular material. Cowin and Hegedus (1976) considered bone remodelling as the change in the porosity of the bone matrix, and postulated it to be driven by the long-term strain history (i.e., that the rate of these changes is very small). It should be noted that, in the paper by Cowin and Hegedus (1976), the balance of mass is postulated for the porous matrix. That being said, the incoming mass is essentially

filling the voids in the matrix. The other important consideration in the study by Cowin and Hegedus (1976) is to consider a different entropy parameter for the perfusant and the chemical reaction between the perfusant and the matrix structure.

Skalak (1981) and Skalak et al. (1982, 1997) studied surface growth in the framework of Continuum Mechanics. In their studies, two notions of growth are introduced. The first kind represents the topological changes due to the rearrangement of the existing mass. The second kind consists in the formation of new tissue that constitutes a new region. Skalak et al. (1997) offered a general description of surface growth in terms of convected curvilinear material coordinates. Using this framework, they modelled different cases of growth of horns in animals. The significance of this group's seminal studies compared to previous ones is that the surface growth velocity is not necessarily orthogonal to the current growth surface. However, they did not address the effective forces associated with the process of growth.

Taber and Humphrey (2001) studied the volumetric growth in the arterial wall based on the local stress at each point. For the growth law, they assumed that the growth rate is a linear function of the local stress. They exploited the opening angle of the arterial wall, which is measured after a transmural radial cut that releases the residual stress. The opening angle is a measure of the degree of growth in the tissue. Another important aspect of this study is having enforced incompressibility during the growth process, although, growth is not isochoric (since the material is incompressible, the new mass occupies additional volume).

Humphrey (1999) studied the remodelling of the collagenous tissue by using the polar decomposition of the deformation gradient to the so called *short-duration, intermittent loading configuration* as the intermediate configuration, which is set to interrogate the material behaviour, in their own words. They used a mixture model with four contributors to the stress: the hydrostatic stress induced by the fluid-dominated ground substance, an isotropic contribution from the amorphous solid constituents, including elastin, an anisotropic contribution from the "originally present" collagen fibres and an anisotropic contribution from the

"newly deposed" collagen fibres. Growth is considered as a dynamic process of degradation and deposition of collagen fibres. The degradation and the deposition of fibres are described by exponential functions, which asymptotically reach prescribed values.

Rodriguez et al. (1994) were among the first who studied cardiac remodelling from the continuum mechanical perspective. They used the Kröner-Bilby decomposition of the deformation gradient into a growth part and an elastic part. In practice, they considered a locally stress-free state before growth (reference configuration) which grows into an intermediate (and generally incompatible) configuration, and finally deforms elastically to the current (and compatible) configuration actually attained by the body. For the constitutive law, they adopted a Fung-type potential (Fung, 1967, 1973). The growth rate in this model is based on the variation of the first Piola-Kirchhoff stress with respect to the no-growth equilibrium stress or, as stated by other scholars, the *homeostatic* stress.

Watton et al. (2004), Watton and Hill (2009) and Watton et al. (2009) studied abdominal aortic aneurysms using the *principle of virtual work*. They considered arteries as two-layered cylinders under constant systolic pressure and under pre-stretch along the axis of symmetry. They employed micro-structural recruitment of the collagen fibres as the remodelling process, which was in turn driven by the enlargement of the aneurysm. The remodelling parameter changes to maintain the strain in the collagen to some equilibrium value. This assumption is consistent with the one in the paper by Humphrey (1999). Kroon (2010) introduced a continuum model of growth and remodelling for collagen fibres, considering three different intermediate configurations. The evolution of reorientation was postulated to be a function of the principal stresses, whereas the collagen production was derived from a mass diffusion equation.

Epstein and Maugin (2000) introduced a theory for growth (creation and resorption of mass) and remodelling (microstructural rearrangement at constant mass), where the evolution is seen as a local rearrangement and change of material inhomogeneities, devising

the first or second order *uniformity transplants*. The balance laws for growing body were introduced considering both volumetric growth and surface growth. Epstein and Maugin (2000) proved that, if the constitutive law is only of first grade, diffusion of mass growth cannot occur. Moreover, volumetric growth is governed by the *inhomogeneity deformation rate*, $\boldsymbol{L_P} = \dot{\boldsymbol{P}}\boldsymbol{P}^{-1}$, where $\boldsymbol{P}^{-1}$ corresponds to the growth tensor of Rodriguez et al. (1994). Moreover, the driving force of growth and remodelling is *Eshelby stress* $\mathfrak{E} = -\mathcal{L}\,\boldsymbol{I}^T - \boldsymbol{F}.\boldsymbol{T}$ (where $\mathcal{L} = K - W$ is the Lagrangian function of the system, with K being the kinetic energy and W the potential energy) or the *Mandel stress* $\mathfrak{M} = \boldsymbol{F}.\boldsymbol{T}$. Nonetheless, the constitutive law can include the elastic strain and its rate, in principle.

Another seminal work is that by DiCarlo and Quiligotti (2002), who introduced the notion of *two-layer dynamics*, with generalised velocities and the conjugated generalised forces. This approach adopts two parallel configurations. The current configuration describes actually placement of the body in space, while the relaxed configuration describes how the body "tends to be placed". Thus, we have two velocities: one is the actual Lagrangian velocity of the body, and the other is a set of virtual velocities that are responsible for the growth. Since the forces are the linear operators that create power over the velocities, we have two force contributions: a *brute force*, which it is the dual of the Lagrangian velocity, and the *remodelling* force, which is dual to the remodelling velocities. For the balance laws, they considered the principle of null working, which implies that the total work on the test velocities is zero, so that the sum of the outer and the inner remodelling working is zero.

In the line of this approach, Ambrosi and Guana (2007) and Ambrosi et al. (2008) proposed a framework to model growth and remodelling of an aneurysm. They considered the axisymmetric deformation of a thick-walled tube comprised of a Fung-type elastic material, and introduced a diagonal growth tensor, representing a non-uniform growth rate in different directions. In their model, growth is triggered by blood pressure increase and the effect of the residual stress can be observed. This boundary-value problem revealed that growth mostly

occurs in the stiffest region. Moreover, the remodelling makes the hoop stress field becomes more uniform throughout the wall cross-section.

Fusi et al. (2006) studied the evolution of mixture composed by an elastic solid and a fluid with exchanging mass. The model employed the decomposition of the deformation gradient for the solid phase combined with the maximisation of the rate of entropy production. Grillo et al. (2015) proposed a mathematical model for the structural reorientation of the collagen fibres in a composite material in which the constitutive law includes a probability distribution of orientation of the fibres. The model is based on the framework proposed by DiCarlo and Quiligotti (2002), and the *remodelling parameter* is the mean angle of the Gaussian-like probability distribution of orientation.

Yavari (2010) introduced a geometric framework for growth and remodelling in which a body undergoing bulk growth is studied as a material manifold with an evolving metric. The time dependence of the metric represents the change of stress-free or natural configuration. The material metric evolves according to the principle of maximum entropy. The governing growth equations were obtained by employing d'Alembert principle and Rayleigh's dissipation functions. Yavari (2010) showed that, even in the case of mass-conserving evolution, i.e. when growth results in only shape changes, one may still see residual stresses. With respect to the standard uniformity theory which uses a non-metric connection with non-zero torsion (Epstein and Maugin, 1990), this approach employs the connection associated with the evolving metric: since it is a metric connection, it has zero torsion but in general a non-zero curvature.

Ateshian (2007) studied growth and remodelling in the framework of mixture theory and provided the balance laws, entropy inequality and the interface jump conditions for reactive mixtures. Using the interface jump condition on the mass flux of individual constituents, a surface growth equation is introduced, which can be employed to predict the deposition or removal of material points from the solid matrix. In this study the configuration map is not

considered one to one as it is considered too restrictive and inappropriate for the growth and remodelling. Following the same line of reasoning, Cowin (2010) argued that when growth is caused by addition of mass without *loss*, the motion is no longer bijective, as there is no one to one correspondence between the points anymore. We will briefly address this issue in the Discussion (Chapter 8).

Chapter 3

Continuum Theory of Fibril Recruitment

We assume that soft biological tissues are comprised of an isotropic matrix reinforced by collagen fibres, that both the matrix and the fibres are hyperelastic, and that the fibres are one-dimensional elements bearing no compression or bending, but only tension. The fibres may or may not have a statistically distributed orientation: in this context, we analyse an individual fibre in its referential direction, described by the unit vector $\boldsymbol{M}$. The overall effect of distributed fibres can be obtained via directional averaging methods (e.g., Lanir, 1983; Hurschler et al., 1997; Gasser et al., 2006; Federico and Herzog, 2008).

We first describe collagen fibres as a bundle of collagen fibrils, then establish the kinematics of recruitment for a single fibril, then introduce the probability distribution of straightening for the fibrils in a fibre, and finally establish the elastic constitutive equations for a single fibril.

3.1 Fibres as Bundles of Fibrils

A collagen fibre consists of a bundle of collagen fibrils connected by proteoglycan (PG) cross-bridges. These bridges transmit the load between fibrils, forming an integrated structure which can elongate significantly (Orgel et al., 2011). The fibrils in a collagen fibre are crimped in the reference configuration, and each of them has a different waviness. Therefore, each fibril bears tensile load only if the stretch $\|\boldsymbol{FM}\|$ in the fibre referential direction $\boldsymbol{M}$ is greater than a certain characteristic stretch λ_s at which the fibril straightens. Overall, the fibre is assumed to start bearing tension when the first fibril straightens, at a value of stretch equal to λ_{min}. We assume that the stretch λ_s at which a fibril straightens is given by a probability distribution. As the stretch increases above the stretch of first straightening,

λ_{min}, there will be a progressive recruitment of the fibrils.

3.2 Kinematics of Fibril Recruitment

Following the notation elucidated in Section 1.3, the reference configuration of our fibre-reinforced body is denoted $\mathcal{B}$, the physical space is denoted $\mathcal{S}$, the configuration map is denoted $\chi : \mathcal{B} \to \mathcal{S}$ and maps material points $X = (X^1, X^2, X^3)$ into spatial points $x = (x^1, x^2, x^3)$, and the deformation gradient is the tensor $\boldsymbol{F}$ with components $F^a{}_A = \chi^a{}_{,A} \equiv \partial\chi^a/\partial X^A$.

We look at a fibril passing by a point X and oriented parallel to the unit vector $\boldsymbol{M}$. The deformation causes the fibre to attain the stretch $\|\boldsymbol{F}\boldsymbol{M}\| = \lambda_{\boldsymbol{M}} \equiv \lambda$. For each of the fibrils constituting the fibre, we follow the kinematical assumption made by Martufi and Gasser (2011), and express the deformation gradient $\boldsymbol{F}$ in Kröner's multiplicative decomposition

$$\boldsymbol{F} = \boldsymbol{F}_e \boldsymbol{F}_s, \tag{3.1}$$

in which $\boldsymbol{F}_s$ is the deformation that the fibril must undergo to pass from its referential crimped configuration $\mathcal{C} \subset \mathcal{B}$ to a straightened configuration $\mathcal{C}_s$, and $\boldsymbol{F}_e$ is the subsequent elastic deformation by which the fibril attains its current stretched configuration $\chi(\mathcal{C}) \subset \chi(\mathcal{B})$. If, with no loss of generality, we assume that $\boldsymbol{M} \equiv \boldsymbol{E}_1$ (where $\boldsymbol{E}_1$ is the basis vector of direction 1), the matrix representation of the straightening deformation $\boldsymbol{F}_s$ is

$$[\![\boldsymbol{F}_s]\!] = \begin{bmatrix} \lambda_s & 0 & 0 \\ 0 & 1 & 0 \\ 0 & 0 & 1 \end{bmatrix}, \tag{3.2}$$

i.e., $\boldsymbol{F}_s$ represents a pure stretch in the direction $\boldsymbol{M} \equiv \boldsymbol{E}_1$, with *no* rotation and *no* change in cross-sectional area, which is justified by the fact that, under $\boldsymbol{F}_s$ the fibril simply unfolds to become straight (see Figure 3.1). More rigorously, with the polar decomposition theorem, we write $\boldsymbol{F}_s = \boldsymbol{R}_s \boldsymbol{U}_s$, and say that the rotational part $\boldsymbol{R}_s$ is represented by an identity matrix, so that the representing matrix $[\boldsymbol{F}_s]$ of $\boldsymbol{F}_s$ coincides with the representing matrix $[\boldsymbol{U}_s]$ of the

stretching part $\boldsymbol{U}_s$, of which λ_s is an eigenvalue. In direction $\boldsymbol{M}$, the stretch $\lambda_{\boldsymbol{M}} \equiv \lambda$ admits the one-dimensional multiplicative decomposition

$$\lambda = \lambda_e \lambda_s, \tag{3.3}$$

in which, analogously to Equation (3.1), λ_s is the straightening stretch of Equation (3.2), and λ_e is the elastic stretch.

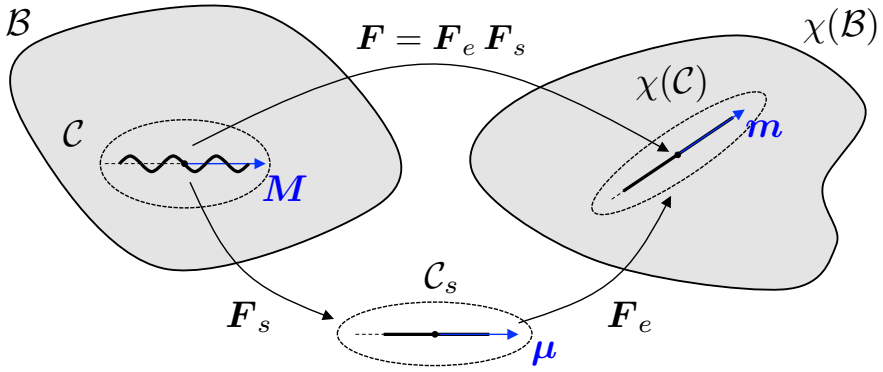

Figure 3.1: Multiplicative decomposition of the deformation of a fibril into $\boldsymbol{F} = \boldsymbol{F}_e\boldsymbol{F}_s$, where the matrix representation of $\boldsymbol{F}_s$ is $[\![\boldsymbol{F}_s]\!] = \mathrm{diag}[\lambda_s,\, 1,\, 1]$, if one assumes, for simplicity, $\boldsymbol{M} \equiv \boldsymbol{E}_1$.

3.3 Recruitment Probability

As discussed in Section 3.1, each fibre can be seen as a bundle of fibrils aligned in the same direction. However, the fibrils can have different "waviness" in the reference configuration, and thus attain a straightened configuration at different values of the straightening stretch λ_s.

Since each fibril has a characteristic straightening stretch λ_s, we need to have two pieces of information, which can both be captured by a *straightening probability distribution*: *i*) at what straightening stretch each fibril is recruited, and *ii*) which fraction of fibrils has been recruited. The general idea can be traced back to the worm-like chain model (Flory, 1969). We also note that numerous studies have been conducted on the experimental determination of the waviness of fibrils (see, e.g., Diamant et al., 1972). We start by recalling the notion

of *support* of a function f. Given a set $\mathcal{D}$ and a function $f : \mathcal{D} \to \mathbb{R}$, the support of f is the subset of the domain $\mathcal{D}$ on which f is non-zero, i.e.,

$$\text{supp}(f) = \{x \in \mathcal{D} : f(x) \neq 0\}. \tag{3.4}$$

The probability distribution could be such that the fibrils are recruited over a *bounded* or *unbounded* interval contained in $[1, +\infty[$, i.e., the probability distribution could have *bounded* or *unbounded* support. The lower extremum of the support of the probability distribution may be 1 or a larger value of stretch λ_{min}.

Physically, the fibrils of a fibre are all recruited at a certain *finite* stretch λ_{max}, so it would seem more sound to use a probability defined piecewise, and equal to zero for values of the stretch greater than λ_{max}, in order for the support to be bounded. This, however, has the disadvantage of requiring piecewise integration and numerical implementation. Examples of probability distributions with bounded support are that of the "triangular" distribution (Martufi and Gasser, 2011) or the beta distribution (Balakrishnan and Nevzorov, 2004). On the other hand, a probability distribution with unbounded support can be made realistic by adjusting the parameters so that the asymptotic behaviour is reached suitably fast. This has the advantage of having a single, continuous function. Examples of recruitment probabilities with unbounded support are those of the Gaussian distribution (Liao and Belkoff, 1999) or the Weibull distribution (Hurschler et al., 1997).

If $\mathfrak{n}_s$ denotes the probability distribution of straightening, the cumulative probability distribution $\mathcal{N}_s$ is given by

$$\mathcal{N}_s(\lambda_s) = \int_{\lambda_{min}}^{\lambda_s} \mathfrak{n}_s(t)\, \mathrm{d}t, \tag{3.5}$$

and provides the fraction of recruited fibrils at the value λ_s of the stretch. Figure 3.2 provides a comparison of three probability functions (triangular, beta and Weibull), along with the respective cumulatives.

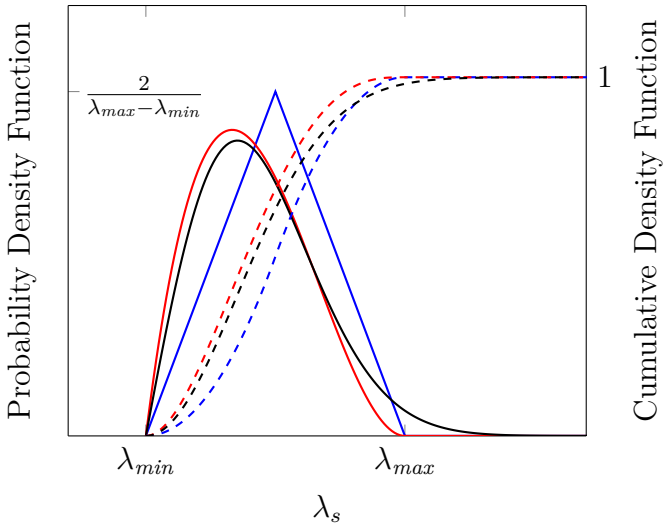

Figure 3.2: Plots of three probability densities, i.e., triangular (blue, solid), beta (red, solid), Weibull (black, solid), and of the corresponding cumulative densities (same colours, dashed). The maximum value λ_{max} is required for the beta and triangular distributions, which have bounded support. The value $2/(\lambda_{max} - \lambda_{min})$ is the peak of the triangular distribution.

3.4 General Form of the Constitutive Equation for a Fibril

We continue to follow standard Continuum Mechanics notation, with uppercase symbols and indices in the reference configuration and lowercase symbols and indices in the current configuration. Moreover, we use uppercase Greek symbols and lowercase Greek indices for quantities referred to the intermediate configuration. Thus, the deformation gradient $\boldsymbol{F}$ has components $F^a{}_B$, the straightening deformation $\boldsymbol{F}_s$ has components $(\boldsymbol{F}_s)^\beta{}_B$, and the elastic deformation $\boldsymbol{F}_e$ has components $(\boldsymbol{F}_e)^a{}_\beta$. Moreover, the Cauchy stress, which is completely spatial, is denoted $\boldsymbol{\sigma}$ (in components, σ^{ab}), whereas the first and second Piola-Kirchhoff stresses are denoted by the usual symbols $\boldsymbol{T}$ and $\boldsymbol{S}$ (in components, T^{aB} and S^{AB}) in the reference configuration and by $\boldsymbol{\Pi}$ and $\boldsymbol{\Sigma}$ (in components, $\Pi^{a\beta}$ and $\Sigma^{\alpha\beta}$) in the intermediate configuration. A "hat" over a symbol denotes the associated constitutive function, e.g., in the expression $\boldsymbol{T} = \hat{\boldsymbol{T}}(\boldsymbol{F})$, $\boldsymbol{T}$ is the physical quantity (first Piola-Kirchhoff stress) and $\hat{\boldsymbol{T}}$ is the associated constitutive function.

The constitutive equation for a fibril should be formulated in its intermediate configuration $\mathcal{C}_s$, in which the fibril is straightened and from which it stretches elastically of λ_e to the

current configuration $\chi(\mathcal{C})$. Thus, the constitutive equation for a fibril should be cast as

$$\Pi_{\text{fibril}} = \hat{\Pi}_{\text{fibril}}(\lambda_e), \tag{3.6}$$

where Π_{fibril} is the one-dimensional first Piola-Kirchhoff stress in the intermediate configuration and $\hat{\Pi}_{\text{fibril}}$ is the constitutive function associated with Π_{fibril}. The constitutive statement (3.6) is the most natural for two reasons: *i*) both the intermediate first Piola-Kirchhoff stress and the elastic stretch map from the intermediate to the current configuration (which is perfectly analogous to the regular first Piola-Kirchhoff stress and deformation gradient, mapping from reference to current configuration), and *ii*) the first Piola-Kirchhoff stress is often the *only* that it is actually possible to measure experimentally, particularly for the case of an object like a collagen fibril, for which it would be practically impossible to measure the change in cross-section.

In order to obtain the correct transformation rules of Π_{fibril}, let us work in tensorial terms, omitting the subscript "fibril" for brevity. The tensorial counterpart of (3.6) is

$$\boldsymbol{\Pi} = \hat{\boldsymbol{\Pi}}(\boldsymbol{F}_e), \tag{3.7}$$

and the stress $\boldsymbol{\Pi}$ is the backward Piola transform of the Cauchy stress (which naturally is defined in the current configuration) with respect to the elastic deformation $\boldsymbol{F}_e$, i.e.,

$$\boldsymbol{\Pi} = J_e\, \boldsymbol{\sigma}\, \boldsymbol{F}_e^{-T}, \qquad \Pi^{a\beta} = J_e\, \sigma^{ab} (\boldsymbol{F}_e^{-T})_b{}^{\beta}. \tag{3.8}$$

With respect to the straightening deformation $\boldsymbol{F}_s$, $\boldsymbol{\Pi}$ can be backward Piola-transformed to the reference configuration into the ordinary first Piola-Kirchhoff stress $\boldsymbol{T}$, i.e.,

$$\boldsymbol{T} = J_s\, \boldsymbol{\Pi}\, \boldsymbol{F}_s^{-T}, \qquad T^{aB} = J_s\, \Pi^{a\alpha} (\boldsymbol{F}_s^{-T})_\alpha{}^{B}, \tag{3.9}$$

so that the regular overall backward Piola transformation,

$$\boldsymbol{T} = J\, \boldsymbol{\sigma}\, \boldsymbol{F}^{-T}, \qquad T^{aB} = J\, \sigma^{ab} (\boldsymbol{F}^{-T})_b{}^{B}, \tag{3.10}$$

is recovered by combining Equations (3.1), (3.8) and (3.9). It should be noted that, because of the assumed representation of $\boldsymbol{F}_s$ shown in Equation (3.2), if the fibre direction is $\boldsymbol{M} \equiv \boldsymbol{E}_1$, we have that $(\boldsymbol{F}_s)^1{}_1 = \lambda_s$, $(\boldsymbol{F}_s^{-1})^1{}_1 = \lambda_s^{-1}$ and $J_s = \lambda_s$. Therefore, the one-dimensional first Piola-Kirchhoff stress for a fibril is *identical* in the reference and in the intermediate configuration, i.e., reinstating the subscript "fibril",

$$T_{\text{fibril}} = \lambda_s \, \Pi_{\text{fibril}} \, \lambda_s^{-1} = \Pi_{\text{fibril}}. \tag{3.11}$$

In general, it is convenient to express the constitutive relation in terms of the first Piola-Kirchhoff stress (current force over undeformed area) because it is the quantity normally measured in fibre/fibril tension tests (e.g., Miyazaki and Hayashi, 1999, Figure 8). From Equations (3.3) and (3.6), the constitutive relation for a single fibril should be of the form

$$T_{\text{fibril}} = \hat{T}_{\text{fibril}}(\lambda/\lambda_s) = \hat{T}_{\text{fibril}} \equiv \hat{\Pi}_{\text{fibril}}(\lambda_e), \tag{3.12}$$

where $\lambda/\lambda_s = \lambda_e$ is the elastic stretch of the one-dimensional multiplicative decomposition of Equation (3.3).

We also intend to show that a constitutive equation in terms of the *second* Piola-Kirchhoff stress is *not* a convenient choice. Indeed, contrary to what seen in the case of the first Piola-Kirchhoff stress (Equation (3.11)), the referential and intermediate second Piola-Kirchhoff stress *do not* coincide:

$$S_{\text{fibril}} \neq \Sigma_{\text{fibril}}. \tag{3.13}$$

In order to prove this relation, let us start from the Cauchy stress, as done above for the case of the first Piola-Kirchhoff stress. First, with respect to the elastic deformation $\boldsymbol{F}_e$, the Cauchy stress $\boldsymbol{\sigma}$ can be backward Piola-transformed on the second leg and pulled-back on the first leg to the intermediate configuration, into the intermediate second Piola-Kirchhoff stress $\boldsymbol{\Sigma}$, i.e.,

$$\boldsymbol{\Sigma} = J_e \, \boldsymbol{F}_e^{-1} \boldsymbol{\sigma} \, \boldsymbol{F}_e^{-T}, \qquad \Sigma^{\alpha\beta} = J_e \, (\boldsymbol{F}_e^{-1})^{\alpha}{}_a \sigma^{ab} (\boldsymbol{F}_e^{-T})_b{}^{\beta}. \tag{3.14}$$

Then, with respect to the straightening deformation $\boldsymbol{F}_s$, the intermediate second Piola-Kirchhoff stress $\boldsymbol{\Sigma}$ can be backward Piola-transformed on the second leg and pulled-back on the first leg to the reference configuration, into the ordinary second Piola-Kirchhoff stress $\boldsymbol{S}$, i.e.,

$$\boldsymbol{S} = J_s\, \boldsymbol{F}_s^{-1} \boldsymbol{\Sigma}\, \boldsymbol{F}_s^{-T}, \qquad S^{AB} = J_s\, (\boldsymbol{F}_s^{-1})^A{}_\alpha \Sigma^{\alpha\beta} (\boldsymbol{F}_s^{-T})_\beta{}^B. \tag{3.15}$$

Note that substitution of (3.14) into (3.15) yields the familiar transformation

$$S^{AB} = J_e\, (\boldsymbol{F}^{-1})^A{}_a \sigma^{ab} (\boldsymbol{F}^{-T})_b{}^B. \tag{3.16}$$

Now, the one-dimensional inequality (3.13) is obtained by using the representation of $\boldsymbol{F}_s$ in Equation (3.2). Indeed, as seen for the case of the first Piola-Kirchhoff stress, if the fibre direction is $\boldsymbol{M} \equiv \boldsymbol{E}_1$, then $(\boldsymbol{F}_s)^1{}_1 = \lambda_s$, $(\boldsymbol{F}_s^{-1})^1{}_1 = \lambda_s^{-1}$ and $J_s = \lambda_s$, and we obtain

$$S_{\text{fibril}} = \lambda_s\, \lambda_s^{-1} \Sigma_{\text{fibril}} \lambda_s^{-1} = \lambda_s^{-1} \Sigma_{\text{fibril}} \neq \Sigma_{\text{fibril}}, \tag{3.17}$$

which, in terms of constitutive functions, reads

$$\hat{S}_{\text{fibril}}(\lambda_e, \lambda_s) = \lambda_s^{-1} \hat{\Sigma}_{\text{fibril}}(\lambda_e) \neq \hat{\Sigma}_{\text{fibril}}(\lambda_e). \tag{3.18}$$

We conclude that the second Piola-Kirchhoff stress is *not* preserved from the intermediate to the reference configuration (Equation (3.18)) and, more importantly, the referential second Piola-Kirchhoff stress $\hat{S}_{\text{fibril}}$ is an *explicit* function not only of λ_e, but *also* of λ_s. These two facts constitute another reason to favour a treatment in terms of the first Piola-Kirchhoff stress.

3.5 Critical Review of Published Fibre Constitutive Models

Here, we review the constitutive relations arising from the recruitment models by Hurschler et al. (1997) and Martufi and Gasser (2011), who used different initial assumptions and integration methods to obtain the stress of a fibre from the contributions of the fibrils. The

stress in a fibre is here denoted by the subscript n, which stands for *non-damaged fibre*, as opposed to that in a damaged fibre, which we shall consider in Section 4. We discuss the advantages and disadvantages of each of the two formulations, in preparation for Section 3.6, in which we shall show that, with the appropriate corrections, the two formulations are in fact equivalent, which establishes our model for recruitment.

Hurschler et al. (1997) did not explicitly consider the multiplicative decomposition of the deformation and worked in terms of the Cauchy stress. They defined the Cauchy stress of a fibre as the integral over the interval $[\lambda_{min}, \lambda]$ of the constitutive function of the Cauchy stress for a single fibril times the straightening probability distribution function $\mathfrak{n}_s$, i.e., in our notation,

$$\sigma_n = \hat{\sigma}_n(\lambda) = \int_{\lambda_{min}}^{\lambda} \hat{\sigma}_{\text{fibril}}(\lambda/t)\ \mathfrak{n}_s(t)\ \mathrm{d}t, \tag{3.19}$$

where the integration variable t has the physical meaning of straightening stretch λ_s, and $\hat{\sigma}_{\text{fibril}}$ is expressed similarly as in Equation (3.12), as a function of $\lambda_e = \lambda/\lambda_s$. The constitutive equation for the fibril stress $\hat{\sigma}_{\text{fibril}}$ was assumed to be linear in the elastic stretch, i.e.,

$$\sigma_{\text{fibril}} = \hat{\sigma}_{\text{fibril}}(\lambda_e) = \hat{\sigma}_{\text{fibril}}(\lambda/\lambda_s) = E_{\text{fibril}}\ (\lambda/\lambda_s - 1), \tag{3.20}$$

where E_{fibril} is the elastic modulus of a fibril and $\varepsilon_e = \lambda/\lambda_s - 1 = \lambda_e - 1$ is the elastic nominal strain. Hurschler et al. (1997) relied on their experimental measurements to support the choice of a linear constitutive equation. We also mention single-fibril experiments performed by Miyazaki and Hayashi (1999).

This approach is simple and elegant in terms of integration. However, the choice of the use of the Cauchy stress has *not* been justified physically and it contrasts with the natural hypothesis that the intermediate first Piola-Kirchhoff stress Π_{fibril} of the fibril be solely a function of the elastic stretch of the fibril λ_e, as in Equation (3.6). In order to show this, let us consider the component Π^{11} (the only non-vanishing one) of the stress $\mathbf{\Pi}$ in Equation (3.8), i.e.,

$$\Pi^{11} = J_e\, \sigma^{11}\, (\boldsymbol{F}_e^{-T})_1{}^1 = J_e\, \sigma^{11}\, \lambda_e^{-1}, \tag{3.21}$$

and substitute the expression $\sigma_{\text{fibril}} = \hat{\sigma}_{\text{fibril}}(\lambda_e)$ proposed by Hurschler et al. (1997) and reported above in Equation (3.20). We obtain that the intermediate first Piola-Kirchhoff stress *must* also depend on J_e, i.e.,

$$\Pi_{\text{fibril}} \equiv \Pi^{11} = J_e \, \hat{\sigma}_{\text{fibril}}(\lambda_e) \, \lambda_e^{-1} = \hat{\Pi}_{\text{fibril}}(\lambda_e, J_e), \tag{3.22}$$

where we remark that, in general, $\boldsymbol{F}_e$ is such that $J_e \neq \lambda_e$, unlike the case of $\boldsymbol{F}_s$, which is *constructed* such that $J_s = \lambda_s$ (see Equation (3.2)). This result is in contrast with the natural assumption in Equation (3.6).

Martufi and Gasser (2011) considered a specific constitutive relation for a single fibril in terms of the second Piola-Kirchhoff stress Σ_{fibril} in the (intermediate) straightened configuration:

$$\Sigma_{\text{fibril}} = \hat{\Sigma}_{\text{fibril}}(\lambda_e) = k \log \lambda_e = k \log(\lambda/\lambda_s). \tag{3.23}$$

From this point on, there are two assumptions in the model by Martufi and Gasser (2011) that need to be rectified. The first incorrect assumption was that, given the form of the straightening deformation $\boldsymbol{F}_s$ with the matrix representation in Equation (3.2), the second Piola-Kirchhoff stress Σ_{fibril} in the intermediate configuration and the second Piola-Kirchhoff stress S_{fibril} in the reference configuration were identical, i.e.,

$$S_{\text{fibril}} = \Sigma_{\text{fibril}}, \tag{3.24}$$

which is incorrect, as it contradicts the relation that we showed in Equation (3.17). Then, Martufi and Gasser (2011) found the stiffness of the relation between the second Piola-Kirchhoff stress of the fibril and the stretch λ. In our notation, we introduce the function

$$h(\lambda, \lambda_s) = \lambda/\lambda_s = \lambda_e \tag{3.25}$$

so that, using the formalism of composite functions, the stress reads

$$\hat{S}_{\text{fibril}}(\lambda_e) = \hat{S}_{\text{fibril}}(h(\lambda, \lambda_s)) = (\hat{S}_{\text{fibril}} \circ h)(\lambda, \lambda_s), \tag{3.26}$$

and the stiffness reads

$$\frac{\partial(\hat{S}_{\text{fibril}} \circ h)}{\partial \lambda}(\lambda, \lambda_s) = \frac{k}{\lambda}. \tag{3.27}$$

The second incorrect assumption was made with the standard relation $\boldsymbol{T} = \boldsymbol{F}\boldsymbol{S}$ in mind, from which Martufi and Gasser (2011) assumed that the derivatives of the first Piola-Kirchhoff stress and of the second Piola-Kirchhoff stress with respect to the stretch λ were related by

$$\frac{\partial(\hat{T}_{\text{fibril}} \circ h)}{\partial \lambda}(\lambda, \lambda_s) = \lambda \, \frac{\partial(\hat{S}_{\text{fibril}} \circ h)}{\partial \lambda}(\lambda, \lambda_s), \tag{3.28}$$

which, in their incremental notation, reads $\mathrm{d}P = \lambda \, \mathrm{d}S$. Based on Equations (3.27) and (3.28), Martufi and Gasser (2011) obtained the *constant* stiffness

$$\frac{\partial(\hat{T}_{\text{fibril}} \circ h)}{\partial \lambda}(\lambda, \lambda_s) = k. \tag{3.29}$$

We show that the assumption (3.28) is incorrect by analysing the corresponding fourth-order elasticity tensors. If the fibre direction is $\boldsymbol{M} \equiv \boldsymbol{E}_1$, the derivative on the right-hand side of Equation (3.28) corresponds to the component $\mathrm{A}^{11}{}_1{}^1$ of the fourth-order tensor $\mathbb{A}$ called *first elasticity tensor* by Marsden and Hughes (1983) (see also Truesdell and Noll, 1965), i.e. (omitting again the subscript "fibril"),

$$\mathbb{A} = \hat{\mathbb{A}}(\boldsymbol{F}) = \frac{\partial \hat{\boldsymbol{T}}}{\partial \boldsymbol{F}}(\boldsymbol{F}), \qquad \mathrm{A}^{aB}{}_c{}^D = \hat{\mathrm{A}}^{aB}{}_c{}^D(\boldsymbol{F}) = \frac{\partial \hat{T}^{aB}}{\partial F^c{}_D}(\boldsymbol{F}), \tag{3.30}$$

where $\hat{\boldsymbol{T}}$ and $\hat{\mathbb{A}}$ are the constitutive functions associated with $\boldsymbol{T}$ and $\mathbb{A}$, respectively. The derivative on the right-hand side of Equation (3.28) corresponds instead to the component $\mathrm{B}^{11}{}_1{}^1$ of the fourth-order tensor $\mathbb{B}$ defined by

$$\mathbb{B} = \hat{\mathbb{B}}(\boldsymbol{F}) = \frac{\partial \hat{\boldsymbol{S}}}{\partial \boldsymbol{F}}(\boldsymbol{F}), \qquad \mathrm{B}^{AB}{}_c{}^D = \hat{\mathrm{B}}^{AB}{}_c{}^D(\boldsymbol{F}) = \frac{\partial \hat{S}^{AB}}{\partial F^c{}_D}(\boldsymbol{F}). \tag{3.31}$$

Tensors $\mathbb{A}$ and $\mathbb{B}$ are *not* related by a push-forward of the type $\boldsymbol{T} = \boldsymbol{F}\boldsymbol{S}$, i.e.,

$$\mathbb{A} \neq \boldsymbol{F}\mathbb{B}, \qquad \mathrm{A}^{aB}{}_c{}^D \neq F^a{}_A \, \mathrm{B}^{AB}{}_c{}^D. \tag{3.32}$$

Indeed,

$$\hat{\mathrm{A}}^{aB}{}_{c}{}^{D} = \frac{\partial \hat{T}^{aB}}{\partial F^{c}{}_{D}} = \frac{\partial (F^{a}{}_{A}\hat{S}^{AB})}{\partial F^{c}{}_{D}} = \delta^{a}{}_{c}\,\delta_{A}{}^{D}\,\hat{S}^{AB} + F^{a}{}_{A}\frac{\partial \hat{S}^{AB}}{\partial F^{c}{}_{D}}$$
$$= \delta^{a}{}_{c}\,\hat{S}^{DB} + F^{a}{}_{A}\,\hat{\mathrm{B}}^{AB}{}_{c}{}^{D} \neq F^{a}{}_{A}\,\hat{\mathrm{B}}^{AB}{}_{c}{}^{D}. \tag{3.33}$$

Thus, the correct incremental expression in the paper by Martufi and Gasser (2011) should have read $\mathrm{d}P = S\,\mathrm{d}\lambda + \lambda\,\mathrm{d}S$, which does not yield a constant stiffness. We are going to correct both issues in Section 3.6.

Finally, since the stiffness in Equation (3.29) was assumed to be constant, Martufi and Gasser (2011) obtained the stress for a fibre as the integral of the stiffness times the *cumulative* straightening distribution $\mathcal{N}_s$, i.e., we have that

$$T_n = \hat{T}_n(\lambda) = \int_{\lambda_{min}}^{\lambda} k\,\mathcal{N}_s(t)\,\mathrm{d}t, \tag{3.34}$$

where the integration variable t has here the meaning of overall stretch λ.

The rationale behind the choice that Martufi and Gasser (2011) made for the constitutive equation (3.23) was that they sought for a stiffness that was *independent* of the straightening stretch λ_s, so that, once straightened, all fibrils would have the same stiffness with respect to the *overall* stretch λ. Note that, similarly to Hurschler et al. (1997), also Martufi and Gasser (2011) chose a fibril linear constitutive equation (although this time in the logarithmic strain $\log\lambda_e$). A linear fibril constitutive equation is the clearly the simplest possible choice, and this is why it has been adopted in both models.

3.6 Fibre Recruitment Constitutive Model

Our proposed fibre constitutive model is, like that by Martufi and Gasser (2011), based on an integration of the stiffness. We shall show that, once we correct the model by Martufi and Gasser (2011), we can show that a linear $\hat{T}_{\text{fibril}}$-$\log\lambda_e$ constitutive equation is the *unique* solution of the differential equation obtained by imposing that the independence of the

stiffness on the straightening stretch λ_s. Once this is achieved, we have two possible choices of integration: one in the first Piola-Kirchhoff stress, which is general, and one in the Cauchy stress, which is limited to the case of incompressibility.

We shall also show that it is possible to relax the hypothesis of a linear $\hat{T}_{\text{fibril}}$-$\log \lambda_e$ constitutive equation, and to obtain a completely general stiffness-based model. Finally, we shall show that this generalised stiffness-based model is in fact equivalent to a slightly adjusted version of the stress-based model by Hurschler et al. (1997).

3.7 Uniqueness

As shown in Section 3.4, the most convenient choice for a fibril constitutive equation is in the first Piola-Kirchhoff stress Π_{fibril} in the intermediate, straightened configuration. If we assume linearity with respect to the elastic logarithmic strain, Equations (3.6) and (3.11) yield the fibril constitutive equation

$$T_{\text{fibril}} = \hat{T}_{\text{fibril}}(\lambda_e) = \hat{\Pi}_{\text{fibril}}(\lambda_e) = k \, \log \lambda_e = k \, \log(\lambda/\lambda_s), \tag{3.35}$$

in terms of the referential first Piola-Kirchhoff stress T_{fibril}.

It is possible to *prove* that the logarithmic constitutive equation (3.35), analogous to that postulated by Martufi and Gasser (2011) in terms of the second Piola-Kirchhoff stress (see Equation (3.23)), is actually the *unique* solution of the differential equation imposing that the stiffness of the relation between $\hat{T}_{\text{fibril}}$ and λ does *not* depend on λ_s.

For brevity, let us use $f(\lambda_e) = f(\lambda/\lambda_s) \equiv \hat{T}_{\text{fibril}}(\lambda_e)$, in this proof. We have

$$\hat{\mathrm{A}}(\lambda, \lambda_s) = \frac{\partial (f \circ h)}{\partial \lambda}(\lambda, \lambda_s) = \left[(f' \circ h) \, \frac{\partial h}{\partial \lambda} \right] (\lambda, \lambda_s) \tag{3.36}$$

where $\mathrm{A} = \hat{\mathrm{A}}(\lambda, \lambda_s)$ is the stiffness of the relation between $f \equiv \hat{T}_{\text{fibril}}$ and λ and, again, h is defined by $h(\lambda, \lambda_s) = \lambda/\lambda_s = \lambda_e$, as in Equation (3.25). We also recall that the stiffness $\mathrm{A} = \hat{\mathrm{A}}(\lambda, \lambda_s)$ corresponds to the first elasticity tensor reported in Equation (3.30). We

impose that the stiffness $\hat{\mathrm{A}}$ does not depend on λ_s, i.e., that its partial derivative with respect to λ_s must vanish, which reads

$$\begin{aligned}\frac{\partial \hat{\mathrm{A}}}{\partial \lambda_s}(\lambda, \lambda_s) &= \frac{\partial}{\partial \lambda_s}\left[(f' \circ h)\,\frac{\partial h}{\partial \lambda}\right](\lambda, \lambda_s) \\ &= \left[(f'' \circ h)\,\frac{\partial h}{\partial \lambda}\,\frac{\partial h}{\partial \lambda_s} + (f' \circ h)\,\frac{\partial^2 h}{\partial \lambda \partial \lambda_s}\right](\lambda, \lambda_s) = 0. \end{aligned} \tag{3.37}$$

Using $h(\lambda, \lambda_s) = \lambda/\lambda_s = \lambda_e$, we obtain the differential equation

$$- f''(\lambda_e)\frac{1}{\lambda_s}\frac{\lambda}{\lambda_s^2} - f'(\lambda)\frac{1}{\lambda_s^2} = 0, \tag{3.38}$$

which can be simplified further, by multiplying by λ_s^2, into

$$f''(\lambda_e)\lambda_e + f'(\lambda_e) = 0. \tag{3.39}$$

Equation (3.39) is a second order linear ordinary differential equation, which admits the general solution

$$f(\lambda_e) = C_1 + C_2 \log \lambda_e. \tag{3.40}$$

Considering the initial condition $\lambda_e = 1$ (zero stress when the elastic stretch λ_e is equal to one), C_1 must be zero. With C_1 being zero, setting $C_2 = k$ yields the constitutive law (3.35) as the *only* possible choice satisfying the requirement that $\hat{\mathrm{A}}$ be independent from λ_s. Note that the three-dimensional counterpart of $\log \lambda_e$ would be the logarithmic strain $\log \boldsymbol{U}_e$, where $\boldsymbol{U}_e$ is the right stretch tensor of the polar decomposition $\boldsymbol{F}_e = \boldsymbol{R}_e.\boldsymbol{U}_e$ (see, e.g., Ogden, 1997; Bonet and Wood, 2008).

Another advantage of working in terms of the first Piola-Kirchhoff stress is that the constitutive equation (3.35) gives two possible choices: *i*) keeping working in terms of the first Piola-Kirchhoff stress, which allows for a general formulation for compressible materials (Section 3.8); *ii*) directly obtaining the Cauchy stress, at the cost of limiting the model to the incompressible case, but with the advantage of a very simple analytical expression for the stress (Section 3.9).

3.8 Stress Evaluated from the T_{fibril}-λ Stiffness

With the constitutive equation (3.35), the stiffness of the relation between $\hat{T}_{\text{fibril}}$ and λ, which corresponds to the first elasticity tensor (3.30), is given by

$$\hat{\mathrm{A}}(\lambda, \lambda_s) = \frac{\partial(\hat{T}_{\text{fibril}} \circ h)}{\partial \lambda}(\lambda, \lambda_s) = k\, \frac{1}{\lambda_e}\, \frac{\partial h}{\partial \lambda}(\lambda, \lambda_s) = k\, \frac{1}{\lambda_e}\, \frac{1}{\lambda_s} = k\, \frac{1}{\lambda}, \tag{3.41}$$

and, as shown in Section 3.7, is independent of the straightening stretch λ_s and can be redefined as a function of λ alone, i.e.,

$$\hat{\mathrm{A}}(\lambda) = \frac{\partial(\hat{T}_{\text{fibril}} \circ h)}{\partial \lambda}(\lambda, \lambda_s) = k\, \frac{1}{\lambda}, \qquad \forall \lambda_s. \tag{3.42}$$

Using the stiffness in Equation (3.42), we can obtain the first Piola-Kirchhoff stress as

$$\hat{T}_n(\lambda) = \int_{\lambda_{min}}^{\lambda} \mathcal{N}_s(t)\, \hat{\mathrm{A}}(t)\, \mathrm{d}t = \int_{\lambda_{min}}^{\lambda} \frac{k}{t}\, \mathcal{N}_s(t)\, \mathrm{d}t, \tag{3.43}$$

where the integration variable t stands for the overall stretch λ. It is important to note that the stiffness in Equation (3.42) and the stress in Equation (3.43) are valid for a general deformation $\boldsymbol{F}$: in particular, we are *not* imposing incompressibility.

3.9 Stress Evaluated from the σ_{fibril}-λ Stiffness

From Equation (3.42) for the first Piola-Kirchhoff stress, it is possible to obtain an expression for the Cauchy stress for the case of incompressibility. We want to prove that, considering that ${F^1}_1 = \lambda$ and assuming incompressible behaviour ($J = 1$), multiplying our Equation (3.42) by λ gives

$$\frac{\partial(\hat{\sigma}_{\text{fibril}} \circ h)}{\partial \lambda}(\lambda, \lambda_s) = \lambda\, \frac{\partial(\hat{T}_{\text{fibril}} \circ h)}{\partial \lambda}(\lambda, \lambda_s) = k, \qquad \forall \lambda_s. \tag{3.44}$$

The tensor corresponding to $\partial(\hat{\sigma}_{\text{fibril}} \circ h)/\partial\lambda$ is the elasticity tensor of the relation between the Cauchy stress $\hat{\boldsymbol{\sigma}}$ and the deformation gradient $\boldsymbol{F}$, i.e.,

$$\hat{\mathbb{D}} = \frac{\partial \hat{\boldsymbol{\sigma}}}{\partial \boldsymbol{F}}, \qquad \hat{\mathrm{D}}^{ab}{}_{c}{}^{D} = \frac{\partial \hat{\sigma}^{ab}}{\partial F^{c}{}_{D}}, \tag{3.45}$$

Since $\boldsymbol{\sigma} = J^{-1}\boldsymbol{T}\boldsymbol{F}^T$, tensors $\mathbb{A}$ and $\mathbb{D}$ are related via

$$\begin{aligned}\hat{\mathrm{D}}^{ab}{}_{c}{}^{D} &= \frac{\partial \hat{\sigma}^{ab}}{\partial F^{c}{}_{D}} = \frac{\partial (J^{-1}\hat{T}^{aB}F^{b}{}_{B})}{\partial F^{c}{}_{D}} \\ &= -J^{-2}\,J\,(\boldsymbol{F}^{-T})_{c}{}^{D}\,\hat{T}^{aB}F^{b}{}_{B} + J^{-1}\frac{\partial \hat{T}^{aB}}{\partial F^{c}{}_{D}}F^{b}{}_{B} + J^{-1}\hat{T}^{aB}\delta^{b}{}_{c}\,\delta_{B}{}^{D} \\ &= -J^{-1}\,(\boldsymbol{F}^{-T})_{c}{}^{D}\,\hat{T}^{aB}F^{b}{}_{B} + J^{-1}\hat{\mathrm{A}}^{aB}{}_{c}{}^{D}\,F^{b}{}_{B} + J^{-1}\hat{T}^{aD}\delta^{b}{}_{c}. \end{aligned} \tag{3.46}$$

We now need to verify whether our Equation (3.44) satisfies the relation between $\mathbb{D}$ and $\mathbb{A}$ in Equation (3.46). Since a fibril can only bear a first Piola-Kirchhoff stress in its direction, only $P_{\text{fibril}} \equiv P^{11}$ is different from zero. Therefore, the components $\partial(\hat{\sigma}_{\text{fibril}} \circ h)/\partial\lambda \equiv \hat{\mathrm{D}}^{11}{}_{1}{}^{1}$ and $\partial(\hat{T}_{\text{fibril}} \circ h)/\partial\lambda \equiv \hat{\mathrm{A}}^{11}{}_{1}{}^{1}$ are related by

$$\begin{aligned}\hat{\mathrm{D}}(\lambda) = \frac{\partial(\hat{\sigma}_{\text{fibril}} \circ h)}{\partial\lambda}(\lambda,\lambda_s) &= -J^{-1}\lambda^{-1}(\hat{T}_{\text{fibril}} \circ h)(\lambda,\lambda_s)\,\lambda \\ &\quad + J^{-1}\frac{\partial(\hat{T}_{\text{fibril}} \circ h)}{\partial\lambda}(\lambda,\lambda_s)\,\lambda + J^{-1}(\hat{T}_{\text{fibril}} \circ h)(\lambda,\lambda_s) \\ &= J^{-1}\lambda\,\frac{\partial(\hat{T}_{\text{fibril}} \circ h)}{\partial\lambda}(\lambda,\lambda_s) = J^{-1}k, \quad \forall\lambda_s. \end{aligned} \tag{3.47}$$

Therefore, if the material is incompressible ($J = 1$), we recover our Equation (3.44), provided that incompressibility is properly enforced by means of a pressure term $-p\,\boldsymbol{g}^{-1}$ (which, in components, reads $-p\,g^{ab}$, where the inverse metric tensor $\boldsymbol{g}^{-1}$ stands for the "contravariant" identity tensor) in the full three-dimensional problem. We now have another stiffness that is independent of the straightening stretch λ_s, i.e.,

$$\hat{\mathrm{D}}(\lambda) = \frac{\partial(\hat{\sigma}_{\text{fibril}} \circ h)}{\partial\lambda}(\lambda,\lambda_s) = \lambda\,\frac{\partial(\hat{T}_{\text{fibril}} \circ h)}{\partial\lambda}(\lambda,\lambda_s) = k, \qquad \forall\lambda_s,\,\forall\lambda. \tag{3.48}$$

The corresponding Cauchy stress is obtained as

$$\hat{\sigma}_n(\lambda) = \int_{\lambda_{min}}^{\lambda} \mathcal{N}_s(t)\,\hat{\mathrm{D}}(t)\,\mathrm{d}t = \int_{\lambda_{min}}^{\lambda} k\,\mathcal{N}_s(t)\,\mathrm{d}t. \tag{3.49}$$

We emphasise again that the expressions of the stiffness (3.48) and the stress (3.49) only hold for *incompressible* materials.

The expression of the Cauchy stress in Equation (3.49) is analogous to the expression of the first Piola-Kirchhoff stress found by Martufi and Gasser (2011) (see Equation (4)

in their paper). However, while the expression found by Martufi and Gasser (2011) must be considered as an approximation, based on the two incorrect assumptions discussed in Section 3.5, Equation (3.49) is *exact*, for incompressible materials.

3.10 Generalised Stiffness-Based Model

In their model, Martufi and Gasser (2011) calculate the stress of a single fibre by integration of the stiffness calculated with respect to λ times the cumulative of the distribution function (Section 3.5). Because of this integration approach, Martufi and Gasser (2011) are forced to require that the stiffness be independent of λ_s in order to have a constitutive equation for the fibre that is independent of λ_s. Actually, this requirement can be bypassed, and here we propose a generalised model that includes, as a particular case, the corrected version of the model by Martufi and Gasser (2011) that we presented in Sections 3.7, 3.8 and 3.9, and in which *any* (physically admissible, e.g., strongly elliptical) fibril constitutive law can be employed.

In order to do so we, introduce the constitutive equation for a single fibre as

$$\hat{T}_n(\lambda) = \int_{\lambda_{min}}^{\lambda} -\frac{\partial(\hat{T}_{\text{fibril}} \circ h)}{\partial \lambda_s}(\lambda, \lambda_s)\, \mathcal{N}_s(\lambda_s)\, \mathrm{d}\lambda_s, \tag{3.50}$$

where, similarly to Hurschler et al. (1997), we integrate over λ_s. It should be noted that the stiffness in (3.50) is calculated as a derivative with respect to λ_s, rather than with respect to λ, as in the case of Martufi and Gasser (2011). Note also the minus sign, which could seem counterintuitive at first, but is turns out to be actually quite natural. Indeed, using the chain rule (recall that $h(\lambda, \lambda_s) = \lambda/\lambda_s = \lambda_e$, Equation (3.25)), we have

$$-\frac{\partial(\hat{T}_{\text{fibril}} \circ h)}{\partial \lambda_s}(\lambda, \lambda_s) = -\frac{\partial \hat{T}_{\text{fibril}}}{\partial \lambda_e}(h(\lambda, \lambda_s)) \, \frac{\partial h}{\partial \lambda_s}(\lambda, \lambda_s)$$
$$= -\frac{\partial \hat{T}_{\text{fibril}}}{\partial \lambda_e}(\lambda_e) \, \left(-\frac{\lambda}{\lambda_s^2}\right)$$
$$= \frac{\partial \hat{T}_{\text{fibril}}}{\partial \lambda_e}(\lambda_e) \, \frac{\lambda}{\lambda_s^2}. \tag{3.51}$$

If the stiffness $\partial \hat{T}_{\text{fibril}}/\partial \lambda_e$ of the relation between the first Piola-Kirchhoff stress and the elastic stretch λ_e is assumed to be positive, as it should be in order to have a strongly elliptic model (Truesdell and Noll, 1965; Marsden and Hughes, 1983; Antman, 1983; Ogden, 1997), then also the stiffness in the definition (3.50), which is calculated with respect to λ_s and includes a negative sign, will result in a positive stress $P_n(\lambda)$, as desired. In order for the stress in Equation (3.50) to be a generalisation of that in our corrected version of the model by Martufi and Gasser (2011), it must coincide with that in Equation (3.43), for the particular choice (3.35) of constitutive equation for the fibril. Using again the chain rule, we have

$$-\frac{\partial(\hat{T}_{\text{fibril}} \circ h)}{\partial \lambda_s}(\lambda, \lambda_s) = -\frac{\partial \hat{T}_{\text{fibril}}}{\partial \lambda_e}(h(\lambda, \lambda_s)) \, \frac{\partial h}{\partial \lambda_s}(\lambda, \lambda_s)$$
$$= -\frac{k}{\lambda_e}\left(-\frac{\lambda}{\lambda_s^2}\right) = -\frac{\lambda_s}{\lambda} k \, \left(-\frac{\lambda}{\lambda_s^2}\right) = \frac{k}{\lambda_s}. \tag{3.52}$$

Now, if we integrate (3.52) according to (3.50), we obtain

$$\hat{T}_n(\lambda) = \int_{\lambda_{min}}^{\lambda} -\frac{\partial(\hat{T}_{\text{fibril}} \circ h)}{\partial \lambda_s}(\lambda, \lambda_s) \, \mathcal{N}_s(\lambda_s) \, \mathrm{d}\lambda_s = \int_{\lambda_{min}}^{\lambda} \frac{k}{\lambda_s} \mathcal{N}_s(\lambda_s) \, \mathrm{d}\lambda_s, \tag{3.53}$$

which is equivalent to (3.43), since λ_s is just the integration variable and could be assigned any symbol.

3.11 Equivalence of Generalised Model and Adjusted Hurschler Model

Here we show that the generalised model presented in Section 3.10 is in fact equivalent to a slightly adjusted version of the model by Hurschler et al. (1997).

We recall that Hurschler et al. (1997) simply integrate the stress of each fibril times the distribution function, which represents the number of fibrils that have identical straightening stretch, and we emphasise that the integration is over λ_s. In contrast, Martufi and Gasser (2011) evaluate the stress of a single fibre by integrating the stiffness of a single fibril calculated with respect to λ times the cumulative of the distribution function. As mentioned in Section 3.10, this forced Martufi and Gasser (2011) to seek for a stiffness that is independent of λ_s. The fact that in the latter model required a specific constitutive function was arguably the reason why the equivalence between the two models has been missed so far. The generalised model that we presented in Section 3.10 is free of any restriction on the constitutive model, and this allows us to show its equivalence with the model by Hurschler et al. (1997).

As mentioned in Section 3.5, the model by Hurschler et al. (1997) has one small inconsistency with respect to the framework that we proposed in Section 3: it is based on a fibril constitutive equation for the Cauchy stress. This can easily be adjusted to fit our framework, by simply replacing the Cauchy stress by the first Piola-Kirchhoff stress. Using Equation (3.12), we can rewrite Equation (3.19) as

$$T_n = \hat{T}_n(\lambda) = \int_{\lambda_{min}}^{\lambda} \hat{T}_{\text{fibril}}(\lambda/t)\ \mathfrak{n}_s(t)\ \mathrm{d}t. \tag{3.54}$$

The proof of the equivalence between our generalised model and that by Hurschler et al. (1997) is quite straightforward. If we use function h of Equation (3.25) and integrate Equation (3.54) by parts, we obtain

$$\begin{aligned}
\hat{T}_n(\lambda) &= \int_{\lambda_{min}}^{\lambda} (\hat{T}_{\text{fibril}} \circ h)(\lambda, \lambda_s)\ \mathfrak{n}_s(\lambda_s)\ \mathrm{d}\lambda_s \\
&= \Big[(\hat{T}_{\text{fibril}} \circ h)(\lambda, \lambda_s)\ \mathcal{N}(\lambda_s)\Big]_{\lambda_s=\lambda_{min}}^{\lambda_s=\lambda} \\
&\quad - \int_{\lambda_{min}}^{\lambda} \frac{\partial(\hat{T}_{\text{fibril}} \circ h)}{\partial \lambda_s}(\lambda, \lambda_s)\ \mathcal{N}_s(\lambda_s)\ \mathrm{d}\lambda_s.
\end{aligned} \tag{3.55}$$

For $\lambda_s = \lambda_{min}$, the cumulative function vanishes, i.e., $\mathcal{N}_s(\lambda_{min}) = 0$ and, for $\lambda_s = \lambda$, the

stress is zero because $\lambda_e = 1$, i.e., $T_{\text{fibril}}(\lambda/\lambda) = 0$. Therefore, Equation (3.55) reduces to

$$\begin{aligned}\hat{T}_n(\lambda) &= \int_{\lambda_{min}}^{\lambda} (\hat{T}_{\text{fibril}} \circ h)(\lambda, \lambda_s)\ \mathfrak{n}_s(\lambda_s)\ \mathrm{d}\lambda_s \\ &= -\int_{\lambda_{min}}^{\lambda} \frac{\partial(\hat{T}_{\text{fibril}} \circ h)}{\partial \lambda_s}(\lambda, \lambda_s)\ \mathcal{N}_s(\lambda_s)\ \mathrm{d}\lambda_s, \end{aligned} \tag{3.56}$$

which shows that the model by Hurschler et al. (1997) is equivalent to our generalisation proposed in (3.50) of the model by Martufi and Gasser (2011).

Chapter 4

Fibre Damage Constitutive Model

In this chapter, we intend to construct a damage model from the constitutive relation proposed in Section 3.10, Equation (3.50), and to prove that this damage model is equivalent to that by Hurschler et al. (1997). The damage model that we propose follows the assumption made on the progressive recruitment of the fibrils when the fibre is stretched, and describes the failure of the collagen fibre via the progressive failure of the fibrils. Although we follow a different approach to construct our damage model, the underlying assumptions are identical to those made by Hurschler et al. (1997) in their model. With an approach similar to that followed for the case of recruitment, we proceed in steps and study the failure kinematics, probability distribution and evaluation of the stress.

4.1 Constitutive Assumptions and Consequences on the Kinematics

Since all fibrils are assumed to have the same mechanical properties, it is reasonable to also assume that each fibril fails at the same elastic failure stretch, called λ_f, evaluated with respect to the straightened configuration $\mathcal{C}_s$. So, for a fibril that gets completely straight at a certain straightening stretch λ_s, the failure stretch evaluated from the reference configuration $\mathcal{C}$ is $\lambda_f\lambda_s$, as depicted in Figure 4.1.

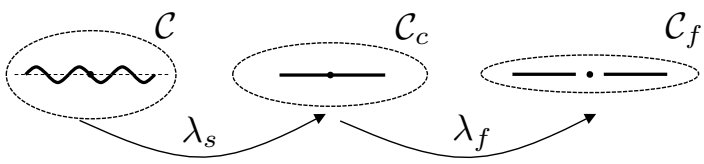

Figure 4.1: Recruitment and failure of a typical fibril; $\mathcal{C}_f$ and λ_f are the configuration and stretch, respectively, at which the fibril fails.

In order to look at fibril failure in the three-dimensional picture, let us recall that the

straightening deformation $\boldsymbol{F}_s$ consists of a pure stretch $\|\boldsymbol{F}_s\boldsymbol{M}\| = \lambda_s$ in the referential direction $\boldsymbol{M}$ of the fibril, and let us consider the "intermediate" direction

$$\boldsymbol{\mu} = \frac{1}{\lambda_s}\boldsymbol{F}_s\boldsymbol{M}, \tag{4.1}$$

which is parallel to $\boldsymbol{M}$ by construction, according to the matrix representation in Equation (3.2) (provided that the bases $\{\boldsymbol{E}_A\}_{A=1}^3$ in the reference configuration and $\{\boldsymbol{\epsilon}_\alpha\}_{\alpha=1}^3$ in the intermediate configuration are chosen to be *coaxial*). Failure is attained at all those elastic deformations $\boldsymbol{F}_e$ such that

$$\|\boldsymbol{F}_e\boldsymbol{\mu}\| = \lambda_f. \tag{4.2}$$

4.2 Failure Probability

The failure of fibrils can be described similarly as their recruitment, which is based on the probability density function $\mathfrak{n}_s$. Since the fibrils straighten orderly following the probability density function $\mathfrak{n}_s$, they also fail in the same order. The failure process begins at $\lambda_f\lambda_{min}$, as the fibril that stretched first (at λ_{min}) reaches its failure stretch. The fibrils will fail progressively until all of them have failed, which corresponds to $\lambda_f\lambda_{max}$. At this point, the stress must equal zero, since there no fibril is capable of bearing any load.

The probability density function $\mathfrak{n}_f$ describing the failure of fibrils is constructed similarly to the straightening probability $\mathfrak{n}_s$, and is in fact related to it by

$$\mathfrak{n}_f(\lambda_s) = \mathfrak{n}_s(\lambda_f\lambda_s). \tag{4.3}$$

Basically, we obtain the failure probability $\mathfrak{n}_f$ by transforming (to be precise, by uniformly stretching, by a factor λ_f) the domain of the straightening probability $\mathfrak{n}_s$ from $[\lambda_{min}, \lambda_{max}]$ to $[\lambda_{minf}, \lambda_{maxf}]$. In order to calculate the stress at a given $\lambda > \lambda_{minf} = \lambda_f\lambda_{min}$, we need a way to exclude the failed fibrils from the fraction of recruited fibres. At a given stretch λ, the fraction of failed fibres is given by the area subtended by $\mathfrak{n}_f$ in the interval $]\lambda_{minf}, \lambda]$. These failed fibrils have been recruited in the interval $]\lambda_{min}, \lambda/\lambda_f]$, and must be "deducted" from

the area subtended by $\mathfrak{n}_s$ in the interval $]\lambda_{min}, \lambda]$, as shown in Figure 4.2. This is equivalent to defining the "transformed" distribution

$$\mathfrak{n}_{sf}(\lambda, \lambda_s) = \begin{cases} 0, & \forall\, \lambda \in]0, \lambda_{minf}], & (4.4a) \\ 0, & \forall\, \lambda \in]\lambda_{minf}, +\infty[\quad \text{and} \quad \forall\, \lambda_s \in]\lambda/\lambda_f, +\infty], & (4.4b) \\ \mathfrak{n}_s(\lambda_s), & \forall\, \lambda \in]\lambda_{minf}, +\infty[\quad \text{and} \quad \forall\, \lambda_s \in]0, \lambda/\lambda_f], & (4.4c) \end{cases}$$

depending on λ and λ_s. The stretch λ is the stretch actually attained by the fibre and, in the definition of $\mathfrak{n}_{sf}$, serves solely as the parameter determining the stretch λ/λ_f below which the fibrils have failed, whereas λ_s is the straightening stretch, which is again used as the integration variable. Figure 4.2 illustrates $\mathfrak{n}_{sf}$ for an arbitrary λ. The cumulative function of $\mathfrak{n}_{sf}$ is obtained by integration in λ_s, as

$$\mathcal{N}_{sf}(\lambda, \lambda_s) = \int_{\lambda_{min}}^{\lambda_s} \mathfrak{n}_{sf}(\lambda, t)\, \mathrm{d}t. \tag{4.5}$$

It is worth mentioning that the cumulative function $\mathcal{N}_{sf}$ represents the area subtended by

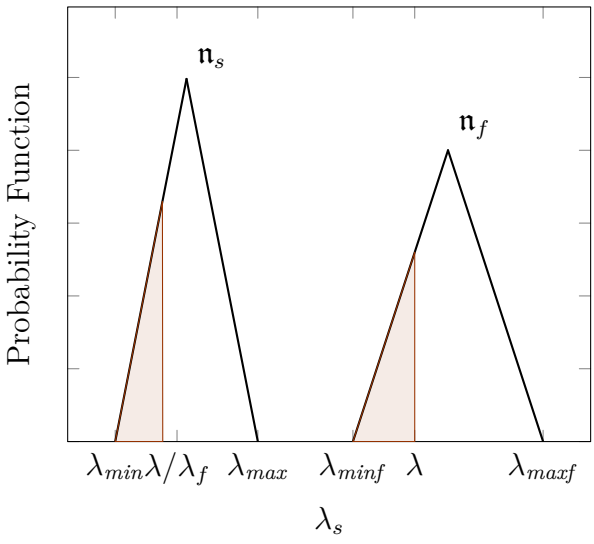

Figure 4.2: The portion of the graph of $\mathfrak{n}_s$ subtending the red triangular area is the non-zero portion of the graph of $\mathfrak{n}_{sf}$.

the graph of $\mathfrak{n}_{sf}$ for a given value of the actually attained stretch λ. The cumulative function $\mathcal{N}_{sf}$ is needed to derive the "loss" of stress due to the failed fibres in a way analogous to how the recruitment cumulative function $\mathcal{N}_s$ is used to evaluate the stress P_f of the recruited

fibres, i.e.,

$$\hat{T}_f(\lambda) = \int_{\lambda_{min}}^{\lambda} -\mathcal{N}_{sf}(\lambda, \lambda_s) \frac{\partial(\hat{T}_{\text{fibril}} \circ h)}{\partial \lambda_s}(\lambda, \lambda_s)\, \mathrm{d}\lambda_s. \tag{4.6}$$

Thus, the actual stress in the damaged fibre can be expressed as

$$\hat{T}(\lambda) = \hat{T}_n(\lambda) - \hat{T}_f(\lambda). \tag{4.7}$$

The cumulative function is

$$\mathcal{N}_{sf}(\lambda, \lambda_s) = \begin{cases} 0, & \forall\, \lambda \in]0, \lambda_{minf}], & \text{(4.8a)} \\ \mathcal{N}_s(\lambda_s), & \forall\, \lambda \in]\lambda_{minf}, +\infty[\text{ and } \forall\, \lambda_s \in]0, \lambda/\lambda_f], & \text{(4.8b)} \\ \mathcal{N}_s(\lambda/\lambda_f), & \forall\, \lambda \in]\lambda_{minf}, +\infty[\text{ and } \forall\, \lambda_s \in [\lambda/\lambda_f, +\infty[. & \text{(4.8c)} \end{cases}$$

Therefore we can split the integration interval of $\hat{T}_f$ of Equation (4.6) into two intervals, $[\lambda_{min}, \lambda/\lambda_f]$ and $]\lambda/\lambda_f, \lambda]$, and obtain:

$$\begin{aligned} \hat{T}_f(\lambda) = &\int_{\lambda_{min}}^{\lambda/\lambda_f} -\mathcal{N}_s(\lambda_s) \frac{\partial(\hat{T}_{\text{fibril}} \circ h)}{\partial \lambda_s}(\lambda, \lambda_s)\, \mathrm{d}\lambda_s + \\ &+ \int_{\lambda/\lambda_f}^{\lambda} -\mathcal{N}_s(\lambda/\lambda_f) \frac{\partial(\hat{T}_{\text{fibril}} \circ h)}{\partial \lambda_s}(\lambda, \lambda_s)\, \mathrm{d}\lambda_s. \end{aligned} \tag{4.9}$$

Thus $\hat{T}(\lambda)$ can be written as:

$$\begin{aligned} \hat{T}(\lambda) = &\int_{\lambda_{min}}^{\lambda} -\mathcal{N}_s(\lambda_s) \frac{\partial(\hat{T}_{\text{fibril}} \circ h)}{\partial \lambda_s}(\lambda, \lambda_s)\, \mathrm{d}\lambda_s - \\ &- \int_{\lambda_{min}}^{\lambda/\lambda_f} -\mathcal{N}_s(\lambda_s) \frac{\partial(\hat{T}_{\text{fibril}} \circ h)}{\partial \lambda_s}(\lambda, \lambda_s)\, \mathrm{d}\lambda_s - \\ &- \int_{\lambda/\lambda_f}^{\lambda} -\mathcal{N}_s(\lambda/\lambda_f) \frac{\partial(\hat{T}_{\text{fibril}} \circ h)}{\partial \lambda_s}(\lambda, \lambda_s)\, \mathrm{d}\lambda_s. \end{aligned} \tag{4.10}$$

We notice that the difference of the first two integrals in Equation (4.10) can be expressed as the integral from λ/λ_f to λ , i.e.,

$$\begin{aligned} \hat{T}(\lambda) = &\int_{\lambda/\lambda_f}^{\lambda} -\mathcal{N}_s(\lambda_s) \frac{\partial(\hat{T}_{\text{fibril}} \circ h)}{\partial \lambda_s}(\lambda, \lambda_s)\, \mathrm{d}\lambda_s - \\ &- \int_{\lambda/\lambda_f}^{\lambda} -\mathcal{N}_s(\lambda/\lambda_f) \frac{\partial(\hat{T}_{\text{fibril}} \circ h)}{\partial \lambda_s}(\lambda, \lambda_s)\, \mathrm{d}\lambda_s \end{aligned} \tag{4.11}$$

Furthermore, we can solve directly the last integral and obtain

$$\begin{aligned}\hat{T}(\lambda) &= \int_{\lambda/\lambda_f}^{\lambda} -\mathcal{N}_s(\lambda_s)\,\frac{\partial(\hat{T}_{\text{fibril}}\circ h)}{\partial\lambda_s}(\lambda,\lambda_s)\,\mathrm{d}\lambda_s + \\ &\quad + \left[\mathcal{N}_s(\lambda/\lambda_f)(\hat{T}_{\text{fibril}}\circ h)(\lambda,\lambda_s)\right]_{\lambda_s=\lambda/\lambda_f}^{\lambda_s=\lambda} \\ &= \int_{\lambda/\lambda_f}^{\lambda} -\mathcal{N}_s(\lambda_s)\,\frac{\partial(\hat{T}_{\text{fibril}}\circ h)}{\partial\lambda_s}(\lambda,\lambda_s)\,\mathrm{d}\lambda_s + \\ &\quad + \mathcal{N}_s(\lambda/\lambda_f)\left[(\hat{T}_{\text{fibril}}\circ h)(\lambda,\lambda) - (\hat{T}_{\text{fibril}}\circ h)(\lambda,\lambda/\lambda_f)\right]. \end{aligned} \tag{4.12}$$

Therefore, since $(\hat{T}_{\text{fibril}}\circ h)(\lambda,\lambda) = \hat{T}_{\text{fibril}}(1) = 0$ and $(\hat{T}_{\text{fibril}}\circ h)(\lambda,\lambda/\lambda_f) = \hat{T}_{\text{fibril}}(\lambda_f)$, we finally obtain the first Piola-Kirchhoff stress in the damage model as

$$T = \hat{T}(\lambda) = \int_{\lambda/\lambda_f}^{\lambda} -\mathcal{N}_s(\lambda_s)\,\frac{\partial(\hat{T}_{\text{fibril}}\circ h)}{\partial\lambda_s}(\lambda,\lambda_s)\,\mathrm{d}\lambda_s - \mathcal{N}_s(\lambda/\lambda_f)\hat{T}_{\text{fibril}}(\lambda_f). \tag{4.13}$$

4.3 Equivalence with the Damage Model by Hurschler et al. (1997)

Now we show that the expression obtained in (4.13) is in fact identical to that proposed by Hurschler et al. (1997). Using integration by parts, we have

$$\begin{aligned}\hat{T}(\lambda) &= \int_{\lambda/\lambda_f}^{\lambda} \mathfrak{n}_s(\lambda_s)(\hat{T}_{\text{fibril}}\circ h)(\lambda,\lambda_s)\,\mathrm{d}\lambda_s \\ &= \left[\mathcal{N}_s(\lambda_s)(\hat{T}_{\text{fibril}}\circ h)(\lambda,\lambda_s)\right]_{\lambda_s=\lambda/\lambda_f}^{\lambda_s=\lambda} - \int_{\lambda/\lambda_f}^{\lambda} \mathcal{N}_s(\lambda_s)\frac{\partial(\hat{T}_{\text{fibril}}\circ h)}{\partial\lambda_s}(\lambda,\lambda_s)\,\mathrm{d}\lambda_s \\ &= \int_{\lambda/\lambda_f}^{\lambda} -\mathcal{N}_s(\lambda_s)\,\frac{\partial(\hat{T}_{\text{fibril}}\circ h)}{\partial\lambda_s}(\lambda,\lambda_s)\,\mathrm{d}\lambda_s - \mathcal{N}_s(\lambda/\lambda_f)\hat{T}_{\text{fibril}}(\lambda_f), \end{aligned} \tag{4.14}$$

and thus Equation (4.14) and Equation (4.13) are identical.

It is noteworthy that we constructed the damage model for generalisation of the model by Martufi and Gasser (2011) independently from Hurschler et al. (1997). However, since both the damage model by Hurschler et al. (1997) and ours are based on the assumption that all fibrils fail at the same stretch λ_f calculated from the straightened configuration, they yield identical results. There is, however, a conceptual difference.

The damage model by Hurschler et al. (1997) is in fact quite straightforward to implement, as it simply requires the modification of the lower limit of integral (compare Equa-

tions (3.54) and (4.14)), which intuitively is a likely physical description of the damage mechanism. In contrast, the approach that we introduce in Section 4.2 is, in a way, more mathematical, in that it explicitly defines a failure probability distribution, which is obtained by *uniformly stretching* the support $[\lambda_{min}, \lambda_{max}]$ of the recruitment distribution into the support $[\lambda_{minf}, \lambda_{maxf}]$ of the failure probability distribution. The equivalence of the two approaches is clear when the failure stretch λ_f is constant. Our approach, however, suggests a greater flexibility in the definition of the damage mechanism. Indeed, a different mechanism would be represented by a *non-uniform* stretch of the support of the straightening probability, performed by a smooth monotonic function φ. In the approach used by Hurschler et al. (1997), this would be obtained by replacing the lower extremum λ/λ_f of the integral in Equation (4.14) by $\varphi(\lambda)$, but this would be less intuitive.

4.4 Unloading Following Damage

Following the same line of thought, we can construct a constitutive equation for the stress in unloading. In order to describe unloading, we must account for the fact that, when unloading from a stretch $\lambda_u > \lambda_{minf} = \lambda_f \lambda_{min}$ the fibrils that have already failed must be disregarded and that no further fibrils fail during unloading. This can be achieved by defining the unloading probability density (see Figure 4.3)

$$\mathfrak{n}_u(\lambda_s, \lambda_u) = \begin{cases} 0, & \forall\, \lambda \in [\lambda_{min}, \lambda_u/\lambda_f[, & \text{(4.15a)} \\ \mathfrak{n}_s(\lambda_s), & \forall\, \lambda \in [\lambda_u/\lambda_f, \lambda_u], & \text{(4.15b)} \end{cases}$$

which gives the cumulative probability

$$\mathcal{N}_u(\lambda_s, \lambda_u) = \begin{cases} 0, & \forall\, \lambda \in]0, \lambda_u/\lambda_f], & \text{(4.16a)} \\ \mathcal{N}_s(\lambda_s) - \mathcal{N}_s(\lambda_u/\lambda_f), & \forall\, \lambda \in]\lambda_u/\lambda_f, \lambda_u], & \text{(4.16b)} \\ \mathcal{N}_s(\lambda_s), & \forall\, \lambda \in]\lambda_u, +\infty[. & \text{(4.16c)} \end{cases}$$

Now we can introduce the stress in the unloading stage as

$$\hat{T}(\lambda, \lambda_u) = \int_{\lambda_{min}}^{\lambda} -\mathcal{N}_u(\lambda_s, \lambda_u)\, \frac{\partial(\hat{T}_{\text{fibril}} \circ h)}{\partial \lambda_s}(\lambda, \lambda_s)\, \mathrm{d}\lambda_s. \qquad (4.17)$$

Considering (4.16a), we can replace the lower limit of the integral in (4.17) by λ_u/λ_f. Moreover, since we only consider the unloading case, we assume that $\lambda_s \in]\lambda_u/\lambda_f, \lambda_u]$. Thus we replace $\mathcal{N}_u(\lambda_s, \lambda_u)$ in (4.17) with the expression of (4.16b) and obtain

$$\hat{T}(\lambda, \lambda_u) = \int_{\lambda_u/\lambda_f}^{\lambda} -\Big[\mathcal{N}_s(\lambda_s) - \mathcal{N}_s(\lambda_u/\lambda_f)\Big] \frac{\partial(\hat{T}_{\text{fibril}} \circ h)}{\partial \lambda_s}(\lambda, \lambda_s)\, \mathrm{d}\lambda_s, \tag{4.18}$$

which, by virtue of the linearity of the integral operator, becomes

$$\begin{aligned}
\hat{T}(\lambda, \lambda_u) &= \int_{\lambda_u/\lambda_f}^{\lambda} -\mathcal{N}_s(\lambda_s) \frac{\partial(\hat{T}_{\text{fibril}} \circ h)}{\partial \lambda_s}(\lambda, \lambda_s)\, \mathrm{d}\lambda_s \\
&\quad + \mathcal{N}_s(\lambda_u/\lambda_f) \Big[\hat{T}_{\text{fibril}}(\lambda/\lambda_s)\Big]_{\lambda_s=\lambda_u/\lambda_f}^{\lambda_s=\lambda} \\
&= \Big[\hat{T}_n(\lambda) - \hat{T}_n(\lambda_u/\lambda_f)\Big] - \mathcal{N}_s(\lambda_u/\lambda_f)\, \hat{T}_{\text{fibril}}(\lambda\lambda_f/\lambda_u).
\end{aligned} \tag{4.19}$$

We note that, if we replace λ_u by λ in Equation (4.19), we recover the case of monotonic loading described by Equation (4.13).

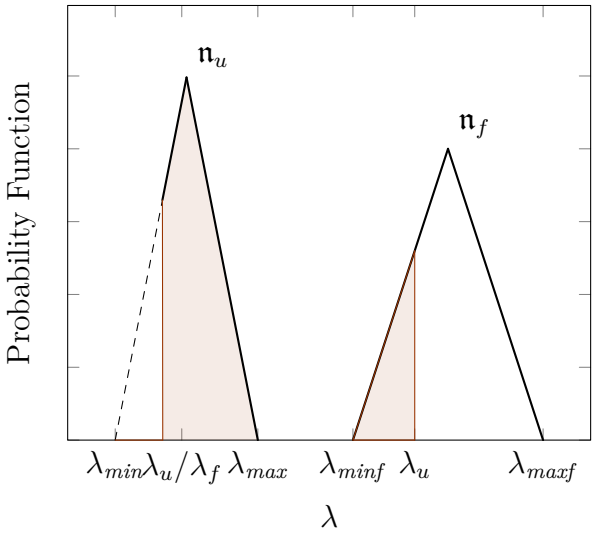

Figure 4.3: The probability density $\mathfrak{n}_u$ is defined as the complementary portion of the area subtended by $\mathfrak{n}_s$ representing the failed fibrils (from λ_{min} to λ_u/λ_f).

4.5 Sensitivity to the Recruitment and Damage Parameters

Here, we discuss the sensitivity of the proposed model to the *anelastic* parameters λ_f and λ_u by means of a numerical example. The choice of the parameter λ_f can affect the model

significantly, not only in terms of the values taken by the stress, but also of the overall damage behaviour, since it affects how recruitment and failure of fibrils, which are the two bases of this constitutive model, interact. As stated before, the progression of damage initiates at $\lambda_{minf} = \lambda_f \lambda_{min}$. Depending on the values of λ_{min}, λ_{max} and λ_f, the failure of fibrils can initiate either while not all fibrils have been recruited yet ($\lambda_f \lambda_{min} = \lambda_{minf} < \lambda_{max}$), or after all fibrils have been recruited ($\lambda_f \lambda_{min} = \lambda_{minf} > \lambda_{max}$). The first scenario corresponds to an overlap between the supports of the recruitment and the failure probabilities (Figure 4.4a), and the second scenario corresponds to non-overlapping supports (Figure 4.4b).

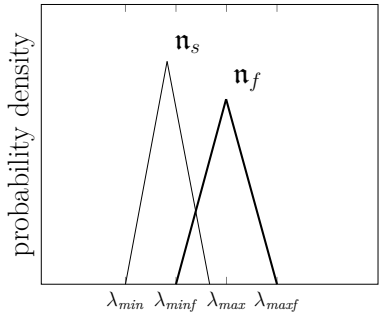

(a) overlapping

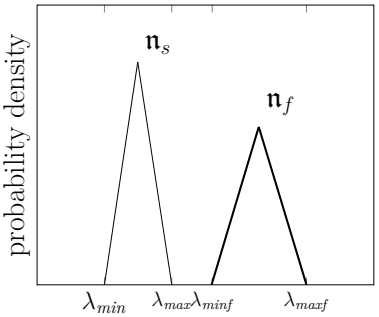

(b) non overlapping

Figure 4.4: Different cases of damage distribution function.

Let us demonstrate the change in the stress-stretch curve depending on the value of λ_f, for fixed λ_{min} and λ_{max}, by means of an example. The values for k, λ_{min} and λ_{max} are taken from the work by Martufi and Gasser (2011). For the scenario with overlap of the supports (Figure 4.4a), three values were selected for λ_f, whereas for the scenario with no overlap

of the supports (Figure 4.4b), one value has been chosen. All parameters are reported in Table 4.1.

Parameter	value
λ_{min}	1.045
λ_{max}	1.117
k [MPa]	63
λ_f (overlapping, as in Fig. 4.4a)	1.03
λ_f (overlapping, as in Fig. 4.4a)	1.04
λ_f (overlapping, as in Fig. 4.4a)	1.06
λ_f (non overlapping, as in Fig. 4.4b)	1.10

Table 4.1: Values of the parameters in our numerical example.

Figure 4.5 demonstrates the change in the stress-stretch curve, for varying λ_f. The stress changes significantly as the value of λ_f increases. The other notable point is that, for lower values of λ_f, the curve is more symmetric. For $\lambda_f = 1.10$, which corresponds to the scenario with non-overlapping supports as depicted in Figure 4.4b, the curve is fairly linear before the maximum, as all the fibrils are engaged for a certain interval of stretch, before the damage process initiates.

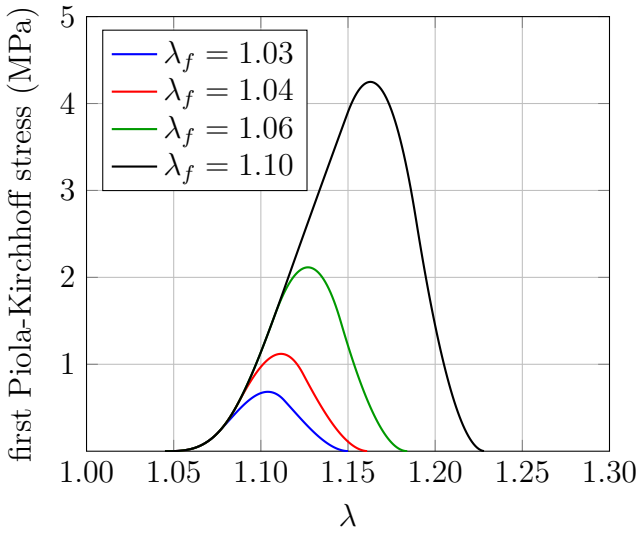

Figure 4.5: Stress-stretch curve for different values of the failure stretch λ_f.

Figure 4.6 shows the stress-stretch curve for unloading, in the scenario with no-overlap in supports depicted in Figure 4.4b, for various values of λ_u. When the fibre is unloaded

after having reached the stretch λ_u, the stress returns to zero at λ_u/λ_f, because the fibrils with $\lambda_s \leq \lambda_u/\lambda_f$ have all failed. When the fibre is being reloaded, the stress-stretch curve coincides with the unloading curve $\hat{T}_u(\lambda)$ for $\lambda < \lambda_u$ and with the curve of $\hat{T}(\lambda)$ for $\lambda \geq \lambda_u$, as the damage initiates again at λ_u, in precisely the same way as the simple loading case. Although no properly called plastic mechanism has been prescribed at the fibril level, the curves show a "plastic" effect, in the sense that the reference stretch is *not* recovered.

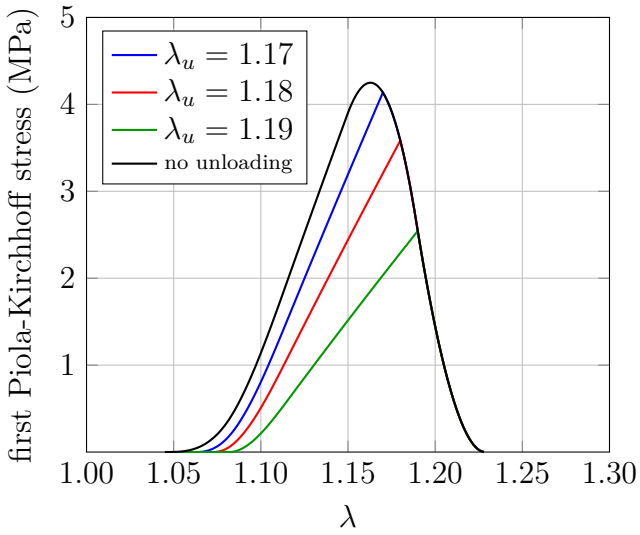

Figure 4.6: Stress-stretch curve for at different values of the stretch λ_u at which unloading begins. The black curve has *no* unloading, as λ_u coincides with the ultimate failure stretch λ_{maxf}.

Chapter 5

Finite Element Implementation

The fibre model has been implemented in the Finite Element package FEAP (Taylor, 2007), using our previously reported framework (Federico and Gasser, 2010), which is capable to also account for statistical fibre orientation. To this end, a quasi-incompressible formulation, based on the mixed Q1P0 finite element (Simo and Taylor, 1991), was followed. We considered a composite comprised of a (soft) matrix phase, denoted by the subscript 0, and a statistically oriented fibre phase, denoted by the superscript 1, and incorporated following the general theory of fibrous tissue (e.g., Lanir, 1983). The matrix is mainly required to regularise the otherwise possibly ill-conditioned fibrous tissue model. The orientation of the collagen fibres is assumed to be described by a probability distribution function Ψ, normalised to unity over the material unit sphere (i.e., the set of all possible directions passing by a given material point). The overall second Piola-Kirchhoff stress is assumed to be given by the integral

$$\boldsymbol{S} = \boldsymbol{S}_0 + \int_{\mathcal{A}} \Psi(\boldsymbol{M})\ \boldsymbol{S}_1\ \mathrm{d}S, \tag{5.1}$$

whose complexity requires a numerical evaluation. In Equation (5.1), the volumetric fractions of matrix and fibres are thought to be lumped into the stresses as multiplicative coefficients, and the integral is performed over $\mathcal{A}$, i.e., the subset of the material unit sphere of all directions $\boldsymbol{M}$ such that a collagen fibre parallel to $\boldsymbol{M}$ is under extension at a given deformation, i.e., $\boldsymbol{C} : (\boldsymbol{M} \otimes \boldsymbol{M}) \geq 1$.

5.1 Matrix and Fibre Constitutive Equations

The strain energy of the matrix is assumed to be neo-Hookean, i.e.,

$$W_0 = \hat{W}_0(\bar{\boldsymbol{C}}) = \tfrac{1}{2}\,\mu_0\,(I_1(\bar{\boldsymbol{C}}) - 3), \tag{5.2}$$

with $I_1(\bar{\boldsymbol{C}}) = \mathrm{Tr}(\bar{\boldsymbol{C}}) = G^{AB}\,\bar{C}_{AB}$ denoting the first invariant of the isochoric right Cauchy-Green deformation $\bar{\boldsymbol{C}} = \bar{\boldsymbol{F}}^T\,\boldsymbol{g}\bar{\boldsymbol{F}} \equiv \bar{\boldsymbol{F}}^T.\bar{\boldsymbol{F}}$ (which is the *isochoric* pull-back of the metric tensor $\boldsymbol{g}$), where the trace Tr is taken with respect to the regular (inverse) material metric tensor $\boldsymbol{G}^{-1}$ (Federico, 2012), and the isochoric deformation gradient is $\bar{\boldsymbol{F}} = J^{-1/3}\boldsymbol{F}$ (Flory, 1961).

Using the first Piola-Kirchhoff stress $\hat{T}_1 \equiv \hat{T}$ for a fibre given in Equation (4.13), the corresponding second Piola-Kirchhoff stress is

$$\boldsymbol{S}_1 = \boldsymbol{F}^{-1}\boldsymbol{T}_1 = \lambda^{-1}T_1\,\boldsymbol{M}\otimes\boldsymbol{M} = \|\boldsymbol{F}\boldsymbol{M}\|^{-1}\hat{T}_1(\|\boldsymbol{F}\boldsymbol{M}\|)\,\boldsymbol{M}\otimes\boldsymbol{M}, \tag{5.3}$$

where, as usual, $\lambda = \|\boldsymbol{F}\boldsymbol{M}\|$. Consequently, the deviatoric second Piola-Kirchhoff stress $\mathrm{Dev}^*(\boldsymbol{S})$ of the collagen fibre reinforced tissue reads

$$\begin{aligned}\mathrm{Dev}^*(\boldsymbol{S}) &= J^{-2/3}\mu_0\,\mathrm{Dev}^*(\boldsymbol{G}^{-1})\\ &\quad + J^{-2/3}\int_{\mathcal{A}}\Psi(\boldsymbol{M})\,\|\boldsymbol{F}\boldsymbol{M}\|^{-1}\hat{T}_1(\|\boldsymbol{F}\boldsymbol{M}\|)\,\mathrm{Dev}^*(\boldsymbol{M}\otimes\boldsymbol{M})\,\mathrm{d}S.\end{aligned} \tag{5.4}$$

In Equation (5.4), $\mathrm{Dev}^*(\,\cdot\,) = (\,\cdot\,) - \frac{1}{3}\,\mathrm{Tr}^*(\,\cdot\,)\,\boldsymbol{C}^{-1}$ denotes the *pulled-back* material deviator operator, with the *pulled-back* trace $\mathrm{Tr}^*(\,\cdot\,)$ calculated with respect to $\boldsymbol{C}$, i.e., $\mathrm{Tr}^*(\boldsymbol{S}) = \boldsymbol{C} : \boldsymbol{S} = C_{AB}\,S^{AB}$ (Federico, 2012), which is the *pull-back* of the spatial metric tensor $\boldsymbol{g}$ (i.e., $\boldsymbol{C} = \chi^*\boldsymbol{g} = \boldsymbol{F}^T\boldsymbol{g}\,\boldsymbol{F} \equiv \boldsymbol{F}^T.\boldsymbol{F}$), and $\boldsymbol{M}$ is the unit direction vector of the generic collagen fibre in the reference configuration.

For an efficient FE implementation, Equation (5.4) is pushed-forward, defining the isochoric Kirchhoff stress

$$\begin{aligned}\mathrm{dev}(\boldsymbol{\tau}) &= \boldsymbol{F}\,[\mathrm{Dev}^*(\boldsymbol{S})]\,\boldsymbol{F}^T\\ &= J^{-2/3}\mu_0\,\mathrm{dev}(\boldsymbol{b})\\ &\quad + J^{-2/3}\int_{\mathcal{A}}\Psi(\boldsymbol{M})\,\|\boldsymbol{F}\boldsymbol{M}\|^{-1}\hat{T}_1(\|\boldsymbol{F}\boldsymbol{M}\|)\,\mathrm{dev}(\boldsymbol{F}\boldsymbol{M}\otimes\boldsymbol{F}\boldsymbol{M})\,\mathrm{d}S.\end{aligned} \tag{5.5}$$

where $\mathrm{dev}(\,\cdot\,) = (\,\cdot\,) - \frac{1}{3}\,\mathrm{tr}(\,\cdot\,)\,\boldsymbol{g}^{-1}$ is the regular spatial deviator operator (where the inverse metric $\boldsymbol{g}^{-1}$, with components g^{ab}, serves as the "contravariant unit tensor") and $\boldsymbol{b}$ denotes the

left Cauchy-Green deformation tensor. The corresponding elasticity tensor can be obtained as outlined in previous works (Gasser et al., 2006; Federico and Gasser, 2010; Federico, 2012).

In order to track the state of damage of an individual collagen fibre, the highest stretch λ previously experienced by the fibre is stored as a history variable at the corresponding integration point.

5.2 Regularisation

In order to ensure FE mesh-independent results, it is usual for smeared fracture models (see Oliver, 1996; Oliver et al., 1999; Comellas et al., 2016) to relate the fracture energy $\mathcal{G}_{\text{fr}}$ to a characteristic length scale, through a relation of the type $\mathcal{G}_{\text{fr}}^{\star} = \mathcal{G}_{\text{fr}}/\xi$, where ξ is a non-dimensional parameter related to the characteristic length scale. We used $\xi = L_{\text{mesh}}/L_{\text{loc}}$ for such a length-scale parameter. Here, $L_{\text{mesh}} = V_{\text{GP}}^{1/3}$ represents the FE mesh-related length scale with V_{GP} denoting the partial volume of the finite element that is allocated to the Gauss point (integration point) at which the constitutive model is evaluated. In addition, L_{loc} is thought to be a material property and represents the length within which the collagen fibre exhibits localisation during failure. Since our constitutive description does not directly give the fracture energy $\mathcal{G}_{\text{fr}}$ to prescribe the stress-strain properties of the collagen fibre, we used an alternative implementation of this regularisation concept. Specifically, at a given stretch λ, we used

$$P^{\star} = \hat{T}^{\star}(\lambda) = \frac{\hat{T}(\lambda)}{\xi}, \qquad \mathrm{K}^{\star} = \hat{\mathrm{K}}^{\star}(\lambda) = \frac{\hat{\mathrm{K}}(\lambda)}{\xi}, \quad \forall\, \mathrm{K}(\lambda) < 0, \tag{5.6}$$

to relate the first Piola-Kirchhoff stress $\hat{T}(\lambda)$ and the related stiffness $\mathrm{K} = \hat{\mathrm{K}}(\lambda) = (\mathrm{d}\hat{T}/\mathrm{d}\lambda)(\lambda)$ of the collagen fibre to the length-scale parameter ξ.

Using the change of variable $\lambda = s + \lambda_0$, the fracture energy reads

$$\mathcal{G}_{\text{fr}} = \int_{\lambda_0}^{+\infty} \hat{T}(\lambda)\, \mathrm{d}\lambda = \int_{0}^{+\infty} \hat{T}(s + \lambda_0)\, \mathrm{d}s. \tag{5.7}$$

Introducing the stretch λ_0 at the point of localisation (i.e., the point at which $\hat{\mathrm{K}}(\lambda_0) = (\mathrm{d}\hat{T}/\mathrm{d}\lambda)(\lambda_0) = 0$ holds), using integration by parts and noting that $\left[\hat{T}(s+\lambda_0)\ s\right]_0^{+\infty} = 0$, we obtain

$$\mathcal{G}_{\mathrm{fr}} = -\int_0^{+\infty} \hat{\mathrm{K}}(s+\lambda_0)\ s\ \mathrm{d}s < 0. \tag{5.8}$$

Due to the linearity of the integral operator, it is equivalent to use the condition $\mathrm{K}^\star = \mathrm{K}/\xi$ in place of $\mathcal{G}_{\mathrm{fr}}^\star = \mathcal{G}_{\mathrm{fr}}/\xi$, which is widely employed (Oliver, 1996; Oliver et al., 2002; Comellas et al., 2016) to ensure FE mesh-independent results.

5.3 Example: Human Achilles Tendon

In order to explore the basic mechanisms of the proposed constitutive model and to demonstrate its Finite Element implementation, we considered a uniaxial tension test on a segment of an Achilles tendon.

The orientation of the collagen fibres within the tendon is assumed to be described by the transversely isotropic von Mises distribution

$$\Psi(\boldsymbol{M}) = \Psi(\boldsymbol{M}(\Theta,\Phi)) = \rho(\Theta) = \frac{1}{\pi}\sqrt{\frac{b}{2\pi}}\frac{\exp[b(\cos(2\Theta)+1)]}{\mathrm{erfi}(\sqrt{2b})}, \tag{5.9}$$

where Θ is the angle with respect to the axis of symmetry of the distribution (Gasser et al., 2006; Federico and Gasser, 2010), b is the *concentration parameter* specifying the distribution, and $\mathrm{erfi}(x) = -i\ \mathrm{erf}(i\ x)$ denotes the imaginary error function at x. For our example, we chose a value of the concentration parameter $b = 2.0$, reflecting a fairly coherent alignment of the fibres along the tendon's axis observed in tendons (Thomopoulos et al., 2003). Although this reflects the qualitative collagen fibre distribution in tendons, detailed quantitative data was not considered in the present computation.

The tendon tissue was treated as a residual stress-free pure solid (i.e., the fluid phase was neglected). The neo-Hookean parameter $\mu_0 = 1.0$ MPa represents the matrix within which the collagen fibres are embedded. The fibres have been modelled with the fibril constitutive

equation (3.35), with a fibril stiffness of $k = 33.6$ MPa, and the T_{fibril}-λ fibre constitutive equation (3.43), which is suitable for the general compressible case, although the overall incompressibility of the model was enforced. The recruitment probability distribution was triangular, with lower and upper extrema $\lambda_{min} = 1.02$ and $\lambda_{max} = 1.12$, respectively. The collagen fibrils were assumed to have a failure stretch $\lambda_f = 1.1$. Finally, localisation was assumed to occur over a length $L_{\text{loc}} = 2.0\,\text{mm}$ around the theoretical point of failure on the collagen fibre. Again, these constitutive properties are plausible estimates rather than data from particular experimental studies. The integral in Equation (5.5) was solved by means of a spherical t-design, with $t = 21$, involving 240 integration points (Hardin and Sloane, 1996).

Parametrised computational grids of an Achilles tendon segment were generated with dimensions as in Figure 5.1. The segment showed a clear neck, to control the onset of tissue failure. The segment's bottom face was fixed, and at its top face the axial displacement u was prescribed such that it increased linearly to the value of 4.5 mm. Then, the stress state was computed at increments of Δu of the prescribed displacement. In order to overcome unstable failure propagation when exceeding the localisation limit, a small degree of viscous behaviour has been introduced at each finite element node. The arising first order transient problem is then solved with the (implicit) Newmark method, and the linearised system of equations is then solved. Simultaneously, tissue incompressibility was enforced by a penalty energy potential, and the associated penalty parameter (bulk modulus) has been updated by a nested loop at each displacement increment Δu (Uzawa scheme, see Simo and Taylor, 1991).

The computed load-elongation curves for different computational grids are shown in Figure 5.1, illustrating how mesh convergence is obtained already with the 480-element mesh. In particular, the coefficient of variation (ratio of standard deviation over average) in the peak stress for the 480-, 1120- and 6400-element meshes is below 1.3%. The curves shown

in Figure 5.1 were computed with the general compressible T_{fibril}-λ fibre constitutive equation (3.43), but since the computation enforces incompressibility, the curves are very close also for the incompressible σ_{fibril}-λ fibre constitutive equation (3.49) shown in 3.9. Figure 5.2 shows the deformed configuration post-localisation for the 6400-element mesh. As shown in Figure 5.1, when exceeding localisation, the stress does not drop completely, but recovers at about two thirds of the maximum. This can be explained by the rotation of still intact collagen fibres in the localised elements towards the loading direction: these intact fibres contribute to supporting the tissue.

The behaviour illustrated in Figure 5.1 is consistent with published experimental data. Eliasson et al. (2013) tested rat Achilles tendons and reported a representative load-displacement curve (which, up to multiplicative constants, is equivalent to a plot of the first Piola-Kirchhoff stress versus the stretch) in their Figure 2. Given the difference in tendon size (rat versus human), we did not attempt to fit our model to their curve. Nonetheless, the behaviour of the curve is remarkably similar. Eliasson et al. (2013) applied a small preload to their sample, as it can be seen from the non-zero load at zero displacement, and thus they have a shorter toe region. However, the J-shape of the curve, the peak, the subsequent drop due to damage and the residual load bearing found by Eliasson et al. (2013) are represented faithfully by our model (Figure 5.1). The failure values of the first Piola-Kirchhoff stresses and stretches that we obtained are quite close to those obtained experimentally by Wren et al. (2001) in their tests on human Achilles tendons, although we have only roughly attempted to fit their results, by calibrating the stiffness k of the collagen fibrils in the constitutive equation (3.35).

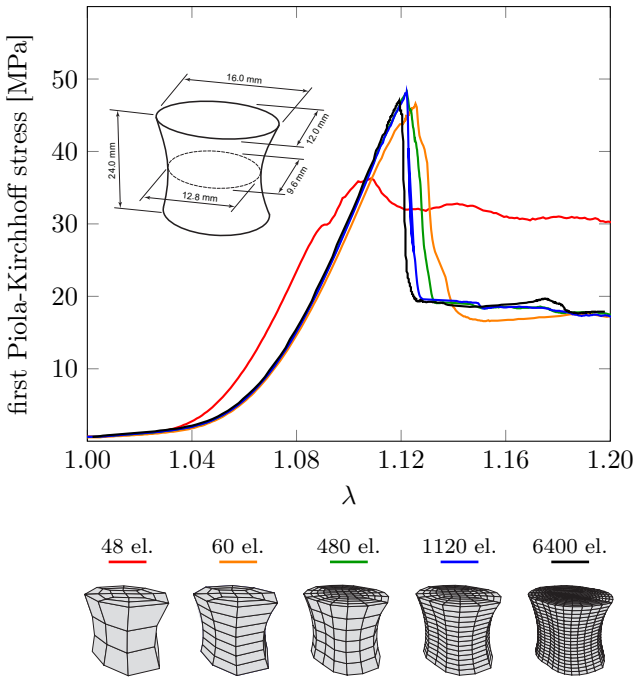

Figure 5.1: Effect of the mesh refinement on the diagram of the first Piola-Kirchhoff stress (evaluated at the narrowest cross-section) versus stretch for the simulated tensile test on an Achilles tendon. The plot shows the average first Piola-Kirchhoff stress, evaluated as total force over undeformed minimal cross-sectional area.

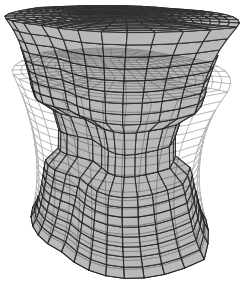

Figure 5.2: Formation of the localisation when exceeding the peak load for the 6400-element mesh. The material parameter L_{loc} determines the width of the localisation zone, in order to ensure mesh-independent results.

Chapter 6

Uniformity Theory and Growth-Remodelling

In this chapter we discuss the material evolution theory from the perspective of the theory of *material uniformity*, as introduced by Noll (1967) and extensively studied by Epstein and Elzanowski (2007). We introduce the balance laws for a uniform simple material, within the framework of Epstein and Maugin (2000), and then we build a constitutive structural model for the remodelling of a fibre-reinforced composite material, which can be used to represent the arterial wall tissue.

Given the extreme complexity of living matter and of the mathematics that is necessary to model it, it is not surprising that the physical and continuum mechanical treatment of growth and remodelling is still in the development stage. Broadly speaking, growth and remodelling can be studied as *anelastic phenomena*. Anelastic processes, the most "classical" example of which is probably plasticity, are accompanied by a change in microstructure, resulting in *configurational forces* and residual stresses (e.g., Hoger, 1997; Gurtin, 2000). Phenomena such as plasticity occur at constant mass, while biological tissues not only experience a change in microstructure, but also an increase (growth) or decrease (resorption) of mass. In addition, living matter can adapt to its environment, which is in many cases in contrast with the classical postulation of the second law of thermodynamics (Cowin and Hegedus, 1976; Epstein and Maugin, 2000).

This study is mainly based on the theoretical framework of Epstein and Maugin (1990), Epstein and Maugin (2000) and Epstein and Elzanowski (2007) and the numerical example presented in Grillo et al. (2015). In the next sections, we discuss the theoretical framework that our study lies upon.

6.1 Balance Laws for Growing Bodies

In this section we briefly discuss the balance laws for a growing body, in the framework introduced by Epstein and Maugin (2000) and Epstein and Elzanowski (2007) and in our notation.

The integral form of the equation of balance of mass reads

$$\partial_t \int_{\mathcal{R}} \rho_R = \int_{\mathcal{R}} \Pi + \int_{\partial\mathcal{R}} \boldsymbol{M}\boldsymbol{N}, \tag{6.1}$$

where ρ_R represents referential mass density, Π is the mass source density per unit referential volume and $\boldsymbol{M}$ is the mass flux density per unit referential area and $\mathcal{R}$ is an arbitrary closed region in the reference. The local form of the balance of mass is expressed as

$$\dot{\rho}_R = \Pi + \operatorname{Div} \boldsymbol{M} \tag{6.2}$$

Rigorously speaking, the balance of linear momentum should deal with *covector* quantities. However, since we have adopted the convention according to which the Cauchy stress and the first Piola-Kirchhoff stress are "contravariant", i.e., have components σ^{ab} and $T^{aB} = J\,\sigma^{ab}\,(\boldsymbol{F}^{-1})^B{}_b$, we have to also treat forces as vectors, and we shall actually write the balance of what, in Newton's words, is called *quantitas motus*, i.e., the product of the mass by the velocity, whose spatial density is $\rho\,\boldsymbol{v}$ and whose material density is $\rho_R\,\dot{\chi}$ (where $\dot{\chi}$ is the Lagrangian velocity, such that $\boldsymbol{v}(x,t) = \dot{\chi}(X,t)$). We allow ourselves an abuse of terminology, and we continue to speak of *linear momentum*. Thus, we write

$$\partial_t \int_{\mathcal{R}} \rho_R\,\dot{\chi} = \int_{\mathcal{R}} [\boldsymbol{f} + \Pi\,\dot{\chi} + \boldsymbol{z}] + \int_{\partial\mathcal{R}} [\boldsymbol{T} + \dot{\chi} \otimes \boldsymbol{M} + \boldsymbol{K}]\,\boldsymbol{N}, \tag{6.3}$$

where $\boldsymbol{f}$ is body force per unit referential volume, $\Pi\,\dot{\chi}$ is the rate of momentum brought about by the volumetric growth, $\boldsymbol{z}$ represents *irreverisble* momentum rate, $\dot{\chi} \otimes \boldsymbol{M}$ is the momentum flux associated with the mass flux and $\boldsymbol{K}$ is the *irreverisble* momentum flux. It should be noted that the *ireversible* momentum rate $\boldsymbol{z}(X,t)$ and momentum flux $\boldsymbol{K}(X,t)$ represent the momentum of growing mass that enter region $\mathcal{R}$ at point X with a velocity

different from the velocity $\dot{\chi}(X,t)$ of the continuum at X (for more details, see Epstein and Elzanowski, 2007). The localised balance of momentum is

$$\partial_t(\rho_R\,\dot{\chi}) = \boldsymbol{f} + \Pi\,\dot{\chi} + \boldsymbol{z} + \mathrm{Div}(\boldsymbol{T} + \dot{\chi}\otimes\boldsymbol{M} + \boldsymbol{K}). \tag{6.4}$$

Denoting the Lagrangian position vector by $\boldsymbol{r}(X,t) \equiv \chi(X,t) - X_O$, where X_O is the point with respect to which moments are evaluated, the balance of angular momentum reads

$$\partial_t \int_{\mathcal{R}} \boldsymbol{r}\times(\rho_R\,\dot{\chi}) = \int_{\mathcal{R}} \boldsymbol{r}\times[\boldsymbol{f} + \Pi\,\dot{\chi} + \boldsymbol{z}] + \int_{\partial\mathcal{R}} \boldsymbol{r}\times\Big[[\boldsymbol{T} + \dot{\chi}\otimes\boldsymbol{M} + \boldsymbol{K}]\,\boldsymbol{N}\Big], \tag{6.5}$$

Localising, and using the balance of mass and the balance of linear momentum, we obtain the symmetry of the modified stress $\tilde{\boldsymbol{T}} = \boldsymbol{T} + \dot{\chi}\otimes\boldsymbol{M} + \boldsymbol{K}$, i.e.,

$$\tilde{\boldsymbol{T}}\,\boldsymbol{F}^T = \boldsymbol{F}\,\tilde{\boldsymbol{T}}^T. \tag{6.6}$$

The integral form of the balance of energy is

$$\begin{aligned}\partial_t \int_{\mathcal{R}} (\tfrac{1}{2}\,\rho_R\,\dot{\chi}\,.\,\dot{\chi} + \rho_R\,\mathcal{E}) = \int_{\mathcal{R}} (\tfrac{1}{2}\,\Pi\,\dot{\chi}\,.\,\dot{\chi} + \Pi\,\mathcal{E} + \boldsymbol{f}\,.\,\dot{\chi} + \mathcal{H} + \mathcal{U} + \boldsymbol{z}\,.\dot{\chi}) \\ + \int_{\partial\mathcal{R}} [\dot{\chi}\,.\,(\boldsymbol{T}+\boldsymbol{K}) + (\mathcal{E} + \tfrac{1}{2}\,\dot{\chi}\,.\,\dot{\chi})\boldsymbol{M} + \boldsymbol{Q}]\boldsymbol{N},\end{aligned} \tag{6.7}$$

where the internal energy per unit mass is denoted by $\mathcal{E}$, the rate of non-mechanical energy supply per unit mass is denoted by $\mathcal{H}$, the non-compliant rate of volumetric internal energy is denoted by $\mathcal{U}$ and $\boldsymbol{Q} = J\,\boldsymbol{q}\circ(\chi,\tau)\,\boldsymbol{F}^{-T}$ denotes the material heat flux. The local form of Equation (6.7) takes the form

$$\begin{aligned}\partial_t \left(\tfrac{1}{2}\rho_R\,\dot{\chi}\,.\,\dot{\chi} + \rho_R\,\mathcal{E}\right) = \tfrac{1}{2}\,\Pi\,\dot{\chi}\,.\,\dot{\chi} + \Pi\,\mathcal{E} + \boldsymbol{f}\,.\,\dot{\chi} + \mathcal{H} + \mathcal{U} + \boldsymbol{z}.\dot{\chi} + \\ + \mathrm{Div}\Big[\dot{\chi}\,.\,(\boldsymbol{T}+\boldsymbol{K}) + (\mathcal{E} + \tfrac{1}{2}\,\dot{\chi}\,.\,\dot{\chi})\boldsymbol{M} + \boldsymbol{Q}\Big].\end{aligned} \tag{6.8}$$

Finally, we need to consider, as a *unilateral constraint*, the Clausius-Duhem inequality, stating the integral form of the Second Principle of Thermodynamics, i.e.,

$$\partial_t \int_{\mathcal{R}} \rho_R\,\mathcal{S} \geq \int_{\mathcal{R}} \left[\Pi\,\mathcal{S} + \frac{(\mathcal{H}+\mathcal{U}+\mathcal{Z})}{\Theta}\right] + \int_{\partial\mathcal{R}} \left[\frac{\boldsymbol{Q}}{\Theta} + \mathcal{S}\,\boldsymbol{M}\right]\boldsymbol{N}, \tag{6.9}$$

where $\mathcal{S}$ represents the entropy per unit referential mass, Θ is the absolute temperature and $\mathcal{Z}$ is the volumetric source of non-compliant entropy. Its localised counterpart can be expressed as:

$$\Theta\,\partial_t(\rho_R\,\mathcal{S}) \geq \Pi\,\Theta\,\mathcal{S} + \mathcal{H} + \mathcal{U} + \mathcal{Z} - \left(\frac{1}{\Theta}\mathrm{Grad}\,\Theta\right)\boldsymbol{Q} + \mathrm{Div}\,\boldsymbol{Q} + \Theta\,(\mathrm{Grad}\,\mathcal{S})\boldsymbol{M} + \Theta\,\mathcal{S}\,\mathrm{Div}\,\boldsymbol{M}. \tag{6.10}$$

Now, by using the mass balance (6.2) and the energy balance (6.8), we obtain

$$\rho_R\Theta\,\dot{\mathcal{S}} \geq \rho_R\,\dot{\mathcal{E}} - [\boldsymbol{g}\,(\boldsymbol{T}+\boldsymbol{K})] : \dot{\boldsymbol{F}} + \mathcal{Z} - \left(\frac{1}{\Theta}\mathrm{Grad}\,\Theta\right)\boldsymbol{Q} - (\mathrm{Grad}\,\mathcal{E} - \Theta\,\mathrm{Grad}\,\mathcal{S})\,\boldsymbol{M}. \tag{6.11}$$

It is customary to write the entropy inequality in terms of the Helmholtz free energy per unit mass, defined by

$$A = \mathcal{E} - \Theta\,\mathcal{S}. \tag{6.12}$$

Noting that its time derivative of which is

$$\dot{A} = \dot{\mathcal{E}} - \dot{\Theta}\,\mathcal{S} - \Theta\,\dot{\mathcal{S}}, \tag{6.13}$$

and substituting into Equation (6.11) the entropy inequality the form

$$-\rho_R\dot{A} - \rho_R\mathcal{S}\,\dot{\Theta} - \mathcal{Z} + [\boldsymbol{g}\,(\boldsymbol{T}+\boldsymbol{K})] : \dot{\boldsymbol{F}} + \left(\frac{1}{\Theta}\mathrm{Grad}\,\Theta\right)\boldsymbol{Q} + (\mathrm{Grad}\,\mathcal{E} - \Theta\mathrm{Grad}\,\mathcal{S})\boldsymbol{M} \geq 0. \tag{6.14}$$

For simplicity, we shall assume to have zero mass flux, i.e., $\boldsymbol{M} = \boldsymbol{0}$, and zero non-compliant terms, i.e., $\boldsymbol{z} = \boldsymbol{0}$, $\boldsymbol{K} = \boldsymbol{0}$, $\mathcal{U} = 0$ and $\mathcal{Z} = 0$. Thus, the balance equations and the entropy inequality reduce to

$$\dot{\rho}_R = \Pi, \tag{6.15a}$$

$$\rho_R\,\boldsymbol{g}\,\ddot{\phi} = \boldsymbol{f} + \mathrm{Div}\,\boldsymbol{T}, \tag{6.15b}$$

$$\boldsymbol{T}\,\boldsymbol{F}^T = \boldsymbol{F}\,\boldsymbol{T}^T, \tag{6.15c}$$

$$\rho_R\,\dot{\mathcal{E}} = (\boldsymbol{g}\,\boldsymbol{T}) : \dot{\boldsymbol{F}} + \mathcal{H} + \mathrm{Div}\,\boldsymbol{Q}, \tag{6.15d}$$

$$0 \leq -\rho_R\dot{A} - \rho_R\mathcal{S}\,\dot{\Theta} + (\boldsymbol{g}\,\boldsymbol{T}) : \dot{\boldsymbol{F}} + \left(\frac{1}{\Theta}\mathrm{Grad}\,\Theta\right)\boldsymbol{Q}. \tag{6.15e}$$

These are identical to the standard equations in the absence of growth, except for the volumetric source of mass Π in the right-hand side of the balance of mass. Note that the balance of angular momentum reduces to the standard one (with the symmetry of the standard Kirchhoff stress $\boldsymbol{\tau} = \boldsymbol{T}\boldsymbol{F}^T$, with components $\tau^{ab} = T^{aB}\, F^b{}_B$), since the Piola-like stress $\tilde{\boldsymbol{T}}$ reduces to the standard first Piola-Kirchhoff stress $\boldsymbol{T}$.

6.2 Uniformity Theory for First Grade Materials

As mentioned above, growth and remodelling can be studies as anelastic phenomena, which in turn can be tackled by means of a variety of approaches. The approach that we follow here is based on the *theory of uniformity*, originally introduced by Noll (1967), in the formulation of Epstein and Maugin (1990). Below, we briefly discuss the history of this mathematical framework of material uniformity and then provide the basic definitions.

The notion of simple material is introduced by Noll (1958), using the principles of material objectivity and determinism of stress. Later, Noll (1967) introduced the concept of *material uniformity*, defined as an isomorphism between the tangent spaces of material points. Noll (1967) distinguished the material uniformity from the material homogeneity explicitly. The postulated notion of uniformity enables us to construct uniform materials with inhomogeneities which leads to the theory of continuous distribution of dislocations in continuum bodies. The theory of continuous dislocations is studied in the pioneering work of Wang (1967) and Wang and Bloom (1974), even though the idea had been introduced before by other scholars (Bilby et al., 1955; Kondo, 1958). Wang (1967) postulated the theory without admitting a global parallelism, as previously assumed by Noll (1967).

The theory of material uniformity concerns with one simple, yet not so trivial question. Considering, two points X_1 and X_2 in the body $\mathcal{B}$, we want to know if they are made of the *same* material. If we look at the microscopic structures, surrounding two materially uniform points, we might not see similar pictures, as one might have been distorted or rotated,

in a different manner, thus we need to distort the pictures accordingly to achieve identical pictures. In other words, the notion of uniformity in this context is somehow indifferent with respect to the affine transformation of two arbitrary material points. From the mathematical point of view, one can establish a *material isomorphism* as follows. Suppose to have an elastic material with elastic potential $W(X,t) = \hat{W}(\boldsymbol{F}(X,t), X)$ depending explicitly on the point and let two material points, X_1 and X_2, be *materially isomorphic*. Then there exists a non-singular linear map $\boldsymbol{P}_{12}(t) : T_{X_1}\mathcal{B} \to T_{X_2}\mathcal{B}$ such that, for any admissible deformation $\boldsymbol{F}$, we have:

$$\hat{W}(\boldsymbol{F}(X_1,t)\boldsymbol{P}_{12}(t), X_1, t) = \hat{W}(\boldsymbol{F}(X_2,t), X_2, t). \tag{6.16}$$

It is of fundamental importance to note that the material isomorphism is an *equivalence relation*, since it is *symmetric*, *reflexive* and *transitive* (Epstein and Elzanowski, 2007). Thus, one can can define an archetypical vector space $\mathcal{A} \equiv \mathbb{R}^3$, called precisely the *archetype*, and a tensor field $\boldsymbol{P}(\,\cdot\,, t)$ such that $\boldsymbol{P}(X,t) : \mathcal{A} \to T_X\mathcal{B}$ is an isomorphism. The tensor field $\boldsymbol{P}(\,\cdot\,, t)$ is called the *uniformity field*, and the isomorphism $\boldsymbol{P}_{12}(t)$ of Equation (6.16) is obtained as

$$\boldsymbol{P}_{12}(t) = \boldsymbol{P}(X_2,t)\,\boldsymbol{P}^{-1}(X_1,t), \tag{6.17}$$

and the elastic potential can be written

$$W(X,t) = \hat{W}(\boldsymbol{F}(X,t), X, t) = J_{\boldsymbol{P}}^{-1}\,\check{W}(\boldsymbol{F}(X,t)\boldsymbol{P}(X,t)), \tag{6.18}$$

where $\check{W}$ is the elastic potential in the archetype, and $J_{\boldsymbol{P}}^{-1}$ comes from the theorem of the change of variables (Epstein and Maugin, 1990). The concept is illustrated in Figure 6.1.

For later use, we find the relation between the uniformity field $\boldsymbol{P}$ and the mass source Π featuring in the simplified balance of mass (6.15a), for the case of a growing uniform body. Because of the uniformity, there is a value $\rho_{\mathcal{A}}$ of the mass density, called *archetypal mass density*, such that

$$\rho_{\mathcal{A}} = J_{\boldsymbol{P}}\,\rho_R. \tag{6.19}$$

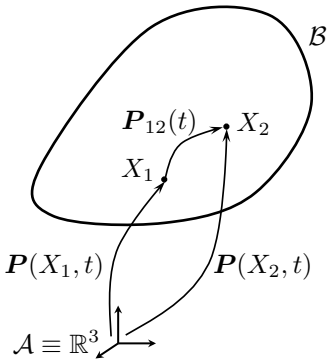

Figure 6.1: The uniformity field and its relation to the material isomorphism between two points X_1 and X_2.

Since $\rho_{\mathcal{A}}$ is a constant and the simplified balance of mass (6.15a) gives $\dot{\rho}_R = \Pi$, if we differentiate Equation (6.19) with respect to time, we obtain

$$0 = \dot{J}_{\boldsymbol{P}}\, \rho_R + J_{\boldsymbol{P}}\, \dot{\rho}_R = J_{\boldsymbol{P}}\, \boldsymbol{P}^{-T} : \dot{\boldsymbol{P}} + J_{\boldsymbol{P}}\, \Pi, \tag{6.20}$$

from which

$$\dot{\rho}_R = \Pi = -\boldsymbol{P}^{-T} : \dot{\boldsymbol{P}}, \tag{6.21}$$

If we define, by analogy with the velocity gradient $\boldsymbol{l} = \dot{\boldsymbol{F}}\boldsymbol{F}^{-1}$, the *inhomogeneity deformation rate* as

$$\boldsymbol{L}_{\boldsymbol{P}} = \dot{\boldsymbol{P}}\boldsymbol{P}^{-1}, \tag{6.22}$$

we have that $\boldsymbol{P}^{-T} : \dot{\boldsymbol{P}} = \operatorname{Tr}(\dot{\boldsymbol{P}}\boldsymbol{P}^{-1}) = \operatorname{Tr}(\boldsymbol{L}_{\boldsymbol{P}})$ and, therefore

$$\dot{\rho}_R = \Pi = -\operatorname{Tr}(\boldsymbol{L}_{\boldsymbol{P}}), \tag{6.23}$$

We can also define the $\boldsymbol{P}$-pull-back of $\boldsymbol{L}_{\boldsymbol{P}}$ as

$$\boldsymbol{\Lambda}_{\boldsymbol{P}} = \boldsymbol{P}^{-1}\boldsymbol{L}_{\boldsymbol{P}}\,\boldsymbol{P} = \boldsymbol{P}^{-1}\dot{\boldsymbol{P}}, \tag{6.24}$$

and, by virtue of the properties of the trace, Equation (6.23) has the alternative form

$$\dot{\rho}_R = \Pi = -\operatorname{Tr}(\boldsymbol{\Lambda}_{\boldsymbol{P}}). \tag{6.25}$$

6.3 The General Recruitment Model

In the first part of this thesis (Chapters 3, 4 and 5), we proposed a framework for recruitment and damage of collagen fibrils within a collagen fibre. Here, we are interested in exploring the recruitment of a whole fibre from the point of view of the theory of uniformity.

Before getting to *fibre recruitment*, let us start by writing the elastic potential for a general *fibril recruitment* model as

$$\hat{W}(\boldsymbol{F}(X), X) \;=\; \int_{\mathbb{R}^+} \int_{\mathbb{S}^2_X \mathcal{B}} \hat{W}_{fib}(\boldsymbol{F}(X), \lambda_s(\boldsymbol{M}(X)), \boldsymbol{M}(X))\; \mathfrak{R}(\lambda_s(\boldsymbol{M}(X)), \boldsymbol{M}(X)), \quad (6.26)$$

where the function $\mathfrak{R}(\lambda_s(\boldsymbol{M}), \boldsymbol{M})$ is the density orientation function that basically gives the population of the fibril with straightening stretch of λ_s along $\boldsymbol{M}$ direction. This function has the two important properties

$$\int_{\mathbb{R}^+} \int_{\mathbb{S}^2_X \mathcal{B}} \mathfrak{R}(\lambda_s(\boldsymbol{M}), \boldsymbol{M}) = 1, \quad (6.27)$$

$$\mathfrak{R}(\lambda_s(\boldsymbol{M}), \boldsymbol{M}) = \mathfrak{R}(\lambda_s(-\boldsymbol{M}), -\boldsymbol{M}). \quad (6.28)$$

If we assume that the waviness of the fibrils does not depend on the direction, we can multiplicatively decompose $\mathfrak{R}(\lambda_s(\boldsymbol{M}), \boldsymbol{M})$ as

$$\mathfrak{R}(\lambda_s(\boldsymbol{M}), \boldsymbol{M}) = \mathfrak{n}_s(\lambda_s)\; \Psi(\boldsymbol{M}), \quad (6.29)$$

where $\mathfrak{n}_s(\lambda_s)$ and $\Psi(\boldsymbol{M})$ have the properties

$$\int_{\mathbb{S}^2 \mathcal{B}} \Psi(\boldsymbol{M})\, \mathrm{d}S = 1, \quad \Psi(\boldsymbol{M}) = \Psi(-\boldsymbol{M}), \quad (6.30)$$

$$\int_{\mathbb{R}^+} \mathfrak{n}_s(\lambda_s)\, \mathrm{d}\lambda_s = 1. \quad (6.31)$$

In this case, the elastic potential becomes

$$\hat{W}(\boldsymbol{F}(X), X) = \int_{\mathbb{R}^+} \int_{\mathbb{S}^2_X \mathcal{B}} \hat{W}_{fib}(\boldsymbol{F}(X), \lambda_s(X), \boldsymbol{M}(X))\; \Psi(\boldsymbol{M}(X))\; \mathfrak{n}_s(\lambda_s(X))\, \mathrm{d}\lambda_s. \quad (6.32)$$

Since in this part of the thesis we focus on remodelling and material evolution, we assume, for simplicity, that the recruitment density $\mathfrak{n}_s$ converges to a Dirac delta in the sense of

distributions (Kolmogorov and Fomin, 1999). In other words, *all* fibrils in a fibre are recruited at the *same* straightening stretch λ_s: therefore, we are dealing with a model of recruitment for *whole fibres* rather than for single fibrils.

6.4 Material Implant for a Single Fibre

The constitutive law for a single fibre is postulated with respect to the elastic deformation, $\boldsymbol{F}_e$, which arises from the decomposition of the overall deformation gradient $\boldsymbol{F}$:

$$\boldsymbol{F} = \boldsymbol{F}_e \boldsymbol{F}_s, \qquad F^i{}_I = (\boldsymbol{F}_e)^i{}_\alpha \, (\boldsymbol{F}_s)^\alpha{}_I. \tag{6.33}$$

In this framework, we can consider the inverse $\boldsymbol{F}_s^{-1}$ of the stretching deformation as the material implant acting on $\boldsymbol{F}$, and construct the elastic deformation $\boldsymbol{F}_e$ as

$$\boldsymbol{F}_e = \boldsymbol{F} \, (\boldsymbol{F}_s)^{-1}, \qquad (\boldsymbol{F}_e)^i{}_\alpha = \boldsymbol{F}^i{}_I (\boldsymbol{F}_s^{-1})^I{}_\alpha. \tag{6.34}$$

As we can see from (6.34), $\boldsymbol{F}_s^{-1}$ plays in fact the same role of the material implant $\boldsymbol{P}$, *without* the need to postulate an "intermediate configuration". Hence, from this point forward, we follow Epstein and Elzanowski (2007) and we identify $\boldsymbol{F}_s^{-1}$ with the material implant $\boldsymbol{P}$, i.e.,

$$\boldsymbol{F}_s^{-1} \equiv \boldsymbol{P}, \quad (\boldsymbol{F}_s^{-1})^I{}_\alpha = P^I{}_\alpha. \tag{6.35}$$

It is noteworthy to examine the physical meaning of this particular material implant. The generic fibre is straight with no undulation in the archetype, and the implant $\boldsymbol{P}(X,t)$ rotates the fibre, crimps it and maps it into the tangent space at X. The implant map can be decomposed into a pure rotation and a pure stretch via the polar decomposition theorem, as

$$\hat{\boldsymbol{P}}(\boldsymbol{M}, \lambda_s) = \hat{\boldsymbol{R}}(\boldsymbol{M}) \, \hat{\boldsymbol{U}}(\lambda_s), \quad P^A{}_\alpha = R^A{}_\beta \, U^\beta{}_\alpha. \tag{6.36}$$

First, we define the straightened archetypical fibre in $\mathcal{A} \equiv \mathbb{R}^3$ as

$$\boldsymbol{\mu} = \mu^\alpha \boldsymbol{a}_\alpha. \tag{6.37}$$

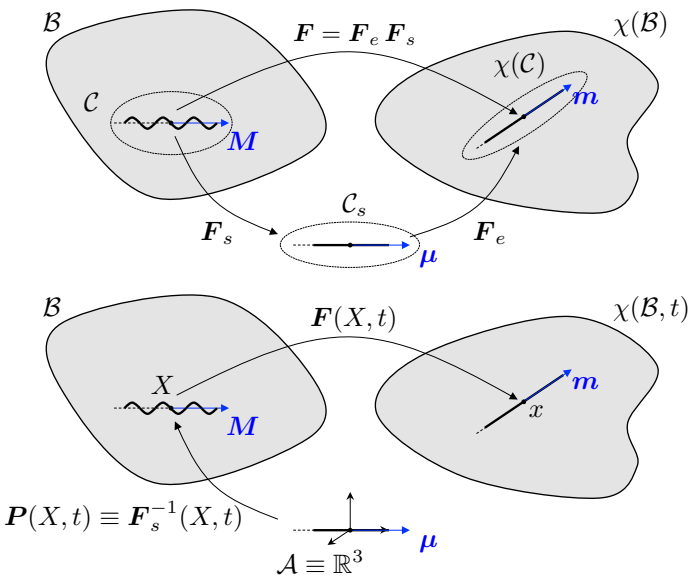

Figure 6.2: Top: Customary view in terms of an intermediate configuration, as seen in Chapters 3, 4 and 5. Bottom: View in terms of the theory of uniformity, with the straightened fibre in the archetype (note that time dependence is considered in this case).

Then, we introduce the pure-stretch part $U^{\beta}{}_{\alpha}$ of the implant $P^{A}{}_{\alpha}$, which in this case is the crimping, as

$$U^{\beta}{}_{\alpha}(X) = (\lambda_s^{-1} - 1)\mu^{\beta}\mu_{\alpha} + \delta^{\beta}{}_{\alpha}, \tag{6.38}$$

where $\mu_{\alpha} = \mathfrak{g}_{\alpha\gamma}\,\mu^{\gamma}$ are the components of the covector $\boldsymbol{\mu}^{\flat}$ associated with $\boldsymbol{\mu}$. To rigorously present the rotation part, we need a little more work.

Let $\mathfrak{g}$ be a metric tensor in the archetype $\mathcal{A} \equiv \mathbb{R}^3$ and $\{\boldsymbol{a}_{\alpha}\}_{\alpha=1}^{3}$ an orthonormal basis in $\mathcal{A}$. Since the body $\mathcal{B}$ is a *trivial* manifold, embedded in the affine space $\mathcal{S} \equiv \mathbb{E}^3$, we have the luxury of having Cartesian coordinates $\{Z^{\alpha}\}$, with associated basis $\{\boldsymbol{I}_{\alpha}\}_{\alpha=1}^{3} \equiv \{\boldsymbol{a}_{\alpha}\}_{\alpha=1}^{3}$ at every tangent space $T_X\mathcal{B}$. In other words, we choose the Cartesian basis in $\mathcal{B}$ such that it coincides with the basis of the archetype $\mathcal{A}$. We also choose a system of curvilinear coordinates $\{X^{A}\}$ in the body $\mathcal{B}$, with associated basis $\{\boldsymbol{E}_{A}\}_{A=1}^{3}$. Note that we are following almost exactly the same notation for Cartesian and curvilinear coordinates used in the book by Marsden and Hughes (1983), except that we use Greek indices for the Cartesian coordinates, since we are making the Cartesian basis vectors coincide with the basis vectors

of the archetype. The change of basis and the transformation rule for vectors are

$$\boldsymbol{E}_A = \frac{\partial Z^\alpha}{\partial X^A}\,\boldsymbol{I}_\alpha, \qquad W^A = \frac{\partial X^A}{\partial Z^\alpha}\,W^\alpha. \tag{6.39}$$

Now we are ready can introduce the pure-rotation part $R^A{}_\beta$ of the implant $P^A{}_\alpha$. The role of the rotation here is simply to rotate the archetypal fibre direction $\boldsymbol{\mu}$ to the direction $\boldsymbol{M}$ of the fibre embedded in the body at point X. We first seek for the rotation matrix $Q^\gamma{}_\beta$ that performs the rotation in Cartesian coordinates. In general, the rotation between two arbitrary unit vectors $\boldsymbol{\mu}$ and $\boldsymbol{M}$ can be uniquely determined by rotation about a unit vector $\boldsymbol{\omega}$, which obtained from the normalisation of the cross-product of the two unit vectors. The angle of rotation θ can be obtained from the scalar product of the two unit vectors. Thus, in Cartesian coordinates

$$\boldsymbol{\omega} = \frac{\boldsymbol{\mu}\times\boldsymbol{M}}{||\boldsymbol{\mu}\times\boldsymbol{M}||}, \qquad \omega^\gamma = \epsilon^\gamma{}_{\alpha\beta}\mu^\alpha M^\beta/||\boldsymbol{\mu}\times\boldsymbol{M}||, \tag{6.40a}$$

$$\theta = \arccos\boldsymbol{\mu}.\boldsymbol{M}, \qquad \theta = \arccos(\mu^\alpha \mathfrak{g}_{\alpha\beta} M^\beta). \tag{6.40b}$$

Then the rotation matrix $[Q]$ can be obtained by exponentiating the skew-symmetric matrix $[\Omega]$ associated with the vector $\boldsymbol{\omega}$, i.e.,

$$[Q] = e^{[\Omega]\theta}, \qquad \Omega^\alpha{}_\gamma = \epsilon^\alpha{}_{\beta\gamma}\omega^\beta, \tag{6.41}$$

which can be convenient expressed by Rodriguez' formula (Koks, 2006), as

$$[Q] = [I] + (\sin\theta)\,[\Omega] + (1-\cos\theta)\,[\Omega]^2, \tag{6.42a}$$

$$Q^\alpha{}_\gamma = \delta^\alpha{}_\gamma + (\sin\theta)\,\Omega^\alpha{}_\gamma + (1-\cos\theta)\,\Omega^\alpha{}_\beta\,\Omega^\beta{}_\gamma. \tag{6.42b}$$

The last step to construct the matrix $[R]$ of the rotation tensor $\boldsymbol{R}$ is to transform the first leg of $[Q]$ to the coordinates $\{X^A\}$, using Equation (6.39), which yields

$$R^A{}_\alpha = \frac{\partial X^A}{\partial Z^\gamma} Q^\gamma{}_\alpha \tag{6.43}$$

Now that we have both tensors $\boldsymbol{R}$ and $\boldsymbol{U}$, we can express our material implant $\boldsymbol{P}$ as

$$P^A{}_\alpha = \frac{\partial X^A}{\partial Z^\gamma} Q^\gamma{}_\beta \left[(\lambda_s^{-1}-1)\mu^\beta\mu_\alpha + \delta^\beta{}_\alpha\right]. \tag{6.44}$$

Since $Q^{\gamma}{}_{\beta}\,\mu^{\beta} = M^{\gamma}$ and $(\partial X^A/\partial Z^{\gamma})\,M^{\gamma} = M^A$, Equation (6.44) can be simplified into

$$P^A{}_{\alpha} = M^A \mu_{\alpha}(\lambda_s^{-1} - 1) + \frac{\partial X^A}{\partial Z^{\gamma}} Q^{\gamma}{}_{\alpha}. \tag{6.45}$$

For an *isochoric* implant $\boldsymbol{P}$, the strecth $\boldsymbol{U}$ must be changed into

$$U^{\beta}{}_{\alpha} = (\lambda_s^{-1} - \lambda_s^{1/2})\mu^{\beta}\mu_{\alpha} + \lambda_s^{1/2}\,\delta^{\beta}{}_{\alpha}, \tag{6.46}$$

so that we have

$$P^A{}_{\alpha} = M^A \mu_{\alpha}(\lambda_s^{-1} - \lambda_s^{1/2}) + \lambda_s^{1/2}\,\frac{\partial X^A}{\partial Z^{\gamma}} Q^{\gamma}{}_{\alpha}. \tag{6.47}$$

6.5 Material Implant for a Distribution of Fibres

We assume that the fibres in our biological tissue have a statistical distribution of orientation. Thus, rather than implanting fibres individually, we can implant a family of statistically oriented fibres as a whole into a material point X. We also assume that the distribution of collagen fibres that is treated as the *archetype* is stress free. As mentioned in Section (2.4), the *ensemble* elastic potential of the fibres (Federico and Herzog, 2008) is

$$\hat{W}_e(\boldsymbol{C}(X,t), X, t) = \int_{\mathbb{S}^2_X \mathcal{B}} \hat{W}_f(\boldsymbol{C}(X,t) : \boldsymbol{N} \otimes \boldsymbol{N}, X, t)\; \Psi(\boldsymbol{N}; X, t), \tag{6.48}$$

where $\boldsymbol{C}(X,t) : \boldsymbol{N} \otimes \boldsymbol{N} = I_4(\boldsymbol{C}(X,t), \boldsymbol{N})$ is the fourth invariant of the right Cauchy-Green deformation in direction $\boldsymbol{N}$, and the probability distribution Ψ depends explicitly on the point and on time. Following the definition (6.18) of material uniformity, the fibre elastic potential $\check{W}$ in the archetype is given by

$$\hat{W}_f(\boldsymbol{C}(X,t) : \boldsymbol{N} \otimes \boldsymbol{N}, X, t) = J_{\boldsymbol{P}}^{-1}(X,t)\; \check{W}_f(\boldsymbol{P}^T(X,t)\boldsymbol{C}(X,t)\boldsymbol{P}(X,t) : \boldsymbol{\nu} \otimes \boldsymbol{\nu}), \tag{6.49}$$

where

$$\boldsymbol{P}^T(X,t)\boldsymbol{C}(X,t)\boldsymbol{P}(X,t) = (\boldsymbol{F}\boldsymbol{P})^T(X,t).(\boldsymbol{F}\boldsymbol{P})(X,t), \tag{6.50}$$

i.e., we have replaced $\boldsymbol{F}$ with $\boldsymbol{FP}$ and multiplied by $J_{\boldsymbol{P}}^{-1}$ to obtain the elastic potential $\hat{W}_f$ from the archetypal one $\check{W}_f$. Note also that we replaced the unit vector $\boldsymbol{N}$ in the body with the unit vector $\boldsymbol{\nu}$ in the archetype.

Now, we can write the ensemble potential as

$$\hat{W}_e(\boldsymbol{C}(X,t),X,t) = J_{\boldsymbol{P}}^{-1}(X,t)\int_{\mathbb{S}^2} \check{W}_f(\check{I}_4(X,t))\,\check{\Psi}(\boldsymbol{\nu}), \tag{6.51}$$

where the simple notation $\mathbb{S}^2$ denotes the unit sphere in the archetype, $\check{\Psi}$ is the archetypal probability distribution and, with a small abuse of notation, we define

$$\check{I}_4(X,t) = \boldsymbol{P}^T(X,t)\boldsymbol{C}(X,t)\boldsymbol{P}(X,t) : \boldsymbol{\nu}\otimes\boldsymbol{\nu}. \tag{6.52}$$

Now the second Piola-Kirchhoff stress can be obtained as (we drop the arguments (X,t) for the sake of a lighter notation)

$$\boldsymbol{S}_e = J_{\boldsymbol{P}}^{-1}\int_{\mathbb{S}^2} 2\,\frac{\partial\check{W}_f}{\partial\check{I}_4}\,\frac{\partial\check{I}_4}{\partial\boldsymbol{C}}\,\check{\Psi}(\boldsymbol{\nu})\,\mathrm{d}S. \tag{6.53}$$

Following (Federico, 2012) we obtain the deviatoric part of the stress as

$$\boldsymbol{S}_{ed} = J_{\boldsymbol{P}}^{-1}\int_{\mathbb{S}^2} 2\,\frac{\partial\check{W}_f}{\partial\check{I}_4}\left[J^{-2/3}\mathbb{M}^* : \frac{\partial\check{I}_4}{\partial\boldsymbol{C}}\right]\check{\Psi}(\boldsymbol{\nu})\,\mathrm{d}S, \tag{6.54}$$

in which, for an arbitrary second-order contravariant tensor $\boldsymbol{A}$, we have

$$J^{-2/3}\mathbb{M}^* : \boldsymbol{A} = \boldsymbol{A} - \frac{1}{3}\mathrm{Tr}^*(\boldsymbol{A})\,\boldsymbol{B} = \boldsymbol{A} - \frac{1}{3}(\boldsymbol{C} : \boldsymbol{A})\,\boldsymbol{B}. \tag{6.55}$$

6.6 Admissible Evolution Laws

The most significant application of implant can be found in the theory of evolution, while the implant $\boldsymbol{P}(X,t)$ changes with time. This perspective of evolution is intuitive in a sense that the material is made of archetype the is deformed and patched to every material point X, so its evolution must occur in the implant. It should be noted that in this context evolution is seen as a differential equation which should be solved *real time* simultaneously with all the

other field and constitutive equations. The evolution differential equation simply provides us with the implant $\boldsymbol{P}$ at each material point X, at any time t. It is noteworthy that the postulation of evolution in the form differential equation, goes back to classical Newtonian mechanics, where time derivative of momentum is given in the form of differential equation. That being said, we can postulate the evolution of material implant as

$$\dot{\boldsymbol{P}}(X,t) = \mathcal{F}(\boldsymbol{P}(X,t), \mathfrak{A}(X,t), X), \tag{6.56}$$

where $\mathcal{F}$ is a tensorial function and $\mathfrak{A}$ is the collection of all other arguments such as Eshelby stress $\mathfrak{E} = W\,\boldsymbol{I}^T - \boldsymbol{F}.\boldsymbol{T}$ or Mandel stress $\mathfrak{M} = \boldsymbol{F}.\boldsymbol{T}$. It is noteworthy that the tensorial function $\mathcal{F}$ does not depend on time explicitly and $\mathcal{F}$ is in a certain sense autonomous. Although this framework is very general, there are some restrictions that are essential for the appropriate choice of evolution law. The first rule regarding the evolution law is, the law of evolution should be invariant with respect to the change of reference configuration, which is called *reduced to the archetype*, in this study Epstein and Elzanowski (2007). Let us define a change of reference configuration $\zeta : \mathcal{B} \to \tilde{\mathcal{B}}$, with tangent map $T\zeta = \boldsymbol{D}$, with components $D^A{}_B = \zeta^A{}_{,B}$. The change of reference configuration for the postulated evolution law reads

$$\dot{\tilde{\boldsymbol{P}}} = \tilde{\mathcal{F}}(\tilde{\boldsymbol{P}}, \tilde{\mathfrak{A}}, \zeta) \tag{6.57}$$

$$\tilde{\boldsymbol{P}} = \boldsymbol{D}\boldsymbol{P}, \tag{6.58}$$

$$\dot{\tilde{\boldsymbol{P}}} = \boldsymbol{D}\dot{\boldsymbol{P}}, \tag{6.59}$$

where, for the case of a "mixed" tensor, such as the Eshelby or Mandel stress, the backward Piola transform $\tilde{\mathfrak{A}}$ is given by

$$\tilde{\mathfrak{A}} = \zeta^* \mathfrak{A} = J_{\boldsymbol{D}}^{-1} \boldsymbol{D}^{-T}\, \mathfrak{A}\, \boldsymbol{D}^T. \tag{6.60}$$

Using Equation (6.57) and (6.60), we have:

$$\dot{\boldsymbol{P}} = \boldsymbol{D}^{-1}\, \tilde{\mathcal{F}}(\boldsymbol{D}\,\boldsymbol{P}, J_{\boldsymbol{D}}^{-1} \boldsymbol{D}^{-T}\, \mathfrak{A}\, \boldsymbol{D}^T, \zeta) \tag{6.61}$$

Now, since the choice of reference is arbitrary, we consider

$$\boldsymbol{D}\boldsymbol{P} = \tilde{\boldsymbol{P}} \equiv \tilde{\boldsymbol{\Upsilon}}, \tag{6.62}$$

where $\tilde{\boldsymbol{\Upsilon}} : \mathcal{A} \to \tilde{\mathcal{B}}$ is the *shifter* from the archetype the reference configuration $\tilde{\mathcal{B}}$ (similarly, $\boldsymbol{\Upsilon} : \mathcal{A} \to \mathcal{B}$ is the shifter from the archetype to the reference configuration $\mathcal{B}$). The situation is illustrated in Figure 6.3.

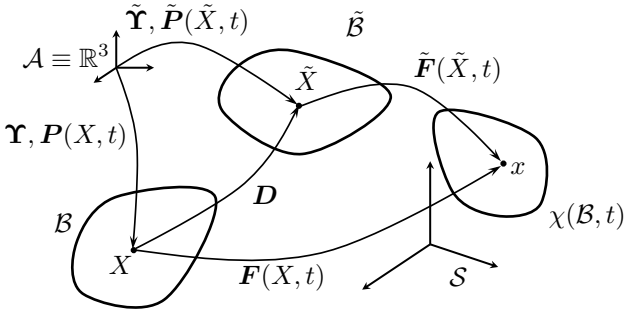

Figure 6.3: A change of reference configuration and the corresponding transformation of the uniformity field.

Considering Equation (6.62), we have,

$$\dot{\boldsymbol{P}} = \boldsymbol{P}\tilde{\boldsymbol{\Upsilon}}^{-1}\,\tilde{\mathcal{F}}(\tilde{\boldsymbol{\Upsilon}}, J_{\boldsymbol{P}}\,\tilde{\boldsymbol{\Upsilon}}^{-T}\boldsymbol{P}^{T}\,\boldsymbol{\mathfrak{A}}\,\boldsymbol{P}^{-T}\tilde{\boldsymbol{\Upsilon}}^{T}, \zeta) \tag{6.63}$$

this shows that

$$\dot{\boldsymbol{P}} = \boldsymbol{P}\,\check{\mathcal{F}}(J_{\boldsymbol{P}}\,\boldsymbol{P}^{T}\,\boldsymbol{\mathfrak{A}}\,\boldsymbol{P}^{-T}). \tag{6.64}$$

We seek for an evolution law for the *inhomogeneity deformation rate* $\boldsymbol{L}_{\boldsymbol{P}}$ defined in Equation (6.22) but, initially, it is easier find one for its $\boldsymbol{P}$-pull-back $\boldsymbol{\Lambda}_{\boldsymbol{P}} = \boldsymbol{P}^{-1}\boldsymbol{L}_{\boldsymbol{P}}\boldsymbol{P}$ (see Equation (6.24)). Indeed, if we right-multiply Equation (6.64) by $\boldsymbol{P}^{-1}$, we obtain

$$\boldsymbol{\Lambda}_{\boldsymbol{P}} = \check{\mathcal{F}}(J_{\boldsymbol{P}}\,\boldsymbol{P}^{T}\,\boldsymbol{\mathfrak{A}}\,\boldsymbol{P}^{-T}). \tag{6.65}$$

The other condition that the evolution law must satisfy is the *objectivity* with respect to the change of the archetype, i.e., with respect to *arbitrary* linear transformations (and not just rotations, in which case we should speak of frame indifference) of the archetype. Since

the evolution is the matter of comparison between the constitutive response of a body point at two different instants of time, the archetype is not involved in this process. Thus, we consider a change of archetype

$$\boldsymbol{P}' = \boldsymbol{P}\boldsymbol{A}, \tag{6.66}$$

where $\boldsymbol{A}$ is a linear map, and observe that

$$\dot{\boldsymbol{P}}' = \dot{\boldsymbol{P}}\boldsymbol{A}, \tag{6.67}$$

and thus

$$\boldsymbol{\Lambda}'_{\boldsymbol{P}} = \boldsymbol{A}^{-1}\boldsymbol{P}^{-1}\dot{\boldsymbol{P}}\boldsymbol{A} = \boldsymbol{A}^{-1}\boldsymbol{\Lambda}_{\boldsymbol{P}}\boldsymbol{A}. \tag{6.68}$$

The evolution equation corresponding to $\boldsymbol{\Lambda}'_{\boldsymbol{P}}$, i.e.,

$$\boldsymbol{\Lambda}'_{\boldsymbol{P}} = \check{\mathcal{F}}(J_{\boldsymbol{P}'}\,\boldsymbol{P}'^{T}\,\mathfrak{A}\,\boldsymbol{P}'^{-T}), \tag{6.69}$$

reads

$$\boldsymbol{A}^{-1}\boldsymbol{\Lambda}_{\boldsymbol{P}}\boldsymbol{A} = \check{\mathcal{F}}\left(J_{\boldsymbol{A}}\,\boldsymbol{A}^{T}(J_{\boldsymbol{P}}\,\boldsymbol{P}^{T}\,\mathfrak{A}\,\boldsymbol{P}^{-T})\boldsymbol{A}^{-T}\right). \tag{6.70}$$

Comparing with Equation (6.65), we finally obtain

$$\boldsymbol{A}^{-1}\check{\mathcal{F}}(J_{\boldsymbol{P}}\,\boldsymbol{P}^{T}\,\mathfrak{A}\,\boldsymbol{P}^{-T})\boldsymbol{A} = \check{\mathcal{F}}\left(J_{\boldsymbol{A}}\,\boldsymbol{A}^{T}(J_{\boldsymbol{P}}\,\boldsymbol{P}^{T}\,\mathfrak{A}\,\boldsymbol{P}^{-T})\boldsymbol{A}^{-T}\right). \tag{6.71}$$

It is noteworthy that the change of archetype is a *symmetry of the evolution law*, if the functions $\check{\mathcal{F}}$ and $\check{\mathcal{F}}'$ in Equation (6.71) are identical. An important consequence of this observation is the concept of *material symmetry consistency*, which demands that the material symmetry group should be a subgroup of evolution symmetry group (for details, see Epstein and Elzanowski, 2007).

In conclusion, using Equations (6.24) and (6.65), we deduce that an admissible evolution law for $\boldsymbol{L}_{\boldsymbol{P}}$ has the form

$$\boldsymbol{L}_{\boldsymbol{P}} = \boldsymbol{P}\,\check{\mathcal{F}}(J_{\boldsymbol{P}}\,\boldsymbol{P}^{T}\,\mathfrak{A}\,\boldsymbol{P}^{-T})\,\boldsymbol{P}^{-1}. \tag{6.72}$$

6.7 Dissipation Inequality and Thermodynamical Admissibility

Here we show that, in order to satisfy the dissipation inequality (6.15e), a good candidate for the still "unspecified" tensor quantity $\mathfrak{A}$ of Equation (6.72), is the *Mandel stress* $\mathfrak{M} = \boldsymbol{F}.\boldsymbol{T}$.

Let us consider the dissipation inequality (6.15e) in the *isothermal* case, i.e., when the temperature field Θ is constant, for every X and t:

$$0 \leq -\rho_R \dot{A} + (\boldsymbol{g}\,\boldsymbol{T}) : \dot{\boldsymbol{F}}. \tag{6.73}$$

Since the elastic potential is related to the Helmholtz free energy by by $W = \rho_R\, A$ (i.e., the elastic potential is nothing but the Helmholtz free energy per unit volume) we have

$$\rho_R\, \dot{A} = \rho_R\, \partial_t \left(\frac{W}{\rho_R}\right) = \dot{W} - \rho_R\, \frac{W}{\rho_R^2}\, \dot{\rho}_R = \dot{W} + W\ \mathrm{Tr}(\boldsymbol{L_P}), \tag{6.74}$$

where we used Equation (6.23). Also, using the uniformity condition (6.18) on the elastic potential, we have

$$\dot{W} = -J_{\boldsymbol{P}}^{-1}(\boldsymbol{P}^{-T} : \dot{\boldsymbol{P}})\, \check{W}(\boldsymbol{FP}) + J_{\boldsymbol{P}}^{-1} \left(\frac{\partial \check{W}}{\partial \boldsymbol{FP}}(\boldsymbol{FP})\right) : (\dot{\boldsymbol{F}}\boldsymbol{P} + \boldsymbol{F}\dot{\boldsymbol{P}}). \tag{6.75}$$

At this point, we need the relation (which we derive with some small of notation)

$$\boldsymbol{g}\,\boldsymbol{T} = \frac{\partial \hat{W}}{\partial \boldsymbol{F}}(\boldsymbol{F}, X, t) = J_{\boldsymbol{P}}^{-1} \left(\frac{\partial \check{W}}{\partial \boldsymbol{FP}}(\boldsymbol{FP})\right) \left(\frac{\partial \boldsymbol{FP}}{\partial \boldsymbol{F}}\right) = J_{\boldsymbol{P}}^{-1} \left(\frac{\partial \check{W}}{\partial \boldsymbol{FP}}(\boldsymbol{FP})\right) \boldsymbol{P}^T, \tag{6.76}$$

from which

$$J_{\boldsymbol{P}}\, \boldsymbol{g}\,\boldsymbol{T}\, \boldsymbol{P}^{-T} = \frac{\partial \check{W}}{\partial \boldsymbol{FP}}(\boldsymbol{FP}). \tag{6.77}$$

Substituting Equation (6.77) together with the identity $\boldsymbol{P}^{-T} : \dot{\boldsymbol{P}} = \mathrm{Tr}(\dot{\boldsymbol{P}}\boldsymbol{P}^{-1}) = \mathrm{Tr}(\boldsymbol{L_P})$ (already seen in the derivation of $\boldsymbol{L_P}$) and $W = J_{\boldsymbol{P}}^{-1}\check{W}(\boldsymbol{FP})$ into Equation (6.75), we obtain

$$\dot{W} = -W\ \mathrm{Tr}(\boldsymbol{L_P}) + (\boldsymbol{g}\,\boldsymbol{T}\,\boldsymbol{P}^{-T}) : (\dot{\boldsymbol{F}}\boldsymbol{P} + \boldsymbol{F}\dot{\boldsymbol{P}}), \tag{6.78}$$

and, using the properties of the double contraction,

$$\dot{W} = -W\ \mathrm{Tr}(\boldsymbol{L_P}) + (\boldsymbol{g}\,\boldsymbol{T}) : (\dot{\boldsymbol{F}}\boldsymbol{P}\boldsymbol{P}^{-1} + \boldsymbol{F}\dot{\boldsymbol{P}}\boldsymbol{P}^{-1}). \tag{6.79}$$

which, using the definition (6.22) of $\boldsymbol{L_P}$, becomes

$$\dot{W} = -W \ \mathrm{Tr}(\boldsymbol{L_P}) + (\boldsymbol{g}\,\boldsymbol{T}) : (\dot{\boldsymbol{F}} + \boldsymbol{F}\boldsymbol{L_P}). \tag{6.80}$$

The final passage is to use once again the properties of the double contraction, which yields

$$\dot{W} = -W\,\mathrm{Tr}(\boldsymbol{L_P}) + (\boldsymbol{g}\,\boldsymbol{T}) : \dot{\boldsymbol{F}} + \mathfrak{M} : \boldsymbol{L_P}, \tag{6.81}$$

where

$$\mathfrak{M} = \boldsymbol{F}\,\boldsymbol{g}\,\boldsymbol{T} = \boldsymbol{F}.\boldsymbol{T} \tag{6.82}$$

is the *Mandel stress*. Now we substitute Equation (6.82) into Equation (6.74) and, with some minimal manipulation, we obtain

$$-\mathfrak{M} : \boldsymbol{L_P} = -\rho_R\,\dot{A} + (\boldsymbol{g}\,\boldsymbol{T}) : \dot{\boldsymbol{F}}. \tag{6.83}$$

Therefore, the entropy inequality (6.73) reads

$$\mathfrak{M} : \boldsymbol{L_P} \leq 0, \tag{6.84}$$

Stating that the *inhomogeneity power*, i.e., the power exerted by the Mandel stress $\mathfrak{M}$ on its conjugated "generalised velocity" $\boldsymbol{L_P}$ must be negative.

6.8 Postulated Evolution Law

We postulate an evolution law i the form reported in Equation (6.72), such that $\mathfrak{A}$ coincides with the *deviatoric* Mandel stress

$$\mathfrak{M}_d = \mathfrak{M} - \tfrac{1}{3}\,\mathrm{Tr}(\mathfrak{M})\boldsymbol{I}^T, \tag{6.85}$$

and

$$\check{\mathcal{F}}(J_{\boldsymbol{P}}\,\boldsymbol{P}^T\,\mathfrak{M}_d\,\boldsymbol{P}^{-T}) = -k\,J_{\boldsymbol{P}}\,\mathfrak{g}^{-1}[\boldsymbol{P}^T\mathfrak{M}_d\boldsymbol{P}^{-T}]\mathfrak{g} \tag{6.86}$$

so that the evolution law reads

$$\boldsymbol{L_P} = -k\ J_{\boldsymbol{P}}\ \boldsymbol{P}\,\mathfrak{g}^{-1}\boldsymbol{P}^T\mathfrak{M}_d\boldsymbol{P}^{-T}\mathfrak{g}\,\boldsymbol{P}^{-1}, \tag{6.87}$$

where k is a positive constant. Note that the inverse metric tensor $\mathfrak{g}^{-1}$ is necessary to properly contract $\boldsymbol{P}^T\mathfrak{M}_d\boldsymbol{P}^{-T}$ with $\boldsymbol{P}$ on the left and $\boldsymbol{P}^{-1}$ on the right, as one can verify in components. We intend to show that the evolution law described by Equation (6.87) is thermodynamically admissible, i.e., it satisfies the dissipation inequality (6.15e) in the form reported in Equation (6.84) for uniform materials in the isothermal case. Therefore, we would like to show that

$$\mathfrak{M} : \boldsymbol{L_P} = -k\ J_{\boldsymbol{P}}\ \mathfrak{M} : \Big[\boldsymbol{P}\,\mathfrak{g}^{-1}\boldsymbol{P}^T\mathfrak{M}_d\boldsymbol{P}^{-T}\mathfrak{g}\,\boldsymbol{P}^{-1}\Big] \leq 0, \tag{6.88}$$

which, since $J_{\boldsymbol{P}}$ must be positive and k is assumed positive, amounts to proving that

$$\mathfrak{M} : \Big[\boldsymbol{P}\,\mathfrak{g}^{-1}\boldsymbol{P}^T\mathfrak{M}_d\boldsymbol{P}^{-T}\mathfrak{g}\,\boldsymbol{P}^{-1}\Big] \geq 0. \tag{6.89}$$

First of all, let us show that the admissibility condition can be further reduced to

$$\mathfrak{M}_d : \Big[\boldsymbol{P}\,\mathfrak{g}^{-1}\boldsymbol{P}^T\mathfrak{M}_d\boldsymbol{P}^{-T}\mathfrak{g}\,\boldsymbol{P}^{-1}\Big] \geq 0. \tag{6.90}$$

Indeed, if we use the definition (6.85) of deviatoric Mandel stress to write the Mandel stress as $\mathfrak{M} = \frac{1}{3}\,\mathrm{Tr}(\mathfrak{M})\boldsymbol{I}^T + \mathfrak{M}_d$, and the property $\mathrm{Tr}(\boldsymbol{B}^{-1}\boldsymbol{A}\boldsymbol{B}) = \mathrm{Tr}(\boldsymbol{A})$ of the trace, we have

$$\begin{aligned}
\tfrac{1}{3}\,\mathrm{Tr}(\mathfrak{M})\boldsymbol{I}^T : \Big[\boldsymbol{P}\,\mathfrak{g}^{-1}\boldsymbol{P}^T\mathfrak{M}_d\boldsymbol{P}^{-T}\mathfrak{g}\,\boldsymbol{P}^{-1}\Big] &= \tfrac{1}{3}\,\mathrm{Tr}(\mathfrak{M})\boldsymbol{I}^T : \Big[(\boldsymbol{P}^{-T}\mathfrak{g}\,\boldsymbol{P}^{-1})^{-1}\mathfrak{M}_d(\boldsymbol{P}^{-T}\mathfrak{g}\,\boldsymbol{P}^{-1})\Big] \\
&= \tfrac{1}{3}\,\mathrm{Tr}(\mathfrak{M})\ \mathrm{Tr}\Big((\boldsymbol{P}^{-T}\mathfrak{g}\,\boldsymbol{P}^{-1})^{-1}\mathfrak{M}_d(\boldsymbol{P}^{-T}\mathfrak{g}\,\boldsymbol{P}^{-1})\Big) \\
&= \tfrac{1}{3}\,\mathrm{Tr}(\mathfrak{M})\ \mathrm{Tr}(\mathfrak{M}_d) = 0,
\end{aligned} \tag{6.91}$$

which implies the reduced condition (6.90). In order to prove (6.90), we employ the property $\boldsymbol{A} : \boldsymbol{B} = \boldsymbol{A}^T\boldsymbol{B}$ of the double contraction and the property $\mathrm{Tr}(\boldsymbol{A}\boldsymbol{B}) = \mathrm{Tr}(\boldsymbol{B}\boldsymbol{A})$ of the trace

and, by setting $\boldsymbol{H} = \boldsymbol{P}^T \mathfrak{M}_d \boldsymbol{P}^{-T}$, we obtain

$$\begin{aligned}
\mathfrak{M}_d : \Big[\boldsymbol{P}\, \mathfrak{g}^{-1} \boldsymbol{P}^T \mathfrak{M}_d \boldsymbol{P}^{-T} \mathfrak{g}\, \boldsymbol{P}^{-1}\Big] &= \mathrm{Tr}\Big(\mathfrak{M}_d^T\, \boldsymbol{P}\, \mathfrak{g}^{-1} \boldsymbol{P}^T \mathfrak{M}_d \boldsymbol{P}^{-T} \mathfrak{g}\, \boldsymbol{P}^{-1}\Big) \\
&= \mathrm{Tr}\Big(\boldsymbol{P}^{-1}\, \mathfrak{M}_d^T\, \boldsymbol{P}\, \mathfrak{g}^{-1} \boldsymbol{P}^T \mathfrak{M}_d \boldsymbol{P}^{-T} \mathfrak{g}\Big) \\
&= \mathrm{Tr}\Big(\boldsymbol{H}^T\, \mathfrak{g}^{-1} \boldsymbol{H}\, \mathfrak{g}\Big) \\
&= \boldsymbol{H} : (\mathfrak{g}^{-1} \boldsymbol{H}\, \mathfrak{g}) \geq 0, \qquad (6.92)
\end{aligned}$$

since the double contraction of a tensor with itself (rigorously, with its counterpart with covariant and contravariant indices inverted: this is precisely the job of the trace of the metric tensor $\mathfrak{g}$ and its inverse) is positive semi-definite. This finally shows that the evolution law (6.87) is thermodynamically admissible.

Chapter 7

Numerical Example: Application to Arterial Walls

In this chapter, we study a benchmark problem previously investigated in the paper by Grillo et al. (2015). We study the remodelling of a fibre-reinforced cylinder under plane strain in the plane orthogonal do the direction $X^3 \equiv Z$ of the axis of the cylinder. The cylinder is under uniform internal pressure, whereas the external pressure is set to be zero. At each material point, we consider two families of statistically oriented fibres, whose distribution evolves with time. We implant two copies of the distribution archetype as shown in Figure 7.1, into each material point, with equal and opposite angles, γ and $-\gamma$, measured from the Z-direction in the Θ-Z-plane. This amounts to defining an implant tensor $\boldsymbol{P}$ and then adapting its expression to the two angles γ and $-\gamma$, which will give two tensors $\boldsymbol{P}_+$ and $\boldsymbol{P}_-$, respectively. We employ a thermodynamically admissible evolution law, based on the arguments made in Section 6.8, Equation (6.87).

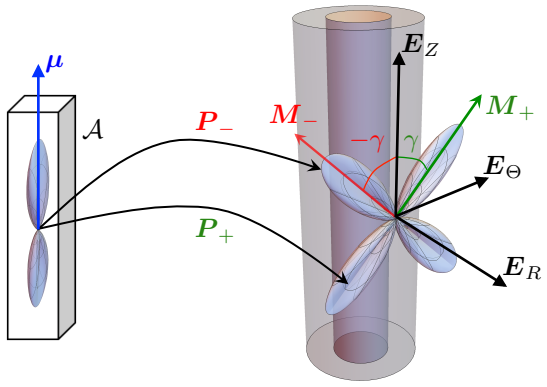

Figure 7.1: The two implanted fibre distributions. The implant tensors corresponding to the angles γ and $-\gamma$ are denoted $\boldsymbol{P}_+$ and $\boldsymbol{P}_-$, respectively. The expressions of the two tensors $\boldsymbol{P}_+$ and $\boldsymbol{P}_-$ are identical, except for the angle.

7.1 Elastic Energy

In this section we introduce the elastic energy for the evolution of a pressurised fibre-reinforced cylinder. The elastic energy is assumed to be given by the sum of an isotropic contribution due to the *matrix*, and isotropic contribution due to the fibres, and an anisotropic contribution due to the fibres, i.e., with some abuse of notation,

$$\hat{W}(\bar{\boldsymbol{C}}, X) = (1-\Phi_f)\hat{W}_m(\bar{\boldsymbol{C}}) + \Phi_f \hat{W}_{fi}(\bar{\boldsymbol{C}}) + \Phi_f \hat{W}_{fa}(\bar{\boldsymbol{C}}, X). \tag{7.1}$$

where

$$\hat{W}_m(\bar{\boldsymbol{C}}) = \frac{1}{2} k_m \left[I_1(\bar{\boldsymbol{C}}) - 3 \right], \tag{7.2}$$

$$\hat{W}_{fi}(\bar{\boldsymbol{C}}) = \frac{1}{2} k_{fi} \left[I_1(\bar{\boldsymbol{C}}) - 3 \right], \tag{7.3}$$

$$\hat{W}_{fa}(\bar{\boldsymbol{C}}, X) = J_{\boldsymbol{P}}^{-1} \int_{\mathbb{S}^2\mathcal{B}} \check{W}_{fib}(\check{\bar{I}}_4(X))\ \Psi(\boldsymbol{\nu}), \tag{7.4}$$

and

$$\check{W}_{fib}(\check{\bar{I}}_4(X)) = \tfrac{1}{4}\, k_{fa}\ \mathcal{H}(\check{\bar{I}}_4(X) - 1)\Big(\check{\bar{I}}_4(X) - 1\Big)^2. \tag{7.5}$$

In Equation (7.5), $\mathcal{H}(x)$, is the step function, equal to 1 for $x > 0$ and equal to 0 for $x \geq 0$. The role of the step function is to remove the contribution of the fibres which are not extended, as it is postulated for recruitment models. Also, $\check{\bar{I}}_4 = \boldsymbol{P}^T \bar{\boldsymbol{C}} \boldsymbol{P} : \boldsymbol{\nu} \otimes \boldsymbol{\nu}$ is the *isochoric* fourth invariant.

The deviatoric stress is derived using Equation (6.54), as

$$\boldsymbol{S}_{d(m)} = \frac{1}{2} k_m [\boldsymbol{G}^\sharp - \frac{1}{3} I_1(\bar{\boldsymbol{C}}) \bar{\boldsymbol{C}}^{-1}], \tag{7.6a}$$

$$\boldsymbol{S}_{d(fi)} = \frac{1}{2} k_{fi} [\boldsymbol{G}^\sharp - \frac{1}{3} I_1(\bar{\boldsymbol{C}}) \bar{\boldsymbol{C}}^{-1}], \tag{7.6b}$$

$$\boldsymbol{S}_{d(fa)} = J_{\boldsymbol{P}}^{-1} \int_{\mathbb{S}^2\mathcal{B}} k_{fa} \mathcal{H}(\check{\bar{I}}_4 - 1)\Big(\check{\bar{I}}_4 - 1\Big) \left[\frac{\partial \check{\bar{I}}_4}{\partial \bar{\boldsymbol{C}}} - \frac{1}{3} \left(\frac{\partial \check{\bar{I}}_4}{\partial \bar{\boldsymbol{C}}} : \bar{\boldsymbol{C}} \right) \bar{\boldsymbol{C}}^{-1} \right]\ \Psi(\boldsymbol{\nu}), \tag{7.6c}$$

where

$$\frac{\partial \check{\bar{I}}_4}{\partial \bar{\boldsymbol{C}}} = \frac{\partial (\boldsymbol{P}^T \bar{\boldsymbol{C}} \boldsymbol{P} : \boldsymbol{\nu} \otimes \boldsymbol{\nu})}{\partial \bar{\boldsymbol{C}}} = \boldsymbol{P}^T \underline{\otimes}\, \boldsymbol{P}^T : \boldsymbol{\nu} \otimes \boldsymbol{\nu} = P^A{}_\alpha P^B{}_\beta\, \nu^\alpha \nu^\beta. \tag{7.7}$$

7.2 Material Implant Formulation

Following the framework of Section 6.5, we obtain the inhomogeneity deformation rate $\boldsymbol{L_P}$ and the deviatoric Mandel stress $\mathfrak{M}_d$, which we need to express in cylindrical coordinates. Here, we prescribe the angle γ as the preferred angle direction for the implanted archetype measured from the Z-axis. It should be noted that rotation is about the R-axis in cylindrical coordinates, meaning that the rotation matrix $[Q]$ of Equation (6.42a) is only function of γ, measured from the Z-axis. We also assume that the archetypal direction of symmetry of the fibre distribution is along the archetypal $\boldsymbol{a}_3$-axis, which gives $\boldsymbol{\mu} = 0\,\boldsymbol{a}_1 + 0\,\boldsymbol{a}_2 + 1\,\boldsymbol{a}_3$ in the archetype $\mathcal{A}$. Therefore, the polar decomposition of the implant $\boldsymbol{P}$ can be expressed as

$$[\![\boldsymbol{U}]\!] = \begin{bmatrix} \sqrt{\lambda_s} & 0 & 0 \\ 0 & \sqrt{\lambda_s} & 0 \\ 0 & 0 & \lambda_s^{-1} \end{bmatrix}, \qquad [\![\boldsymbol{R}]\!] = \begin{bmatrix} 1 & 0 & 0 \\ 0 & \cos\gamma & \sin\gamma \\ 0 & -\sin\gamma & \cos\gamma \end{bmatrix}, \tag{7.8}$$

so that the implant has the matrix representation

$$[\![\boldsymbol{P}]\!] = [\![\boldsymbol{R}\boldsymbol{U}]\!] = \begin{bmatrix} \sqrt{\lambda_s} & 0 & 0 \\ 0 & \cos\gamma\,\sqrt{\lambda_s} & \frac{\sin\gamma}{\lambda_s} \\ 0 & -\sin\gamma\,\sqrt{\lambda_s} & \frac{\cos\gamma}{\lambda_s}. \end{bmatrix} \tag{7.9}$$

Having $\boldsymbol{P}$ in matrix form, we can obtain $\dot{\boldsymbol{P}}$ as a function of λ_s and γ as:

$$[\![\dot{\boldsymbol{P}}]\!] = \begin{bmatrix} \frac{\dot{\lambda}_s}{2\sqrt{\lambda_s}} & 0 & 0 \\ 0 & \frac{\cos\gamma\,\dot{\lambda}_s - 2\lambda_s\dot{\gamma}\sin\gamma}{2\sqrt{\lambda_s}} & \frac{\lambda_s\,\dot{\gamma}\,\cos\gamma - \sin\gamma\,\dot{\lambda}_s}{\lambda_s^2} \\ 0 & \frac{2\lambda_s\dot{\gamma}\cos\gamma + \sin\gamma\,\dot{\lambda}_s}{2\sqrt{\lambda_s}} & -\frac{\lambda_s\dot{\gamma}\sin\gamma + \cos\gamma\,\dot{\lambda}_s}{\lambda_s^2} \end{bmatrix}. \tag{7.10}$$

7.3 Geometry and Governing Equations

Following Olsson and Klarbring (2008) and Grillo et al. (2015), we study the remodelling of thick-walled cylinder which is made of hyperelastic material, the ground matrix and the fibre. The cylinder goes under pure inflation. We also assume that the cylinder is axially

symmetric, subjected to an isochoric deformation. The fibres are oriented according to the modified von Mises distribution (Holzapfel et al., 2015; Gizzi et al., 2018),

$$\Psi(a,b) = \sqrt{\frac{2b}{\pi}} \frac{\exp(a\cos 2\beta)\exp(b(\cos 2\alpha + 1))}{2\pi I_0(a)\ \mathrm{erfi}\left(\sqrt{2b}\right)}, \tag{7.11}$$

where erfi is the *imaginary error function* and I_0 is the *Bessel function* of zero kind (see Abramowitz and Stegun, 1964). In this study, we used $a = -1$ and $b = 5$, which give rise to the orientation distribution illustrated in Figure 7.1. This particular choice of parameters are chosen to have distributed fibres mostly aligned along the Θ-axis and in the Θ-Z-plane.

We also assume that the cylinder undergoes pure remodelling with no growth: in the sense of the material implant theory, this means that $J_{\boldsymbol{P}} = 1$ and $\mathrm{Tr}(\boldsymbol{L}_{\boldsymbol{P}}) = 0$, as it can be deduced from Equation (6.23). We also assume that system is closed and thus the balance equations are as in (6.15). The tensorial differential equations are

$$\mathrm{Div}(\boldsymbol{T}) = 0, \qquad \text{in } \mathcal{B} \tag{7.12a}$$

$$\boldsymbol{T}.\boldsymbol{N} = \boldsymbol{f}, \qquad \text{on } \partial\mathcal{B} \tag{7.12b}$$

$$J = 1 \qquad \text{in } \mathcal{B} \tag{7.12c}$$

$$\dot{\boldsymbol{P}} = -k_r\ J_{\boldsymbol{P}}\, \boldsymbol{P}\, \mathfrak{g}^{-1} \boldsymbol{P}^T \mathfrak{M}_d \boldsymbol{P}^{-T} \mathfrak{g}, \tag{7.12d}$$

where the evolution law (7.12d) is obtained via the definition (6.22) and by right-multiplying Equation (6.87) by $\boldsymbol{P}$.

7.4 Plane Strain Incompressible Deformation

We cover the body manifold with a polar chart, denoted by (R, Θ, Z), in which, $R \in [R_i, R_o], \Theta \in [0, 2\pi], Z \in [0, L]$. R_i and R_o, are the inner and outer radii respectively, Θ is the referential polar angle and L is the length of the cylinder. The current configuration is obtained under the assumption of pure inflation as:

$$(R, \Theta, Z) \mapsto (r, \theta, z) = (\chi^r(R, t), \Theta, Z). \tag{7.13}$$

For convenience, from this point forward, we refer to $\xi \equiv \chi^r$. Since ξ is a function solely of the radial coordinate R, we denote its derivative imply by $\xi' \equiv \partial\chi^r/\partial R$. The orthonormal bases for the tangent spaces of the referential and the current configurations are denoted by $\{\boldsymbol{E}_R, \boldsymbol{E}_\Theta, \boldsymbol{E}_Z\}$ and $\{\boldsymbol{e}_r, \boldsymbol{e}_\theta, \boldsymbol{e}_z\}$, respectively. Thus, the deformation gradient $\boldsymbol{F}$ reads

$$\boldsymbol{F}(R,t) = \xi'(R,t)\,\boldsymbol{e}_r \otimes \boldsymbol{E}^R + \frac{\xi(R,t)}{R}\,\boldsymbol{e}_\theta \otimes \boldsymbol{E}^\Theta + \boldsymbol{e}_z \otimes \boldsymbol{E}^Z. \tag{7.14}$$

Since we imposed incompressibility, we should have $\det \boldsymbol{F} = 1$, which implies

$$\xi'(X,t)\xi(X,t) = R. \tag{7.15}$$

Equation (7.15) is a separable ordinary differential equation which admits the solution

$$\xi(R,t) = \sqrt{R^2 + \upsilon(t)}, \tag{7.16}$$

in which υ is a function, *independent* of R, which should be determined from the boundary conditions. Also, we have

$$\xi'(R,t) = \frac{R}{\sqrt{R^2+\upsilon(t)}} = \frac{R}{\xi(R,t)}, \tag{7.17}$$

Therefore, we can express the deformation gradient as

$$[\![\boldsymbol{F}(R,t)]\!] = \begin{bmatrix} \frac{R}{\xi(R,t)} & 0 & 0 \\ 0 & \frac{\xi(R,t)}{R} & 0 \\ 0 & 0 & 1 \end{bmatrix} = \begin{bmatrix} \frac{R}{\sqrt{R^2+\upsilon(t)}} & 0 & 0 \\ 0 & \frac{\sqrt{R^2+\upsilon(t)}}{R} & 0 \\ 0 & 0 & 1 \end{bmatrix}. \tag{7.18}$$

7.5 Boundary Conditions and Integration

Here we follow the same procedure as in the example reported by Grillo et al. (2015). The inner and outer circumferences constitute the boundary of the pressurised cylinder. We prescribe Neumann boundary conditions as

$$\boldsymbol{\tau} = \boldsymbol{\sigma}.\boldsymbol{n} = -\wp_o\,\boldsymbol{n}, \qquad \text{on}\,\chi(\partial\mathcal{B}_o), \tag{7.19a}$$

$$\boldsymbol{\tau} = \boldsymbol{\sigma}.\boldsymbol{n} = -\wp_i\,\boldsymbol{n}, \qquad \text{on}\,\chi(\partial\mathcal{B}_i), \tag{7.19b}$$

where $\boldsymbol{\tau}$ represents the distribution of contact forces for the inner and the outer radius, $\boldsymbol{n}$ denotes the normal vector to the boundary and $\wp_o$ and $\wp_i$ are the imposed pressures. Note that the normal vectors to both portions of the boundary are parallel to $\boldsymbol{e}_r$ by virtue of the axial symmetry of the problem. Using Nanson's formula $\boldsymbol{f} = J\sqrt{\boldsymbol{N}.\boldsymbol{C}^{-1}.\boldsymbol{N}}\ \boldsymbol{\tau}$, which accounts for the change of area from the current boundary $\chi(\partial\mathcal{B})$ to the reference boundary $\partial\mathcal{B}$ (Bonet and Wood, 2008), and imposing the incompressibility condition $J = 1$, we have

$$\boldsymbol{f} = \boldsymbol{T}.\boldsymbol{N} = -\wp_o\, \boldsymbol{g}^{\sharp}\, \boldsymbol{F}^{-T}.\boldsymbol{N}, \qquad \text{on } \partial\mathcal{B}_o, \tag{7.20a}$$

$$\boldsymbol{f} = \boldsymbol{T}.\boldsymbol{N} = -\wp_i\, \boldsymbol{g}^{\sharp}\, \boldsymbol{F}^{-T}.\boldsymbol{N}, \qquad \text{on } \partial\mathcal{B}_i, \tag{7.20b}$$

where, again, the normal vector $\boldsymbol{N}$ are parallel to $\boldsymbol{E}_R$ for both portions of the boundary. Since we consider an axisymmetric problem, the first Piola-Kirchhoff stress is independent of Θ and Z. Also, the boundary conditions ensure that the first Piola-Kirchhoff stress is diagonal, i.e.,

$$[\![\boldsymbol{T}(R,t)]\!] = \begin{bmatrix} T^{rR} & 0 & 0 \\ 0 & T^{\theta\Theta} & 0 \\ 0 & 0 & T^{zZ} \end{bmatrix}. \tag{7.21}$$

The first Piola-Kirchhoff stress can be expressed as the sum of its hydrostatic and deviatoric components, and in terms of the deviatoric second Piola-Kirchhoff stress, as

$$\boldsymbol{T} = \boldsymbol{T}_h + \boldsymbol{T}_d = -J\, p\, \boldsymbol{g}^{\sharp}\boldsymbol{F}^{-T} + \boldsymbol{F}\, \boldsymbol{S}_d. \tag{7.22}$$

Since both the deformation gradient (7.18) and the first Piola-Kirchhoff stress (7.21) are diagonal, also the second Piola-Kirchhoff stresses is diagonal, and the radial component of the first Piola-Kirchhoff stress is expressed by

$$T^{rR}(R,t) = -\frac{\xi(R,t)}{R}\, p(R,t) + \frac{R}{\xi(R,t)} S_d^{RR}(R,t), \tag{7.23}$$

where we considered that $J = 1$.

Comparing Equations (7.23) and (7.20), and recalling that the axial symmetry of the problem ensures that $\boldsymbol{N} \equiv \boldsymbol{E}_R$, we can reformulate the boundary conditions as

$$T^{rR}(R_o,t) = -\frac{\xi(R_o,t)}{R_o}\,p(R_o,t) + \frac{R_o}{\xi(R_o,t)} S_d^{RR}(R_o,t) = -\wp_o(t)\,\frac{\xi(R_o,t)}{R_o}, \tag{7.24a}$$

$$T^{rR}(R_i,t) = -\frac{\xi(R_i,t)}{R_i}\,p(R_i,t) + \frac{R_i}{\xi(R_i,t)} S_d^{RR}(R_i,t) = -\wp_i(t)\,\frac{\xi(R_i,t)}{R_i}. \tag{7.24b}$$

or, in terms of the pressure term p, and using $R/\xi(R,t) = R/\sqrt{R^2+\upsilon(t)}$ (Equation (7.17)), as

$$p(R_o,t) = \wp_o(t) + \frac{R_o^2}{R_o^2+\upsilon(t)}\, S_d^{RR}(R_o,t), \tag{7.25a}$$

$$p(R_i,t) = \wp_i(t) + \frac{R_i^2}{R_i^2+\upsilon(t)}\, S_d^{RR}(R_i,t). \tag{7.25b}$$

The balance of linear momentum (7.12a) must be expressed in cylindrical coordinates,

$$\frac{\partial T^{rR}}{\partial R} + \frac{T^{rR} - T^{\theta\Theta}}{R} = 0, \tag{7.26}$$

and can then be integrated with the boundary conditions (7.24), which yields the pressure term as

$$p(R,t) = \left[\frac{R}{\xi(R,t)}\right]^2 S_d^{RR}(R,t) + \wp_i(t) - \int_{R_i}^{R} \frac{\eta(H,t)}{\xi(H,t)}\mathrm{d}H, \tag{7.27}$$

where $H \in [R_i, R]$ is the integration variable, and

$$\eta(H,t) = \frac{\xi(H,t)}{H} S_d^{\Theta\Theta}(H,t) - \left[\frac{H}{\xi(H,t)}\right]^3 S_d^{RR}(H,t). \tag{7.28}$$

In order to determine the function υ featuring in the expression of the radial deformation $\xi(R,t) = \sqrt{R^2+\upsilon(t)}$ of Equation (7.16), we calculate p at R_o and use the first of the (7.25). Finally, imposing the simplifying condition $\wp_o(t) = 0$, for every t, the consistency condition

$$\wp_i(t) = \int_{R_i}^{R_o} \frac{\eta(R,t)}{\xi(R,t)}\mathrm{d}R \tag{7.29}$$

is obtained.

7.6 Evolution Differential Equation and Numerical Algorithm

Using Equations (7.9), (7.10) and (7.12d), the final form of the evolution equation is

$$\frac{\dot{\lambda_s}}{\lambda_s} = k_r \, (\hat{\mathfrak{M}}_d)_R{}^R, \tag{7.30a}$$

$$\frac{\frac{1}{2}\lambda_s^2(3\cos(2\gamma)-1)\dot{\lambda}_s - (\lambda_s^6-1)\,\dot{\gamma}\sin(2\gamma)}{\lambda_s^3} = k_r \, (\hat{\mathfrak{M}}_d)_\Theta{}^\Theta. \tag{7.30b}$$

To study the numerical example discussed in the previous sections the beginning of Chapter 7, a code is developed in *Wolfram Mathematica*. The main focus of the numerical algorithm in this study is to have high *accuracy* and *precision* as we are studying a model with a simple geometry (isochoric inflation of a hollow cylinder). Although the geometry is simple, the evolution equation (7.30) makes the model computationally heavy. In this numerical study, we have two types of integrals: the surface integral over the unit sphere $\mathbb{S}^2$, which describe the fibre distribution, and the integral over the interval bounded by the inner and the outer radii $[R_i, R_o]$.

For the surface integral, we use the *Lebedev quadrature* (Lebedev, 1977), in which the grid points and the corresponding weights are obtained from the exact integration of *spherical harmonics* up to an arbitrary order. In this sense, the Lebedev scheme can be given expressed as

$$\int_{\mathbb{S}^2\mathcal{B}} f(\boldsymbol{M}) \approx \tilde{I}[f] = 4\pi \sum_{i=1}^{N} w_i f(\hat{\boldsymbol{M}}(\alpha_i, \beta_i)). \tag{7.31}$$

in which α_i and β_i are the polar and the azimuthal angles corresponding to the grid points and w_i is the weight of the i-th grid point. The Lebedev scheme is analogous to the *Gauss-Legendre* scheme in one dimension. For the integral over the interval $[R_i, R_o]$, we used the well-known *Gauss-Legendre* scheme, by solving the Legendre polynomials to find the grid points and the corresponding weights. For details, see Abramowitz and Stegun (1964).

It is obvious that having more grid points results in higher accuracy. We used 20 grid points for the Gauss points and 86 points for the spherical integrals. The number of grid points are chosen to keep the margin of error below one percent for each integral point.

7.7 Numerical Results

In this section, we present the results from the numerical analysis of the benchmark problem described in the previous sections. The required parameters for the problem is given in Table 7.1.

Parameter	Value	Symbol
inner radius	1 mm	R_i
outer radius	2 mm	R_o
internal pressure	0.02 MPa	$\wp_i$
initial angle	45°	γ_0
initial λ_s	1.014	λ_{s0}
matrix stiffness	0.0375 MPa	k_m
fibre isotropic stiffness	0.0375 MPa	k_{fi}
fibre anisotropic stiffness	0.0375 MPa	k_{fa}
remodelling stiffness	5×10^{-8} [t]/Pa *	k_r
fibre volume fraction	0.2	Φ_f

Table 7.1: Parameters for Numerical Analysis

Since we did not impose any condition to stop the remodelling, we carried out the analysis for 800 time steps for all the following cases. Figure 7.2 represents the evolution of the straightening stretch λ_s.

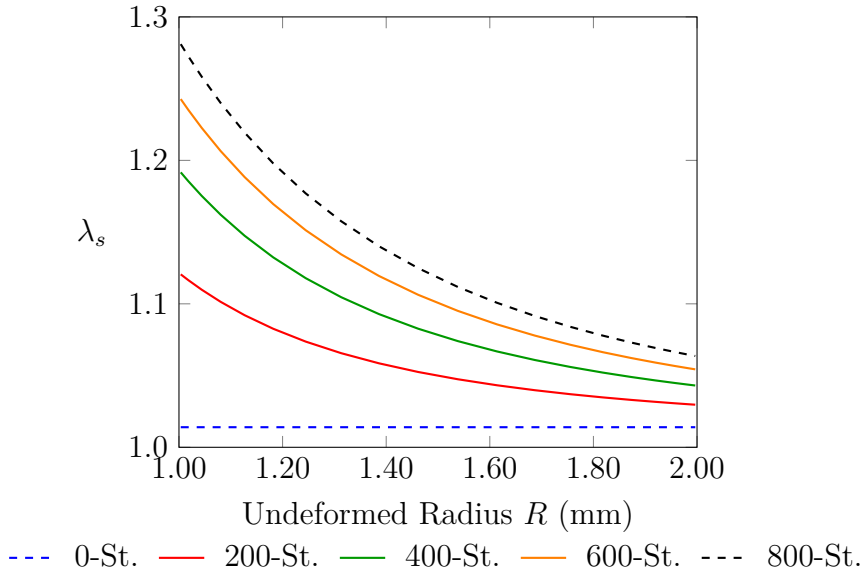

Figure 7.2: Evolution of the straightening stretch (λ_s) with time

As we can see, the largest value of λ_s is at the inner radius R_i, i.e., $\lambda_s(R_i) = 1.28$, whereas $\lambda_s(R_o) = 1.06$). The difference $\lambda_s(R_i, t) - \lambda_s(R_o, t)$ between the value of λ_s for the inner and out radius becomes more pronounced with time. The behaviour of λ_s is monotonically decreasing in the radius R throughout the evolution.

Figure 7.3 shows the evolution of the behaviour of the angle γ describing the direction of symmetry of the fibre family with time. After remodelling, the maximum and minimum angles occur at the inner and outer angle, respectively. The difference $\gamma(R_i, t) - \gamma(R_o, t)$ between the angle at the inner radius and that at the outer radius is more pronounced for the early cycles.

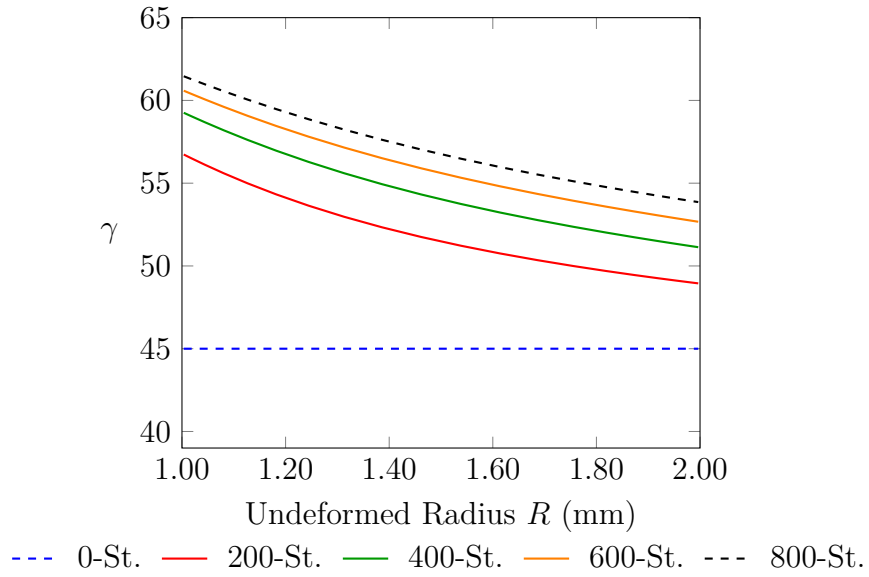

Figure 7.3: Evolution of the fibre angle γ with time

Figure 7.4 shows the evolution of the radial first Piola-Kirchhoff stress T^{rR} (dashed lines) and circumferential first Piola-Kirchhoff stress $T^{\theta\Theta}$ (solid lines) for the deformed radius. The results are shown for 1-cycle, 400-cycle and 800-cycle. The behaviour of the circumferential stress tends to become more homogeneous throughout the thickness of the tube. The difference $T^{\theta\Theta}(R_i, t) - T^{\theta\Theta}(R_o, t)$ between the circumferential stresses of the inner and outer radii before remodelling is around 23 kPa at time equal to zero, whereas for the 400-cycle the difference reduced to 16 kPa and for the 800-cycle is 14 kPa. It is noteworthy that the

variation of $T^{\theta\Theta}(R_i,t)-T^{\theta\Theta}(R_o,t)$ from $t=0$ cycles and $t=400$ cycles is significantly higher (7 kPa) than the variation from $t=400$ cycles and $t=800$ cycles (2 kPa). The absolute values of the radial stress at the inner and outer radii remain constant ($T^{rR}(R_i,t)=20$ kPa and $T^{rR}(R_0,t)=0$ kPa) according to the imposed boundary conditions ($\wp_i=20$ kPa and $\wp_o=0$ kPa).

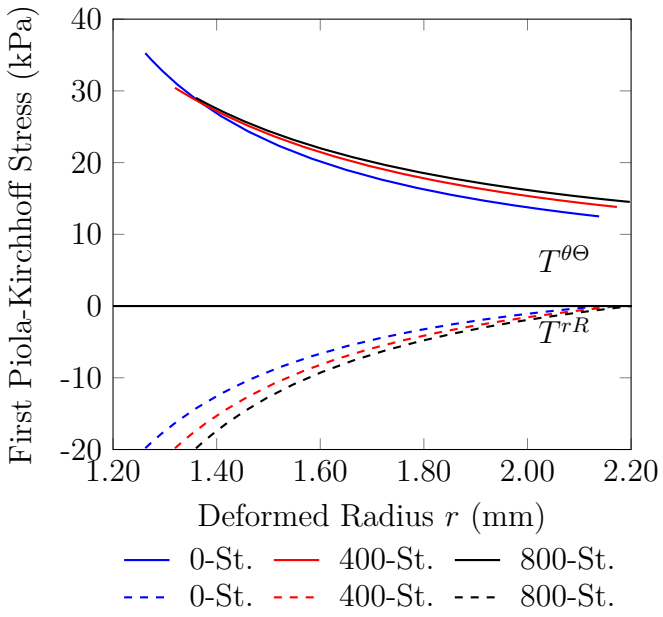

Figure 7.4: First Piola-Kirchhoff stresses T^{rR} and $T^{\theta\Theta}$.

One of the most prominent and well-known mechanical aspect of biological tissues, particularly the arterial wall, is the presence of residual stresses. There are numerous explanations and hypotheses on what the role of residual stress is and how it affects the structural integrity of the tissue. Choung and Fung (1986) argued that the residual stresses reduce the magnitude of the stress of the artery under internal pressure. In the same line of reasoning, Fung (1983) pointed out that residual stresses cannot be uniformly distributed across the arterial wall and the profile of the residual circumferential stress (along Θ-axis) is compressive for the inner wall and tensile for the outer wall. The profile of the residual stresses for our benchmark problem is shown in Figure 7.5. All three principal residual stresses increase monotonically. It is noteworthy that the residual circumferential stress (*red* curve), similarly

to what Fung (1983) stated, is compressive in the inner wall and tensile in the outer wall. Moreover, the circumferential stress is more uniform (smaller gradient in direction R) in the outer wall.

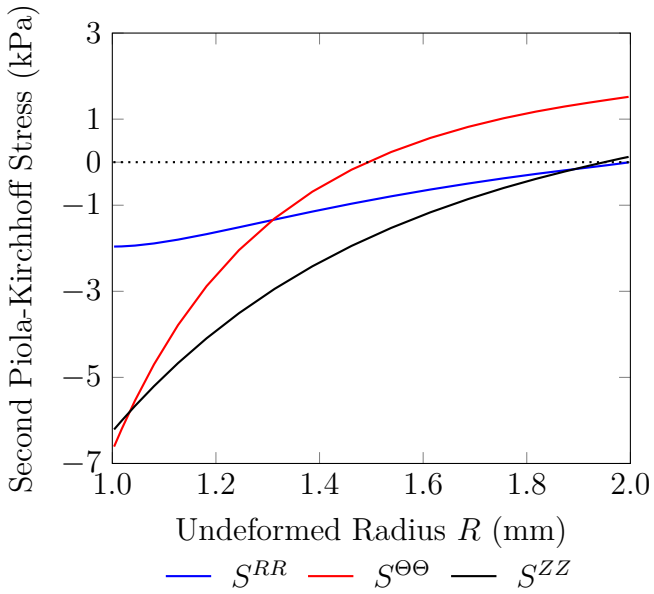

Figure 7.5: Residual Stresses.

7.8 Sensitivity Analysis

Here we study the sensitivity of the model to the initial conditions of straightening stretch and angle.

First, we fix the initial straightening stretch λ_{s0} and change the initial angle γ_0 in the range from 35° to 55°. Figure 7.6 shows the evolution of λ_s after 800 steps for different values of the initial angle. The evolution of the angle after 800 steps is shown in Figure 7.7. The behaviour of λ_s is very weakly affected by a change in the initial angle. In contrast, the larger the initial angle, the smaller the difference between the initial angle at the inner and outer radii.

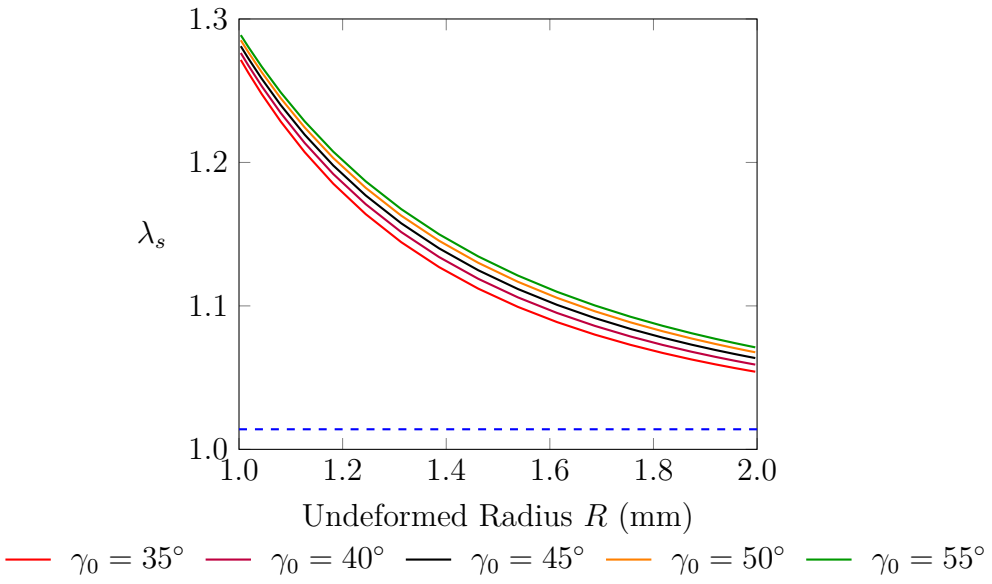

Figure 7.6: Behaviour of λ_s at 800 steps for different initial angles γ_0.

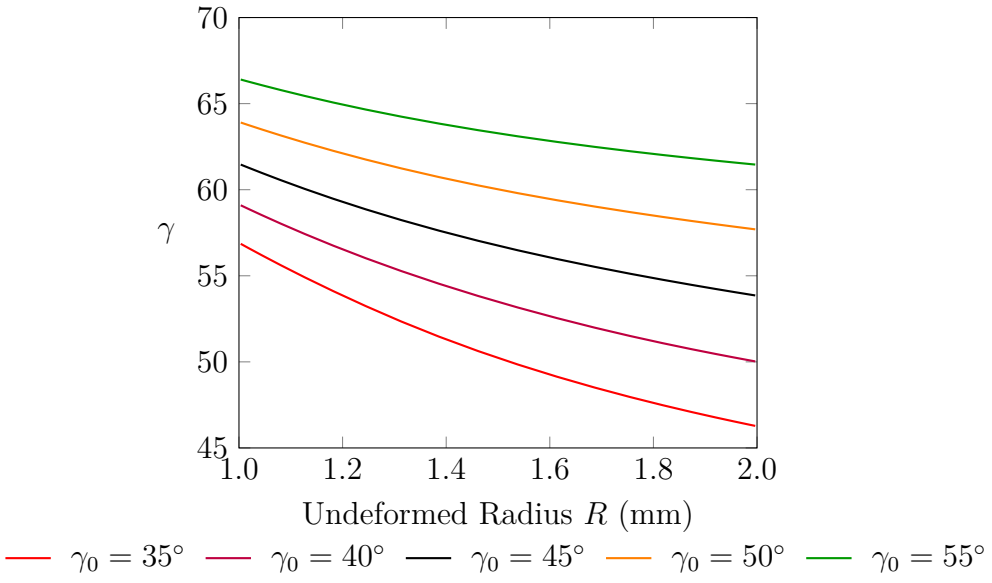

Figure 7.7: Behaviour of γ at 800 steps for different initial angles γ_0

Second, we fix the initial angle γ_0 at 45° for all the cases, whereas λ_s varies from 1.02 to 1.18. Figure 7.8 shows the behaviour of λ_s after 800 steps for different initial values λ_{s0}, and Figure 7.9 illustrates the behaviour of the angle γ after 800 steps for different initial values λ_{s0}. Figure 7.8 shows that the difference in initial condition for the straightening stretch is carried almost identically through the radius. Figure 7.9 shows a similar situation for the angle gamma: the difference between the angle at the inner and outer radius is almost unchanged with varying initial condition for the straightening stretch. This is in contrast with the case described by Figure 7.9, when the variation of the difference between the angle at the inner and outer radius with the initial angle was pronounced. We also note that we do not observe any evolution for the region close to outer circumference for the cases $\lambda_{s0} = 1.22$ and $\lambda_{s0} = 1.18$. This is due to fact that, since the fibres are not stretching with respect to the archetypal (straightened) configuration ($\breve{\breve{I}}_4 < 1$, which means that the stretch in the fibre is still greater than one, but smaller than λ_s), the Heaviside step function in the fibre potential (7.5) implies a corresponding zero deviatoric Mandel stress for the fibres.

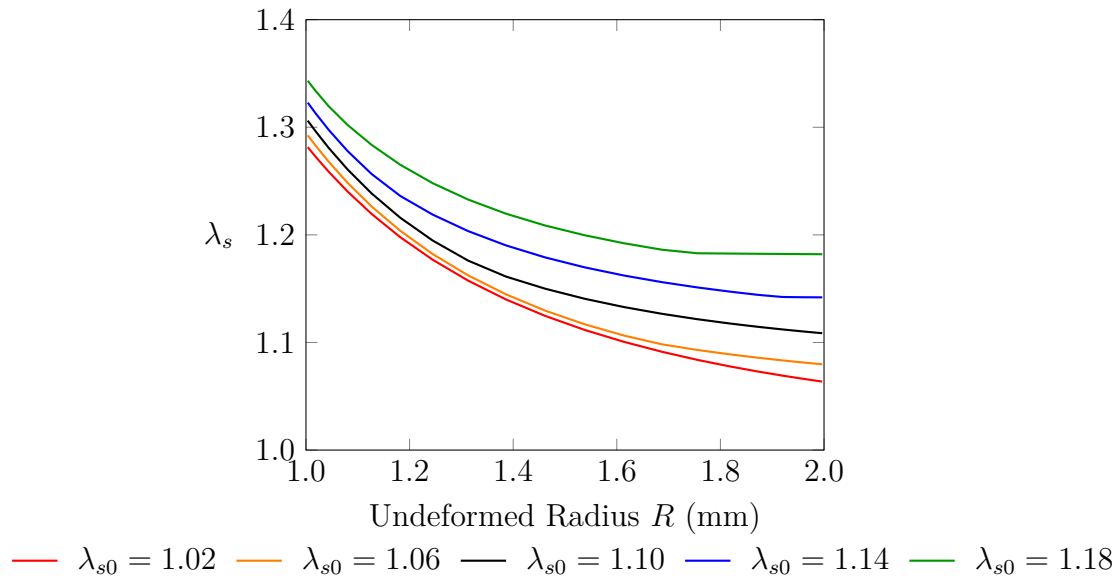

Figure 7.8: Behaviour of λ_s at 800 cycles for different values of λ_{s0}

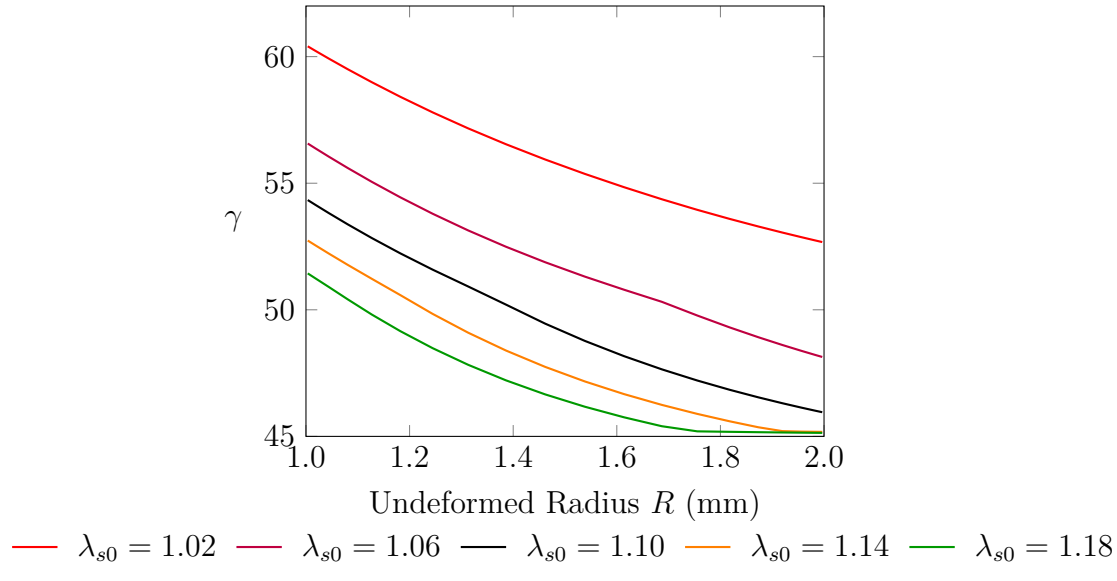

Figure 7.9: Behaviour of γ at 800 cycles for different values of λ_{s0}.

Chapter 8

Discussion

This study consists of two major parts, conceptually. The first part (Chapter 3–5) concerns with damage in soft tissue models with progressive fibril recruitment, whereas the second part (Chapter 6–7) constructs a framework for the remodelling of biological tissues described by models with fibre recruitment, based on the theory of material evolution (Epstein and Elzanowski, 2007).

8.1 Damage

This part of the thesis is based on a paper accepted for publication (Hamedzadeh et al., 2018). The focus of the damage part of this thesis was on the modelling of the progressive recruitment and damage of individual fibrils in a collagen fibre. We describe the progressive recruitment of the collagen fibrils in a fibre by means of a suitable probability distribution, which is a function of the straightening stretch λ_s. The probability distribution can be defined on bounded or superiorly unbounded intervals of stretches. The probability distribution for damage can be obtained directly from that of straightening if one assumes that all fibrils fail at the same value of stretch λ_f, evaluated from when their straightened configuration.

The aims were essentially three, and coincide with Objectives 1, 2 and 3, which are addressed in Chapters 3, 4 and 5, respectively:

1. To describe recruitment rigorously in a continuum mechanical framework, to conduct a critical review of the models proposed by Hurschler et al. (1997) and Martufi and Gasser (2011), to propose a novel recruitment model, based on correcting that by Martufi and Gasser (2011) and on generalising it to any general fibril constitutive law, and to demonstrate that this generalisation is

in fact equivalent to the model previously proposed by Hurschler et al. (1997);

2. To employ the proposed generalised recruitment model to also construct a damage model, which was eventually shown to be equivalent to that by Hurschler et al. (1997) under specific assumptions;

3. To propose a robust Finite Element implementation of the recruitment-damage model, including the regularisation procedure necessary to address the issue of damage localisation.

The proposed generalised recruitment model (Equation (3.50)) may or may not retain the fibril constitutive equation originally proposed by Martufi and Gasser (2011), which was linear in the logarithmic strain. If this constitutive law holds, the generalised model allows for a formulation in terms of the first Piola-Kirchhoff stress, which can be compressible as well, and for a formulation in terms of the Cauchy stress, which is valid in the incompressible case only.

The proof of the equivalence of the model by Hurschler et al. (1997) and of our generalised model is based upon the application of the Theorem of Integration by Parts (Equation (3.56)), and on the fact that the cumulative probability is zero when the straightening stretch λ_s is precisely that of first recruitment λ_{min} and that the stress goes to zero when the overall stretch λ equals the straightening stretch λ_s.

Based on the equivalence of the two recruitment models, it is possible to show that a damage model stemming from the proposed recruitment model is equivalent to the damage model proposed in the same paper by Hurschler et al. (1997). Furthermore, a procedure for obtaining the stress-strain relationship in the case of unloading following partial damage was obtained. We also studied the sensitivity of the model to the failure stretch λ_f and the bounds λ_{min} and λ_{max} of the recruitment probability through a numerical example.

We implemented the proposed model into Finite Elements, with a proper regularisation procedure to solve the problem of damage localisation. We simulated, as an example of

application, the uniaxial tension of a human Achilles tendon. Mesh sensitivity has been performed to check the convergence of the model. It is noteworthy that, although the Finite Element implementation has been performed solely to demonstrate the capability of the proposed model, it has been able to capture the essential characteristics of an experimental test on a rat Achilles tendon performed by Eliasson et al. (2013), as well as the numerical values of the first Piola-Kirchhoff stress at failure and stretch at failure obtained by Wren et al. (2001) in their tests on human Achilles tendons.

It is noteworthy to remark that our model is able to predict the residual deformation after unloading from a damaged state. This sheds new light on the interpretation of experimental data, which always shows such residual deformations. Specifically, it is interesting that this effect can be predicted by our fibre-based damage mechanism, without the introduction of any type of plastic sliding mechanism at the fibril level. To our knowledge, this conclusion has never been drawn before, and constitutes one of the most important non-intuitive findings of our work.

We would like to note that our model covers the stress-strain properties including strain localisation. The representation of strain localisation within continuous FE descriptions requires displacement interpolations that are flexible enough to avoid stress locking. Despite the mixed FE formulation (FEAP's Q1P0 element) used in this work effectively avoids volume locking, it may not be ideal for the problem of strain localisation; other approaches such as FE methods based on assumed enhance strain fields might be advantageous. Nonetheless, our model allows for computing the stresses well beyond the purely elastic domain and for predicting the progression of tissue damage associated with the rupture of collagen fibril. Clinically, this region is very important to estimate the degree of injury that a soft tissue attains during mechanical trauma (Frank et al., 1999; Comellas et al., 2016). Such tissue damage (injury) triggers well known healing processes (Williamson and Harding, 2004; Enoch and Leaper, 2008) and, as such, links mechanics to biology.

In summary, we provide a consistent framework to formulate damage models for collagen fibres in fibrous tissues. The compressible T_{fibril}-λ model (Section 3.8) and the incompressible σ_{fibril}-λ model (Section 3.9) that we present are only two specific particularisations, and indeed we presented a completely general stiffness-based model in Section 3.10 (recruitment) and Section 4 (damage), which is equivalent to the stress-based model by Hurschler et al. (1997). The formulation can be facilitated with any type of fibril properties and allows for incorporating rate effects.

8.2 Remodelling

In this part of the thesis, which fulfils Objective 4 and is contained in Chapters 6 and 7, we approached the *anelastic* phenomenon of remodelling in the light of the *material implant theory* (Epstein and Elzanowski, 2007) based on the notion of *first grade uniformity* as proposed in the classical work by Noll (1967).

We expressed the balance laws for a body undergoing growth-remodelling, including balance of mass, balance of momentum, balance of angular momentum, balance of energy and dissipation inequality, in the general case first, and then in the simplified case of non-zero mass source term but zero mass flux and non-compliant terms. We discussed the premises leading to the recruitment implant $\boldsymbol{P}$ by using the polar decomposition of the implant into a pure*rotation* and a pure *stretch*. The rotational part of the implant is responsible for rotating the fibre and parallel-transporting it from the archetype to the tangent space of the material point. The stretching part is responsible for mapping a fibre from its natural, straightened, stress-free state, into a crimped state in a material point in the reference configuration. In the subsequent step, we introduced the notion of *distribution implant*, which considers a collection of statistically oriented fibres, represented by an archetypical probability distribution of orientation, which then is implanted into each material point. In addition, we discussed the admissibility of evolution laws and the notion of *reduction to the*

archetype. We proposed a simple evolution law, in which the inhomogeneity deformation rate is linearly dependent on the *deviatoric Mandel* stress, and showed that it satisfied the dissipation inequality.

Using the prescribed evolution law, we solved a benchmark numerical problem describing a pressurised thick-walled cylinder under plane strain conditions, with uniform internal pressure, as in the work by Grillo et al. (2015). We considered two families of fibres, represented by a modified von Mises distribution (Holzapfel et al., 2015). The two families are such that the vectors describing the direction of symmetry of their distributions are oriented with opposite angles in the Θ-Z plane. With some abuse of terminology, we can call these angles the *mean angles*, although, rigorously speaking, the parameters in a modified von-Mises distribution could be such that the direction of symmetry is *not* the most probable direction. We used the same constitutive laws as in the work by Grillo et al. (2015). However, in the paper by Grillo et al. (2015), the distribution of fibre orientation is Gaussian-like, with the fibres being evenly distributed with a variable mean angle about the Z-axis and a fixed dispersion, and the only evolution parameter is the mean angle of the distribution, as opposed to our two remodelling parameters (straightening stretch λ_s and mean angles $\pm\gamma$).

Nonetheless, qualitatively speaking, the results for the remodelling angle are similar to those by Grillo et al. (2015). Both models predict that the angle increases, with the mean angle at the inner radius R_i being the largest. Moreover, the dependence on radius and time of the *radial* and *circumferential* stresses in our model (Figure 7.4) is similar to those in the paper by Grillo et al. (2015). However, while in Grillo et al. (2015) the cylinder deflates as it becomes stiffer *circumferentially*, in our study the cylinder inflates. This is not surprising, as we have two evolving mechanisms that work simultaneously, namely the relaxation of the fibres (increasing λ_s) and the change in fibre angle (increasing γ). Indeed when λ_s increases, it causes a *relaxation* of the fibres, and the cylinder needs to inflate so that the fibres reach their straightening stretch and are able to bear load.

Clearly, since Grillo et al. (2015) do not accommodate for the change in recruitment stretch λ_s, we cannot compare our results for the remodelling of λ_s. Nonetheless, other studies (e.g., Humphrey, 1999; Taber and Humphrey, 2001; Watton and Hill, 2009; Watton et al., 2009) considered a change of undulation of the fibres (Humphrey, 1999) or fibrils (Watton and Hill, 2009; Watton et al., 2009), and they agree with our findings, despite being fundamentally different in the basic assumptions: Humphrey (1999) considers resorption and generation of fibres, and Watton and Hill (2009) and Watton et al. (2009) consider pre-stretch in Z-direction. The relaxation effect that our model predicts has been observed by Kamiya and Togawa (1980). In addition, the overall profile of the *residual stress* for circumferential stress agrees with that described by Fung (1983): the residual stress is compressive in the inner layer and tensile in the outer layer.

It should be noted that, in this model, we did not prescribe our evolution law in accordance to experimental observations. Rather, we postulated an evolution law solely based on the *reduction to the archetype* and the *thermodynamical admissibility*. The evolution law is purposely of the simplest possible form, yet it could qualitatively reproduce the remodelling behaviour seen in other studies. This indicates that the framework of evolving material uniformity can be a viable and promising paradigm to explore growth and remodelling of biological tissues.

We recall that, in Section 2.7, we discussed the two different points of views on growth and remodelling offered by Epstein and Maugin (2000) and DiCarlo and Quiligotti (2002). Broadly speaking, Epstein and Maugin (2000) employ the theory of uniformity with a time-dependent implant $\boldsymbol{P}$, whereas DiCarlo and Quiligotti (2002) construct their evolution law follow the framework of Analytical mechanics, with generalised forces as linear operators on generalised velocities and a two-layer dynamics that distinguishes standard forces and velocities from the remodelling ones. We believe that these two points of view, although seemingly different in nature, are complementary. In both approaches, we have a modified

version of the *thermodynamics inequality* to accommodate for the non compliant entropy term and we see the arising of Eshelby-type stresses, as the driving forces of evolution. It is noteworthy that, although the study by Grillo et al. (2015) was based on that by DiCarlo and Quiligotti (2002) and ours on that by Epstein and Maugin (2000) and Epstein and Elzanowski (2007), the qualitative outcomes are rather similar. We believe that these similarities are the consequence of imposing the system to obey the *dissipation inequality*, a *universal law* that can be postulated and interpreted in different ways as the *imago Dei*, yet brings to the same results.

It is noteworthy to mention some controversial points with regards growth and remodelling, as arising from assumptions related to the configuration map. Some authors (Ateshian, 2007; Cowin, 2010) argue that, since we have addition or resorption of mass in a growing living matter, the deformation map cannot be bijective in principle. In this point of view, the material points are considered as particles bearing a mass and, therefore, one needs to track the source and the destination of each point to understand growth and remodelling appropriately. Indeed, this view is in-line with the atomistic point of view, which describes a material as a collection of a *finite number* of particles with mass. However, we should note that Continuum Mechanics, as any *Field Theory*, treats a body as being *fundamentally* different from a cluster of particles. In a continuum body, adding or subtracting no matter how many particles would not change the total number of particles, since the *cardinality* of a continuum body is $\aleph_1$ (See Munkres, 2000): roughly speaking, the number of particles is already infinite, so adding more particles does not make it "more infinite". Moreover, in Continuum Mechanics, the mass contained in a region of space is defined as the integral of the density over the region and, therefore, a single point has no mass according to measure theory. We should also point out that some of the fundamental theorems in Continuum Mechanics are founded upon the bijectivity of the configuration map, relaxing which might be detrimental to our framework. Indeed, we do not dismiss the idea of considering alterna-

tive theories and assumptions to accommodate the alternative point of view, which can be insightful and valuable. Nonetheless, we believe the assumption of bijective map can be still useful even in the realm of growth and remodelling.

8.3 Limitations and Future Work

We employed the framework of the material implant theory to develop a model applicable to the growth and remodelling of the arterial wall. We emphasise that the example we presented here is by no means a viable model for arterial walls, unless we consider the physiological conditions under which the remodelling occurs. There are fundamental differences between different types of *anelastic* phenomena in arterial walls. Moreover, the parameters that we introduced in this study are mostly selected in order to obtain a reasonable evolution. Indeed, we know from the histology of arterial walls that there are three distinct layers in the arterial walls (Holzapfel et al., 2000, intima, media and adventitia), whereas, in our study, we started the evolution from a homogenous initial condition. For a proper model of the arterial wall, we need to take into account the differences between these layers by means of a three-layer model, at the very minimum. Moreover, when solving a simple boundary-value problem, we can address more complex cases by implementing the model in a Finite Element (FE) package.

From the theoretical perspective, we can postulate proper conditions to stop the remodelling or to enhance our model by considering a *rate dependent* evolution law to capture asymptotic behaviour of remodelling. Moreover, we can easily extend the model to consider the case of growth, just by changing our implant from *isochoric* to non-isochoric. In this study, we ignored the presence of the non-complaint entropy. By incorporating the non-complaint entropy, we can couple the diagonal components (R, Θ and Z) of Mandel stress in different manners and explore the consequences. The stability of the prescribed differential equations is of great interest from the mathematical point of view, since there is no straight-

forward well-honed theorem, to the best of our knowledge, to obtain the stability domain of the evolution differential equation.

Another avenue to pursue in the realm of growth-remodelling constitutive modelling is to consider the damage of fibres as explored in the first part of this study. With some minor modifications to the constitutive law of the fibres, we can incorporate damage and explore new applications for our model such as the phenomenon of *healing*. The concept of recruitment that has been employed in this study can also be considered as a case of *wrinkling*. It would be of interest to conjoin the theory of wrinkling (Steigmann, 1990; Epstein and Forcinito, 2001; Epstein, 2002), which can produce a more sophisticated model, in comparison to our current model.

As a final remark, we would like to emphasise that the fields of physics and mechanics, as desired by scientists throughout the history from Newton to Einstein, represents the strive to find the universal laws of Nature, which can be simple yet powerful. Although in our limited and beginner's view, we tried to align with this endeavour in this thesis. We are certainly aware that modelling living matter, which puzzled and is puzzling the greatest minds of our generation, can by no means be achieved by a simple model like ours. Nonetheless, this is a small step towards a better understating of biological tissues.

When it comes to reproducing any experimental data, we can employ sophisticated regression analysis techniques and produce multivariable complex models. However, these approaches are more similar to curve-fitting, as humorously put by von Neumann (see Dyson, 2004):

> "*With four parameters I can fit an elephant, and with five I can make him wiggle his trunk*".

Bibliography

Abramowitz, M. and Stegun, I. A. (1964). *Handbook of mathematical functions: with formulas, graphs, and mathematical tables*, volume 55. Courier Corporation.

Alastrué, V., Rodríguez, J. F., Calvo, B., and Doblaré, M. (2007). Structural damage models for fibrous biological soft tissues. *Int. J. Solids Struc.*, 44:5894–5911.

Ambrosi, D. and Guana, F. (2007). Stress-modulated growth. *Math. Mech. Solids*, 12(3):319–342.

Ambrosi, D., Guillou, A., and Di Martino, E. (2008). Stress-modulated remodeling of a non-homogeneous body. *Biomech. Model. Mechanobiol.*, 7(1):63–76.

Antman, S. S. (1983). The influence of elasticity on analysis: modern developments. *Bul. Am. Math. Sco.*, 9:267–291.

Arnoux, P. J., Bonnoit, J., Chabrand, P., Jean, M., and Pithioux, M. (2002). Numerical damage models using a structural approach: application in bones and ligaments. *Euro. Physl. J. App. Phys.*, 26:65–73.

Ateshian, G. A. (2007). On the theory of reactive mixtures for modeling biological growth. *Biomech. Model. Mechanobiol.*, 6:423–445.

Baek, S., Rajagopal, K., and Humphrey, J. (2006). A theoretical model of enlarging intracranial fusiform aneurysms. *J. Biomech. Eng.*, 128(1):142–149.

Balakrishnan, N. and Nevzorov, V. B. (2004). *A Primer on Statistical Distributions*. John Wiley & Sons.

Balzani, D., Schroeder, J., and Gross, D. (2006). Simulation of discontinuous damage incorporating residual stresses in circumferentially overstretched atherosclerotic arteries. *Acta Biomat.*, 2:609–618.

Beck, K. and Brodsky, B. (1998). Supercoiled protein motifs: the collagen triple-helix and the α-helical coiled coil. *J. Struct. Biol.*, 122(1-2):17–29.

Best, T. M., McElhaney, J., Garrett Jr., W. E., and Myers, B. S. (1994). Characterization of passive response of live skeletal muscle using quasilinear viscoelastic theory of viscoelasticity. *J. Biomech.*, 27:413–419.

Betten, J. (1987b). Formulation of anisotropic constitutive equations. In Boehler, J. P., editor, *Applications of Tensor Functions in Solid Mechanics*, pages 227–250. Springer-Verlag, Wien. CISM Courses and Lectures No. 292, International Centre for Mechanical Sciences.

Bilby, B., Bullough, R., and Smith, E. (1955). Continuous distributions of dislocations: a new application of the methods of non-riemannian geometry. *Proceedings of the Royal Society of London A*, 231:263–273.

Bischoff, J. E., Arruda, E. M., and Grosh, K. (2004). A rheological network model for the continuum anisotropic and viscoelastic behavior of soft tissue. *Biomech. Model. Mechanobiol.*, 3:56–65.

Bonet, J. and Wood, R. D. (2008). *Nonlinear Continuum Mechanics for Finite Element Analysis (Second Edition)*. Cambridge University Press, Cambridge, UK.

Born, G. V. R. and Richardson, P. D. (1990). Mechanical properties of human atherosclerotic lesions. In Glagov, S., Newman, W. P., and Schaffer, S. A., editors, *Pathology of Human Atherosclerotic Plaques*, pages 413–423. Springer-Verlag, New York.

Brodland, G. W. (2002). The differential interfacial tension hypothesis (dith): A comprehensive theory for the self-rearrangement of embryonic cells and tissues. *J. Biomech. Eng.*, 124(2):188.

Calvo, B., Peña, E., Martinez, M. A., and Doblaré, M. (2007). An uncoupled directional damage model for fibred biological soft tissues. Formulation and computational aspects. *Int. J. Num. Meth. .Eng.*, 69:2036–2057.

Canham, P. B., Finlay, H. M., Dixon, J. G., Boughner, D. R., and Chen, A. (1989). Measurements from light and polarised light microscopy of human coronary arteries fixed at distending pressure. *Cardiovasc. Res.*, 23:973–982.

Cauvin, A. and Testa, R. B. (1999). Damage mechanics : basic variables in continuum theories. *Int. J. Solids Struct.*, 36(5):747–761.

Cavalcanti-Adam, E. A., Volberg, T., Micoulet, A., Kessler, H., Geiger, B., and Spatz, J. P. (2007). Cell spreading and focal adhesion dynamics are regulated by spacing of integrin ligands. *Biophys. J.*, 92(8):2964–2974.

Chaboche, J.-L. (1986). Time-independent constitutive theories for cyclic plasticity. *Int. J. Plasticity*, 2(2):149–188.

Chew, P. H., Yin, F. C., and Zeger, S. L. (1986). Biaxial stress-strain properties of canine pericardium. *J. Mol. Cell Cardiol.*, 18(6):567–578.

Choi, H. S. and Vito, R. (1990). Two-dimensional stress-strain relationship for canine pericardium. *J. Biomech. Eng.*, 112(2):153–159.

Choung, C. J. and Fung, Y. C. (1986). Residual stress in arteries. In Schmid-Schoenbein, G. W., Woo, S. L., and Zweifach, B. W., editors, *Frontiers in Biomechanics*, pages 117–129. Springer.

Coleman, B. D. and Noll, W. (1961). Foundations of linear viscoelasticity. *Rev. Modern Phys.*, 3:239–249.

Comellas, E., Gasser, T. C., Bellomo, F. J., and Oller, S. (2016). A homeostatic-driven turnover remodelling constitutive model for healing in soft tissues. *J. R. Soc. Interface*, 13:20151081.

Cordebois, J. and Sidoroff, F. (1982). Damage induced elastic anisotropy. In *Mechanical Behavior of Anisotropic Solids/Comportment Méchanique des Solides Anisotropes*, pages 761–774. Springer.

Cosgrove, D. (1986). Biophysical control of plant cell growth. *Annual Review of Plant Physiology*, 37(1):377–405.

Cosgrove, D. J. (1985). Cell wall yield properties of growing tissue: evaluation by in vivo stress relaxation. *Plant physiology*, 78(2):347–356.

Cowin, S. and Hegedus, D. (1976). Bone remodeling i: theory of adaptive elasticity. *Journal of Elasticity*, 6(3):313–326.

Cowin, S. C. (2010). Continuum kinematical modeling of mass increasing biological growth. *International Journal of Engineering Science*, 48(11):1137–1145.

Davis, F. M. and De Vita, R. (2012). A Nonlinear Constitutive Model for Stress Relaxation in Ligaments and Tendons. *Ann. Biomed. Eng.*, 40:1–10.

Decraemer, W., Maes, M., Vanhuyse, V., and Vanpeperstraete, P. (1980). A non-linear viscoelastic constitutive equation for soft biological tissues, based upon a structural model. *J. Biomech.*, 13:559–564.

Demer, L. L. and Yin, F. C. P. (1983). Passive biaxial mechanical properties of isolated canine myocardium. *J. Physiol. London*, 339:615–630.

Demiray, H. (1972). A note on the elasticity of soft biological tissues. *J. Biomech.*, 5:309–311.

Demiray, H. and Vito, R. P. (1976). Large deformation analysis of soft biomaterials. *Int. J. Eng. Sci.*, 14:789–793.

Diamant, J., Keller, A., Baer, E., Litt, M., and Arridge, R. G. C. (1972). Collagen: Ultrastructure and its relation to mechanical properties as a function of ageing. *Proc. Roy. Soc. Lond. B: Biol. Sci.*, 180:293–315.

DiCarlo, A. and Quiligotti, S. (2002). Growth and balance. *Mech. Res. Commun.*, 29:449–456.

Dokos, S., LeGrice, I. J., Smaill, B. H., Kar, J., and Young, A. A. (2000). A triaxial-measurement shear-test device for soft biological tissues. *J. Biomech. Eng.*, 122:471–478.

Dyson, F. (2004). A meeting with Enrico Fermi. *Nature*, 427(6972):297.

Eliasson, P., Andersson, T., Hammerman, M., and Aspenberg, P. (2013). Primary gene response to mechanical loading in healing rat achilles tendons. *J. Appl. Physiol.*, 114:1519–1526.

Enoch, S. and Leaper, D. J. (2008). Basic science of wound healing. *Surgery (Oxford)*, 26:31–37.

Epstein, M. (2002). From saturated elasticity to finite evolution, plasticity and growth. *Math. Mech. Solids*, 7(3):255–283.

Epstein, M. and Elzanowski, M. (2007). *Material inhomogeneities and their evolution: a geometric approach*. Springer Science & Business Media.

Epstein, M. and Forcinito, M. A. (2001). Anisotropic membrane wrinkling: theory and analysis. *Int. J. Solids Struct.*, 38(30-31):5253–5272.

Epstein, M. and Maugin, G. A. (1990). The energy-momentum tensor and material uniformity in finite elasticity. *Acta Mech.*, 83(3-4):127–133.

Epstein, M. and Maugin, G. A. (2000). Thermomechanics of volumetric growth in uniform bodies. *Int. J. Plasticity*, 16(7):951–978.

Epstein, M. and Maugin, G. A. (2010). Remarks on the Universality of the Eshelby Stress. *Math. Mech. Solids*, 15(2):137–143.

Eringen, A. C. (1980). *Mechanics of Continua*. Robert E. Krieger Publishing Company, Huntington, NY, USA.

Federico, S. (2012). Covariant formulation of the tensor algebra of non-linear elasticity. *Int. J. Non Lin. Mech.*, 47:273–284.

Federico, S. (2015a). Porous materials with statistically oriented reinforcing fibres. In Dorfmann, L. and Ogden, R. W., editors, *Nonlinear Mechanics of Soft Fibrous Materials*, pages 49–120. Springer, Berlin. CISM Courses and Lectures No. 559, International Centre for Mechanical Sciences.

Federico, S. (2015b). Some remarks on metric and deformation. *Math. Mech. Solids*, 20:522–539.

Federico, S. and Gasser, T. G. (2010). Non-linear elasticity of biological tissues with statistical fibre orientation. *J. Roy. Soc. Interface*, 7:955–966.

Federico, S. and Grillo, A. (2012). Elasticity and permeability of porous fibre-reinforced materials under large deformations. *Mech. Mat.*, 44:58–71.

Federico, S., Grillo, A., Giaquinta, G., and Herzog, W. (2008). Convex Fung-type potentials for biological tissues. *Meccanica*, 43:279–288.

Federico, S., Grillo, A., La Rosa, G., Giaquinta, G., and Herzog, W. (2005). A transversely isotropic, transversely homogeneous microstructural-statistical model of articular cartilage. *J. Biomech.*, 38:2008–2018.

Federico, S. and Herzog, W. (2008). Towards an analytical model of soft tissues. *J. Biomech.*, 41:3309–3313.

Flory, P. J. (1961). Thermodynamic relations for high elastic materials. *Trans. Faraday Soc.*, 57:829–838.

Flory, P. J. (1969). *Statistical Mechanics of Chain Molecules*. Wiley - Interscience, New York.

Frank, C., Shrive, N., Hiraoka, H., Nakamura, N., Kaneda, Y., and Hart, D. (1999). Optimisation of the biology of soft tissue repair. *Journal of Science and Medicine in Sport*, 2:190–210.

Fratzl, P. (2008). *Collagen: structure and mechanics*. Springer Science & Business Media.

Fratzl, P., Misof, K., Zizak, I., Rapp, G., Amenitsch, H., and Bernstorff, S. (1997). Fibrillar structure and mechanical properties of collagen. *J. Struct. Biol.*, 122:119–122.

Fung, Y. C. (1967). Elasticity of soft tissues in simple elongation. *Am. J. Physiol.*, 213:1532–1544.

Fung, Y. C. (1968). Biomechanics: its scope, history, and some problems of continuum mechanics in physiology. *Appl. Mech. Rev.*, 21:1–20.

Fung, Y. C. (1973). Biorheology of soft tissues. *Biorheol.*, 10:139–155.

Fung, Y. C. (1983). On the foundations of biomechanics. *J. Appl. Mech.*, 50:1003–1009.

Fung, Y. C. (1987). Mechanics of soft tissues. In Skalak, R. and Chien, S., editors, *Handbook of Bioengineering*. McGraw-Hill.

Fung, Y. C. (1990). *Biomechanics. Motion, Flow, Stress, and Growth*. Springer-Verlag, New York.

Fung, Y. C. (1993). *Biomechanics. Mechanical Properties of Living Tissues*. Springer-Verlag, New York, 2nd edition.

Fung, Y. C. (1995). Stress, strain, growth, and remodeling of living organisms. *Z. Angew. Math. Phys.*, 46:469–482.

Fung, Y. C. and Liu, S. Q. (1989). Change of residual strains in arteries due to hypertrophy caused by aortic constrictions. *Circ. Res.*, 65:1340–1349.

Fung, Y. C., Liu, S. Q., and Zhou, J. B. (1993). Remodeling of the constitutive equation while a blood vessel remodels itself under stress. *J. Biomech. Eng.*, 115:453–459.

Fusi, L., Farina, A., and Ambrosi, D. (2006). Mathematical modeling of a solid–liquid mixture with mass exchange between constituents. *Math. Mech. Solids*, 11(6):575–595.

Gasser, T. C. (2011). An irreversible constitutive model for fibrous soft biological tissue: A 3-D microfiber approach with demonstrative application to abdominal aortic aneurysms. *Acta Biomat.*, 7:2457–2466.

Gasser, T. C. and Holzapfel, G. A. (2007). Modeling dissection failure during balloon angioplasty. *Ann. Biomed. Eng.*, 35:711–723.

Gasser, T. C., Ogden, R. W., and Holzapfel, G. A. (2006). Hyperelastic modelling of arterial layers with distributed collagen fibre orientations. *J. Roy. Soc. Interface*, 3:15–35.

Gizzi, A., Pandolfi, A., and Vasta, M. (2018). A generalized statistical approach for modeling fiber-reinforced materials. *Journal of Engineering Mathematics*, 109:211–226.

Goudreau, G. L. and Taylor, R. L. (1972). Evaluation of numerical integration methods in elastodynamics. *Comput. Meth. Appl. Mech. Eng.*, 2:69–97.

Grillo, A., Wittum, G., Tomic, A., and Federico, S. (2015). Remodelling in statistically oriented fibre-reinforced materials and biological tissues. *Math. Mech. Solids*, 20(9):1107–1129.

Gurson, A. L. (1977). Continuum theory of ductile rupture by void nucleation and growth: Part i—yield criteria and flow rules for porous ductile media. *J. of Eng. mater. Tech.*, 99(1):2–15.

Gurtin, M. E. (2000). Configurational Forces as Basic Concepts of Continuum Physics. *Configurational Forces*.

Hamedzadeh, A., Gasser, T. C., and Federico, S. (2018). On the constitutive modelling of recruitment and damage of collagen fibres in soft biological tissues. *Eur. J. Mech. A/Solids*, in press.

Hansen, K. A., Weiss, J. A., and Barton, J. K. (2002). Recruitment of tendon crimp with applied tensile strain. *J. Biomech. Eng.*, 124(1):72–77.

Hardin, R. H. and Sloane, N. J. A. (1996). McLaren's improved snub cube and other new spherical designs in three dimensions. *Discrete Comput. Geom.*, 15:429–441.

Hayashi, K., Igarashi, Y., and Takamizawa, K. (1985). Stiffness of coronary arteries. In *ASME 1985 Biomechanics Symposium, AMD-Vol. 68*, pages 129–132, New York. American Society of Mechanical Engineers.

Hegedus, D. M. and Cowin, S. C. (1976). Bone remodeling, II: Small strain adaptive elasticity. *J. Elasticity*, 6:337–352.

Hoffman, A. H. and Grigg, P. (1984). A method for measuring strains in soft tissue. *J. Biomech.*, 17:795–800.

Hoger, A. (1997). Virtual configurations and constitutive equations for residually stressed bodies with material symmetry. *J. Elasticity*, 48:125–144.

Hokanson, J. and Yazdani, S. (1997). A constitutive model of the artery with damage. *Mech. Res. Commun.*, 24:151–159.

Holzapfel, G. and Ogden, R. (2007). On planar biaxial tests for anisotropic nonlinearly elastic solids: a continuum mechanical framework. *Math. Mech. Solids*, pages 474–489.

Holzapfel, G. A., Eberlein, R., Wriggers, P., and Weizsäcker, H. W. (1996). A new axisymmetrical membrane element for anisotropic, finite strain analysis of arteries. *Comput. Meth. Appl. Mech. Eng.*, 12:507–517.

Holzapfel, G. A., Gasser, T. C., and Ogden, R. W. (2000). A new constitutive framework for arterial wall mechanics and a comparative study of material models. *J. Elasticity*, 61:1–48.

Holzapfel, G. A., Niestrawska, J. A., Ogden, R. W., Reinisch, A. J., and Schriefl, A. J. (2015). Modelling non-symmetric collagen fibre dispersion in arterial walls. *J. R. Soc. Interface*, 12(106):20150188.

Hsu, F.-H. (1968). The influences of mechanical loads on the form of a growing elastic body. *J. Biomech.*, 1(4):303–311.

Hulmes, D. J. S. (2002). Building collagen molecules, fibrils, and suprafibrillar structures. *J. Struct. Biol.*, 137:2–10.

Humphrey, J. and Yin, F. (1987). On constitutive relations and finite deformations of passive cardiac tissue: I. A pseudostrain-energy function. *J. Biomech. Eng.*, 109(4):298–304.

Humphrey, J. D. (1999). Remodeling of a collagenous tissue at fixed lengths. *J. Biomech. Eng.*, 121:591–597.

Humphrey, J. D. (2003). Continuum biomechanics of soft biological tissues. *Proc. Roy. Soc. Lond. A*, 459:1–44.

Humphrey, J. D., Kang, T., Sakarda, P., and Anjanappa, M. (1993). Computer-aided vascular experimentation: A new electromechanical test system. *Ann. Biomed. Eng.*, 21:33–43.

Hurschler, C., Loitz-Ramage, B., and Vanderby Jr., R. (1997). A structurally based stress-stretch relationship for tendon and ligament. *J. Biomech. Eng.*, 119:392–399.

Huxley, J., Strauss, R. E., and Churchill, F. B. (1932). *Problems of relative growth*. Methuen London.

Ju, J. (1989). On energy-based coupled elastoplastic damage theories: Constitutive modeling and computational aspects. *Int. J. Solids Struct.*, 25(7):803–833.

Kachanov, L. M. (1986). *Introduction to Continuum Damage Mechanics*. Martinus Nijhoff Publishers, Dordrecht, The Netherlands.

Kadler, K. E., Baldock, C., Bella, J., and Boot-Handford, R. P. (2007). Collagens at a glance. *J. Cell Sci.*, 120(12):1955–1958.

Kadler, K. E., Holmes, D. F., Trotter, J. A., and Chapman, J. A. (1996). Collagen fibril formation. *Bioc. J.*, 316(Pt 1):1–11.

Kamiya, A. and Togawa, T. (1980). Adaptive regulation of wall shear stress to flow change in the canine carotid artery. *Am. J. Physiol.*, 239:H14–H21.

Kestin, J. and Rice, J. R. (1969). *Paradoxes in the application of thermodynamics to strained solids*. Division of Engineering, Brown University.

Koks, D. (2006). *Explorations in mathematical physics: the concepts behind an elegant language*. Springer Science & Business Media.

Kolmogorov, A. N. and Fomin, S. V. (1999). *Elements of the Theory of Functions and Functional Analysis*. Dover.

Kondo, K. (1958). *Memoirs of the unifying study of the basic problems in engineering sciences by means of geometry*. Gakujutsu Bunken Fukyu-Kai.

Kratky, O. and Porod, G. (1949). Röntgenuntersuchung gelöster fadenmoleküle. *Recueil des Travaux Chimiques des Pays-Bas*, 68:1106–1122.

Kroon, M. (2010). A continuum mechanics framework and a constitutive model for remodelling of collagen gels and collagenous tissues. *Journal of the Mechanics and Physics of Solids*, 58(6):918–933.

Lanir, Y. (1983). Constitutive equations for fibrous connective tissues. *J. Biomech.*, 16:1–12.

Lebedev, V. (1977). Spherical quadrature formulas exact to orders 25–29. *Siberian Mathematical Journal*, 18(1):99–107.

Lemaitre, J. and Chaboche, J. (1975). A non-linear model of creep-fatigue damage cumulation and interaction(for hot metallic structures). *Mech. of visc. media and bodies*.

Liao, H. and Belkoff, S. M. (1999). A failure model for ligaments. *J. Biomech.*, 32:183–188.

Lubliner, J. (1986). Normality rules in large-deformation plasticity. *Mech. Mater.*, 5(1):29–34.

Marsden, J. E. and Hughes, T. J. R. (1983). *Mathematical Foundations of Elasticity*. Prentice-Hall, Englewood Cliff, NJ, USA.

Martufi, G. and Gasser, T. C. (2011). A constitutive model for vascular tissue that integrates fibril, fiber and continuum levels with application to the isotropic and passive properties of the infrarenal aorta. *J. Biomech.*, 44:2544–2550.

von Maltzahn, W.-W., Besdo, D., and Wiemer, W. (1981). Elastic properties of arteries: A nonlinear two-layer cylindrical model. *J. Biomech.*, 14:389–397.

Mendler, M., Eich-Bender, S. G., Vaughan, L., Winterhalter, K. H., and Bruckner, P. (1989). Cartilage contains mixed fibrils of collagen types ii, ix, and xi. *J. Cell Biol.*, 108(1):191–197.

Miehe, C. (1988). *Zur numerischen Behandlung thermomechanischer Prozesse, Technischer Bericht F88/6*. PhD thesis, Institut für Baumechanik und numerische Mechanik der Universität Hannover.

Miyazaki, H. and Hayashi, K. (1999). Tensile tests of collagen fibers obtained from the rabbit patellar tendon. *Biomedical Microdevices*, 2:151–157.

Munkres, J. R. (2000). *Topology*. Prentice Hall.

Murakami, S. (1988). Mechanical modeling of material damage. *J. Appl. Mech.*, 55(2):280–286.

Murakami, S. (2012). *Continuum damage mechanics: a continuum mechanics approach to the analysis of damage and fracture*, volume 185. Springer Science & Business Media.

Murakami, S., Hayakawa, K., and Liu, Y. (1998). Damage evolution and damage surface of elastic-plastic-damage materials under multiaxial loading. *Int. J. Damage*, 7(2):103–128.

Myllyharju, J. and Kivirikko, K. I. (2004). Collagens, modifying enzymes and their mutations in humans, flies and worms. *Trends in Genetics*, 20(1):33–43.

Natali, A. N., Pavan, P. G., Carniel, E. L., and Dorow, C. (2005a). A transversally isotropic elasto-damage constitutive model for the periodontal ligament. *Comp. Meth. Biomech. Biomed.l Eng.*, 6:329–336.

Natali, A. N., Pavan, P. G., Carniel, E. L., Lucisano, M. E., and Taglialavoro, G. (2005b). Anisotropic elasto-damage constitutive model for the biomechanical analysis of tendons. *Med. Eng. Phys.*, 27:209–214.

Noll, W. (1958). A mathematical theory of the mechanical behavior of continuous media. *Archive for rational Mechanics and Analysis*, 2(1):197–226.

Noll, W. (1967). Materially uniform simple bodies with inhomogeneities. *Arch. Rat. Mech. Anal.*, 27:1–32.

Novak, V. P., Yin, F. C. P., and Humphrey, J. D. (1994). Regional mechanical properties of passive myocardium. *J. Biomech. Eng.*, 27:403–412.

Ogden, R. W. (1997). *Non-linear Elastic Deformations*. Dover, New York, USA.

Oliver, J. (1996). Modelling strong discontinuities in solid mechanics via strain softening constitutive equations. Part 1: Fundamentals. *Int. J. Numer. Meth. Eng.*, 39:3575–3600.

Oliver, J., Cervera, M., and Manzoli, O. (1999). Strong discontinuites and continuum plasticity models: The strong discontinuity approach. *Int. J. Plasticity*, 15:319–351.

Oliver, J., Huespe, A., Pulido, M., and Chaves, E. (2002). From continuum mechanics to fracture mechanics: The strong discontinuity approach. *Engr. Fracture Mech.*, 69:113–136.

Olsson, T. and Klarbring, A. (2008). Residual stresses in soft tissue as a consequence of growth and remodeling: application to an arterial geometry. *European Journal of Mechanics-A/Solids*, 27(6):959–974.

Orgel, J. P. R. O., San Antonio, J. D., and Antipova, O. (2011). Molecular and structural mapping of collagen fibril interactions. *Connec. Tiss. Res.*, 52:2–17.

Peña, E., Peña, J., and Doblaré, M. (2008). On modelling nonlinear viscoelastic effects in ligaments. *J. Biomech.*, 41:2659–2666.

Rabier, P. (1989). Some remarks on damage theory. *Int. J. Eng. Sci.*, 27(1):29–54.

Rausch, M. K. and Humphrey, J. D. (2016). A microstructurally inspired damage model for early venous thrombus. *J. Mech. Behav. Biomed. Mat.*, 55:12–20.

Rice, J. R. (1971). Inelastic constitutive relations for solids: an internal-variable theory and its application to metal plasticity. *J. Mech. Phys. Solids*, 19(6):433–455.

Rodriguez, E. K., Hoger, A., and McCulloch, A. D. (1994). Stress-dependent finite growth in soft elastic tissues. *J. Biomech.*, 27:455–467.

Rodriguez, E. K., Omens, J. H., Waldman, L. K., and McCulloch, A. D. (1993). Effect of residual stress on transmural sarcomere length distributions in rat left ventricle. *Am. J. Physiol.*, 264:H1048–H1056.

Rodriguez, J. F., Alastrue, V., and Doblare, M. (2008). Finite element implementation of a stochastic three dimensional finite-strain damage model for fibrous soft tissue. *Comp. Meth. App. Mech. Eng.*, 197:946–958.

Rodríguez, J. F., Cacho, F., Bea, J. A., and Doblaré, M. (2006). A stochastic-structurally based three dimensional finite-strain damage model for fibrous soft tissue. *J. Mech. Phys. Solids*, 54:864–886.

Roeder, B. A., Kokini, K., Sturgis, J. E., Robinson, J. P., and Voytik-Harbin, S. L. (2002). Tensile mechanical properties of three-dimensional type I collagen extracellular matrices with varied microstructure. *J. Biomech. Eng.*, 124:214–222.

Rumpler, M., Woesz, A., Dunlop, J. W., van Dongen, J. T., and Fratzl, P. (2008). The effect of geometry on three-dimensional tissue growth. *J. R. Soc. Interface*, 5(27):1173–1180.

Sacks, M. S. and Chuong, C. J. (1993). Biaxial mechanical properties of passive right ventricular free wall myocardium. *J. Biomech. Eng.*, 115:202–205.

Sasaki, N., Shukunami, N., Matsushima, N., and Izumi, Y. (1999). Time-resolved X-ray diffraction from tendon collagen during creep using synchrotron radiation. *J. Biomech.*, 32:285–292.

Schwartz, T. L., Rayancha, S., Rashid, A., Chlebowksi, S., Chilton, M., and Morell, M. (2007). Modafinil treatment for fatigue associated with fibromyalgia. *J. Clin. Rheumat.*, 13(1):52.

Sim, J. H., Puria, S., and Steele, C. R. (2007). On large deformation generalized plasticity. *Math. Mech. Solids*, 2(October).

Simo, J. C. and Taylor, R. L. (1991). Quasi-incompressible finite elasticity in principal stretches. Continuum basis and numerical algorithms. *Comput. Meth. Appl. Mech. Eng.*, 85:273–310.

Skalak, R. (1981). Growth as a finite displacement field. In Carlson, D. E. and Shield, R. T., editors, *Proceedings of the IUTAM Symposium on Finite Elasticity, 1981*, The Hague. Martinus Nijhoff Publishers.

Skalak, R., Dasgupta, G., Moss, M., Otten, E., Dullemeijer, P., and Vilmann, H. (1982). Analytical description of growth. *Journal of theoretical biology*, 94(3):555–577.

Skalak, R., Farrow, D. A., and Hoger, A. (1997). Kinematics of surface growth. *J. Math. Biol.*, 35:869–907.

Spencer, A. J. M. (1984). Constitutive theory for strongly anisotropic solids. In Spencer, A. J. M., editor, *Continuum Theory of the Mechanics of Fibre-Reinforced Composites*, pages 1–32. Springer-Verlag, Wien, Austria. CISM Courses and Lectures No. 282, International Centre for Mechanical Sciences.

Steigmann, D. (1990). Tension-field theory. In *Proceedings of the Royal Society of London A: Mathematical, Physical and Engineering Sciences*, volume 429, pages 141–173. The Royal Society.

Sun, D. D. N. and Leong, K. W. (2003). Functional engineering of load-supporting soft tissues. In *Comprehensive Structural Integrity*, volume 9, pages 97–130.

Sverdlik, A. and Lanir, Y. (2002). Time-dependent mechanical behavior of sheep digital tendon, including the effects of preconditioning. *J. Biomech.*, 124:78–84.

Taber, L. A. (1998a). Biomechanical growth laws for muscle tissue. *J. Theor. Biol.*, 193:201–213.

Taber, L. A. (1998b). Mechanical aspects of heart development. *Prog. Biophys. Molec. Biol.*, 69:225–254.

Taber, L. A. (1998c). A model for aortic growth based on fluid shear and fiber stress. *J. Biomech. Eng.*, 120:348–354.

Taber, L. A. and Humphrey, J. D. (2001). Stress-modulated growth, residual stress, and vascular heterogeneity. *J. Biomech. Eng.*, 123:528–535.

Taylor, R. L. (2007). *FEAP - A Finite Element Analysis Program, Version 8.2 User Manual*. University of California at Berkeley, CA, USA.

Thomopoulos, S., Williams, G. R., Gimbel, J. A., Favata, M., and Soslowsky, L. J. (2003). Variation of biomechanical, structural, and compositional properties along the tendon to bone insertion site. *J. Orthop. Res.*, 21(3):413–419.

Tower, T. T., Neidert, M. R., and Tranquillo, R. T. (2002). Fiber alignment imaging during mechanical testing of soft tissues. *Ann. Biomed. Eng.*, 30:1221–1233.

Truesdell, C. and Noll, W. (1965). *The Non-Linear Field Theories of Mechanics*, volume III of *Flügge. S., Ed., Encyclopedia of Physics*. Springer-Verlag, Berlin, Germany.

Valanis, K. C. (1995). The concept of physical metric in thermodynamics. *Acta Mech.*, 113(1-4):169–184.

Wang, C. and Bloom, F. (1974). Material uniformity and inhomogeneity in anelastic bodies. *Archive for Rational Mechanics and Analysis*, 53(3):246–276.

Wang, C.-C. (1967). On the geometric structures of simple bodies, a mathematical foundation for the theory of continuous distributions of dislocations. *Archive for Rational Mechanics and Analysis*, 27(1):33–94.

Watton, P. and Hill, N. (2009). Evolving mechanical properties of a model of abdominal aortic aneurysm. *Biomechanics and modeling in mechanobiology*, 8(1):25–42.

Watton, P. N., Hill, N. A., and Heil, M. (2004). A mathematical model for the growth of the abdominal aortic aneurysm. *Biomech. Model. Mechanobiol.*, 3:98–113.

Watton, P. N., Ventikos, Y., and Holzapfel, G. A. (2009). Modelling the growth and stabilization of cerebral aneurysms. *Mathematical medicine and biology: a journal of the IMA*, 26(2):133–164.

Weiss, J. A., Gardiner, J. C., and Bonifasi-Lista, C. (2002). Ligament material behavior is nonlinear, viscoelastic and rate-independent under shear loading. *J. Biomech.*, 35:943–950.

Williamson, D. and Harding, K. (2004). Wound healing. *Medicine*, 32:4–7.

Wren, T. A. L., Yerby, S. A., Beaupré, G. S., and Carter, D. R. (2001). Mechanical properties of the human Achilles tendon. *Clin. Biomech.*, 16:245–251.

Wuyts, F. L., Vanhuyse, V. J., Langewouters, G. J., Decraemer, W. F., Raman, E. R., and Buyle, S. (1995). Elastic properties of human aortas in relation to age and atherosclerosis: A structural model. *Phys. Med. Biol.*, 40:1577–1597.

Yavari, A. (2010). A geometric theory of growth mechanics. *J. of Non-linear Sci.*, 20(6):781–830.

Yin, F. C. P., Strumpf, R. K., Chew, P. H., and Zeger, S. L. (1987). Quantification of the mechanical properties of noncontracting canine myocardium under simultaneous biaxial loading. *J. Biomech.*, 20:577–589.

Zulliger, M. A., Fridez, P., Hayashi, K., and Stergiopulos, N. (2004). A strain energy function for arteries accounting for wall composition and structure. *J. Biomech.*, 37:989–1000.